Order N°:

Democratic and Popular Republic of Algeria
Ministry of Higher Education and Scientific Research

Djillali Liabes University of Sidi Bel Abbes
Faculty of Exact Sciences

THESIS

Presented at Faculty of Exact Sciences

In order to obtain the degree of:

DOCTOR OF SCIENCES

Option: Materials Physics

By

Ismail OUADHA

Title

Structural, mechanical, electronic and thermodynamic investigations of the new quaternary MAX phase $(Zr_{1-x}Ti_x)_3AlC_2$ with (x=0, 0.5, 1) by the first-principales study.

Publicly defended on ../../ 2021, in front of the following dissertation committee:

Pr. Boualem ABIDRI	***Chair***	***UDL-SBA***
Pr. Nour-Eddine BENKHETTOU	***Examiner***	***UDL-SBA***
Pr. Ali BENTOUAF	***External Examiner***	***U. Saida***
Pr. Djillali BENSAID	***External Examiner***	***U. Ain Temouchent***
Pr. Habib RACHED	***Supervisor***	***UHB-Chlef***
Pr. Djamel RACHED	***Co-supervisor***	***UDL-SBA***

University year 2020-2021

ACKNOWLEDGMENTS

*First and before all things, I would like to thank **ALLAH** the Almighty who gives me the power to go forward in a way illuminated with his merciful guidance.*

*I extend my warmest thank to my supervisor **Prof. Habib Rached** and co-supervisor **Prof. Djamel Rached** for giving me the chance to be one of their students and for their generous advices, patience and valuable discussions which helped me greatly.*

I would like to thank the chair and members of my dissertation committee, Pr. ABIDRI Boualem, Pr. BENKHETTOU Nour-Eddine, Pr. BENTOUAF Ali and Pr. BENSAID Djillali for generously offering their time.

I am so grateful to all my teachers and professors throughout my academic career, from the elementary school to the university.

Finally, I would like to thank my family and friends for their continued support and encouragement over the years.

Dedication

I dedicate this thesis to:

My lovely parents.

My lovely wife.

My children Mohammed Anes.

Contents

General Introduction

Chapter I. *Presentation of the MAX phases*

Chapter II. *Density functional theory DFT*

Chapter III. *Full-Potential Linearized Augmented Plane Wave Method*

Chapter IV. *Results and Discussion*

Conclusion

Abstract

International Publications

List of Figures

List of Tables

List of Symbols

DFT	Density Functional Theory
H	Hartree
HF	Hartree-Fock
XC	Exchange Correlation
KS	Kohn-Sham
LDA	Local Density Approximation
GGA	Generalized Gradient Approximation
PBEsol	Perdew-Burke-Ernzerhof functional for solids
APW	Augmented Plane Wave
LAPW	Linearized Augmented Plane Wave
FP	Full Potential
MT	Muffin-Tin region
I	Interstitial region
BM	Birch Murnaghan
$\mathbf{E}_l$	The linearization energies
$\mathbf{U}_l$	The radial functions
PVD	Physical vapor deposition
PLD	Pulsed laser Deposition
TDOS	Total Density Of States
PDOS	Partial Density Of States
V	Volume
P	Pressure
$\mathbf{C}_{ij}$	The elastic constants
B	The bulk modulus
G	Shear modukus
ν	Poisson's coefficient
$\boldsymbol{\theta_D}$	Debye temperature
$\boldsymbol{v_m}$	The average sound velocities
$\boldsymbol{v_l}$	Longitudinal sound velocities
$\boldsymbol{v_t}$	Transverse sound velocities
$\mathbf{E}_f$	Fermi energy level
$\mathbf{C}_v$	Constant volume heat capacity
$\mathbf{C}_p$	Constant pressure heat capacity

General Introduction

General Introduction

The growing interest in materials science has led to a true technological revolution of our time. The need to develop new materials that can meet the rapidly changing and renewable needs of society is one of the major challenges in the field of engineering and new technologies. Materials science is concerned with the elaboration and characterization of materials of whatever types, and constantly searching for new materials that meet the increasing demands of technological applications. In fact, before choosing a material to be used in a particular technological application, the possibilities of its use must be first studied by determining its physical and chemical properties (structural, electronic, mechanical … etc) through both experimental and theoretical methods. For example, improving aircraft engines must include an increase in operating temperature, so the materials used should be lighter and more resistant to high temperatures. In recent decades, researchers have shown that even the strongest metal alloys become soft at temperatures above 1000°C. Scientists have developed a new class of materials known as ceramics, but unfortunately it is characterized by fragility that limits its use despite undeniable progress in this field. Generally, brittleness, hardness and low usability are closely related to good resistance to high temperatures.

During the 1990s, the team Barsoum et al. [1] from Drexel University in Philadelphia, discovered interesting properties of Ti_3SiC_2. In addition to being inexpensive, this material is distinguished by its hardness, lightness, useable, resistance to oxidation and thermal shock and ability to remain solid at temperature above 1300°C in air. About fifty compounds with similar properties were synthesized and classified into a new family known as MAX phases, referring to their formulations.

MAX phases are ternary ceramic materials based on carbides or nitrides which constitute a new class of nanolamellar materials combining the properties of metals and ceramics which give them exceptional properties such as high elastic stiffness, high melting temperature, high thermal shock resistance and high electrical conductivity [2,3]. Due to the exceptional and desirable properties of MAX phases materials, they are well known to be used in many industrial applications such as in aerospace, automotive, defense, medical and nuclear reactors [4-7].

Recently in 2016, a successful experimental study of the new compound Zr_3AlC_2 of MAX family was reported [8]. After that, Zapata-Solvas et al. synthesized experimentally solid solutions $(Zr_{1-x}Ti_x)_3AlC_2$ by mixing Zr with Ti for different x concentration [4, 9,10].

In addition to experimental work, there are many theoretical studies related to the properties of MAX phases, for example, elastic properties and electronic-structure calculations. Moreover, theoretical study has significance in stimulating experimental research on the synthesis and application of new MAX phases compounds with better characteristics, reaching some results that are difficult to reach experimentally.

According to the theory of quantum mechanics, the electronic structures of materials can be theoretically determined by solving the Schrödinger equation, where defining the electronic structures of materials is fundamental to understanding and explaining experimental results obtained on their properties or even predicting their properties even if they have not yet been experimentally determined.

In order to widen previous works on Zr_3AlC_2 and Ti_3AlC_2 compounds and enriched literature by the uninvestigated MAX phase compounds, we have investigated the structural, mechanical electronic and thermodynamic properties of the new quaternary MAX phases $(Zr_{1-x}Ti_x)_3AlC_2$ for different concentrations (x = 0, 1/3, 1/2, 2/3, 1) using the first-principle full potential linearized augmented plane wave (FP-LAPW) method [11], in the framework of density functional theory (DFT) [12,13] and implemented in the WIEN2k code [14].

References

[1] M.W. Barsoum, T. El-Raghy. J. Am. Ceram. Sos. 79 (1996) 1953-1956.

[2] M.W. Barsoum, T. El-Raghy, Am. Sci. 89 (2001) 334-343.

[3] H. Yoo, M.W. Barsoum, T. El-Raghy, Nature 407 (2000) 581.

[4] E. Zapata-Solvas, S.-R.G. Christopoulos, N. Ni, D.C. Parfitt, D. Horlait, M.E. Fitzpatrick, A. Chroneos, W.E. Lee, J. Am. Ceram. Soc. 100 (2017) 1377.

[5] T. El-Raghy, M.W. Barsoum, A. Zavaliangos, S.R. Kolidindi, J. Am. Ceram. Soc. 82 (1999) 2855.

[6] M.W. Barsoum, L. Farber, T. El-Raghy, Metall. Mater. Trans. 30 (1999) 1727.

[7] D. Tallman, Acta Mater. 85 (2014) 132.

[8] T. Lapauw, J. Halimc, J. Lu, T. Cabioc'h, L. Hultman, M.W. Barsoum, K. Lambrinou, J. Vleugels, Euro. Ceram. Soc 36 (2016) 943.

[9] M.A. Hadi, Y. Panayiotatos, A. Chroneos, J. Mater. Sci. Mater. Electron. 28 (2016) 3386-3393.

[10] M.A. Hadi, M. Roknuzzaman, A. Chroneos, S.H. Naqib, A.K.M.A. Islam, R.V. Vovk, K. Ostrikov, Comput. Mater. Sci. 137 (2017) 318.

[11] J.C. Slater, Adv. Quant. Chem. 1 (1994) 5564.

[12] P. Hohenberg, W. Kohn, Phys. Rev. B 136 (1964) 864.

[13] W. Kohn, L.S. Sham, Phys. Rev. 140 (1965) 113.

[14] P. Blaha, K. Schwarz, G.K.H. Madsen, D. Kvasnicka, J. Luitz, WIEN2K, an Augmented Plane Wave þLocal Orbitals Program for Calculating Crystal Properties, 2001, ISBN 3-9501031-1-2.

CHAPTER I.
Presentation of the MAX phases

I.1. Introduction

The MAX phases $M_{n+1}AX_n$ are compounds with specific composition where M is an early transition metal, A is an A-group element and X is C and/or N, knows as 211, 312, 413 MAX phases for n = 1, 2 and 3, respectively. They have attracted an intensive interest at the community of science for nearly two decades. The first study of this type of compounds was done in 1960s on the Ti_3SiC_2 powder to determine its specific properties [1]. However, interest in these phases remained limited for many years. Significantly renewed interest in the MAX phases since mid-1990s after the intrinsic properties of the compounds became known, where Barsoum and El-Raghy reported on the synthesis and characterization of bulk and pure samples of Ti_3SiC_2, which combine the best properties of metals and ceramics that seemed very promising [2-4]. A major research effort has been carried out to synthesize pure MAX phases compounds, in the form of bulk or thin film [5,6]. Several MAX phases have been synthesized and many have been investigated for their interesting properties. Characterization and understanding of their physical, mechanical and chemical properties have fundamental and development goals for potential applications. Many recent articles focus on compounds such as Ti_3SiC_2 [7] and Ti_3AlC_2 [8], especially on their elastic and mechanical properties.

In 2016, T. Laupauw et al. were the first team to experimentally synthesized a new compound Zr_3AlC_2 of MAX family (312) [9]. Barsoum et al also successfully in synthesizied Ti_4AlN_3 compound of MAX family (413) [10].

The MAX phases have now been shown to include over 90 different compounds. The majority consists of 211 compounds, most of which were discovered by Nowotny [11]. There is a lot of work being done regarding the theoretical prediction of the stability of these types of compounds and there is still definitely an undiscovered chemical group [12]. Finally, it is interesting to note that it is possible to make a large number of solid solutions at sites M, A, and X, of which only a few have been synthesized thus far, so this will be particularly important to modify and improve the properties of these materials.

I.2. Chemical elements

The MAX phases take their name from their chemical composition $\mathbf{M_{n+1}AX_n}$, where:

- **M** is a transition metal (Sc, Ti, Zr, Nb,…).
- **A** is an element of group A (Al, Si, P,…).
- **X** is either C and /or N.

The index n varies from 1 to 3 and the corresponding structures M_2AX, M_3AX_2 and M_4AX_3 are named 211, 312 and 413 respectively [5]. The Fig I.1 shows the different possible elements used and gives the list of thermodynamically stable MAX phases.

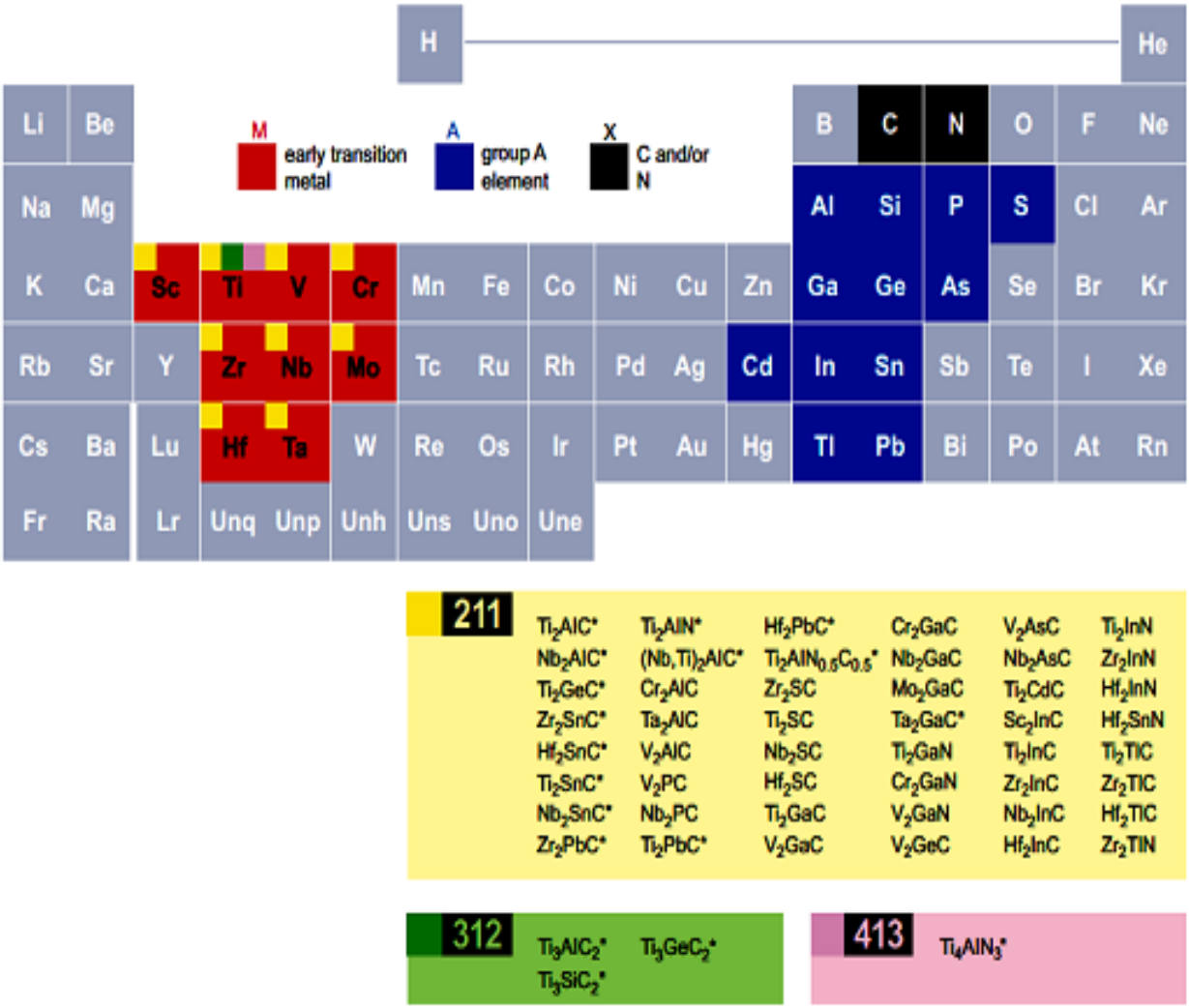

Fig I.1. Elements known to make up the MAX phases. Red indicates M-elements, blue A-elements and grey X-elements, and a list of the different thermodynamically stable phases [13].

I.3. Crystal structure

$M_{n+1}AX_n$ phases are hexagonal lamellar compounds which crystallize in the $P6_3/mmc$ space group. The Fig I.2 represents the hexagonal unit cell 211, 312 and 413 MAX phase, respectively. The size of the unit cell increases along the c-axis with increasing values of n.

The atoms in the MAX phases are arranged in alternate nanolaminate layers consisting of close-packed layers of M and X atoms – where the X atoms fill the octahedral sites between M

layers – intertwined with layers of pure A elements [5]. Wyckoff's positions for the atom sites in structures 211, 312, and 413 are listed in Table I.1.

The difference MAX phases between the three structures is due to the number of M layers separating the A layers, so that there are two layers in 211, three in 312 and four in 413 MAX phases. This difference in particular, is a fundamental factor in the origin of the mechanical properties of the MAX phase. The unit cells consisting of M_6X octahedral, for example Nb_6C, interleaved with layers of A-elements (such as As, In, Ga, or Ge). The M_6X edge-sharing octahedral building block in the MAX phases is the same as in the binary carbides and nitrides, MX. In MAX phases, the MX layers are twinned with respect to each other and separated by the A-layer which acts as mirror plane. This is shown in the Fig I.3, which is a cross-section image of a Ti_3SiC_2 structure taken with a high-resolution transmission electron microscope (TEM) [13].

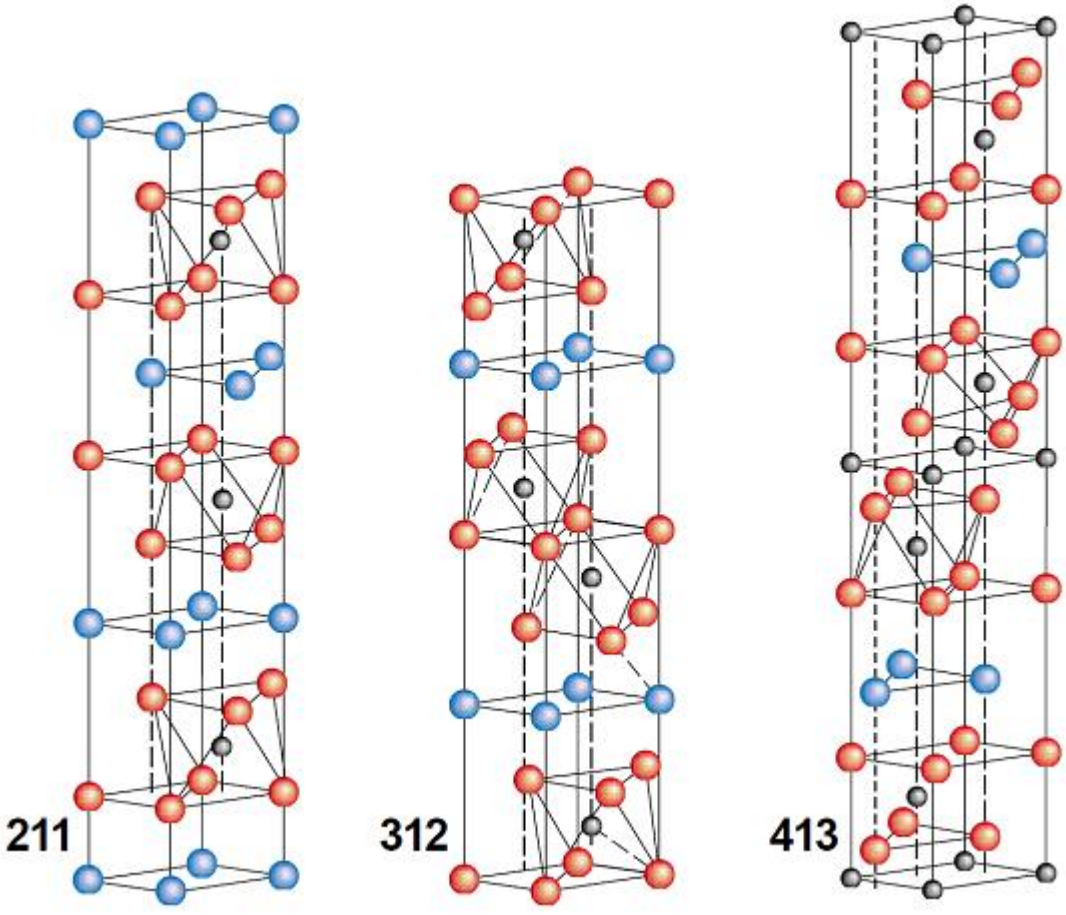

Fig I.2. Crystal structures of the three MAX groups. Early transition metal atoms are colored in red, A-group elements in blue, carbon or nitrogen in black [14].

Phases	Atoms	Wyckoff	*x*	*y*	*z*
211 M_2AX	M	4f	1/3	2/3	$Z_M \approx 0.08$
	A	2d	1/3	2/3	3/4
	X	2a	0	0	0
312 α-M_3AX_2	M_1	2a	0	0	0
	M_2	4f	2/3	1/3	$Z_M \approx 0.14$
	A	**2b**	0	0	1/4
	X	4f	1/3	2/3	$Z_M \approx 0.07$
312 β-M_3AX_2	M_1	2a	0	0	0
	M_2	4f	2/3	1/3	$Z_M \approx 0.14$
	A	**2d**	1/3	2/3	3/4
	X	4f	1/3	2/3	$Z_M \approx 0.07$
413 α-M_4AX_3	M_1	**4e**	0	0	$Z_M \approx 0.16$
	M_2	4f	1/3	2/3	$Z_M \approx 0.05$
	A	2c	1/3	2/3	1/4
	X_1	4f	2/3	1/2	$Z_M \approx 0.10$
	X_2	**2a**	0	0	0
413 β-M_4AX_3	M_1	**4f**	1/3	1/3	$Z_M \approx 0.66$
	M_2	4f	1/3	2/3	$Z_M \approx 0.05$
	A	2c	1/3	2/3	1/4
	X_1	**4e**	0	0	$Z_M \approx 0.10$
	X_2	**2a**	0	0	0

Table I.1. The Wyckoff positions for the atom sites in 211, 312 and 413 MAX phases.

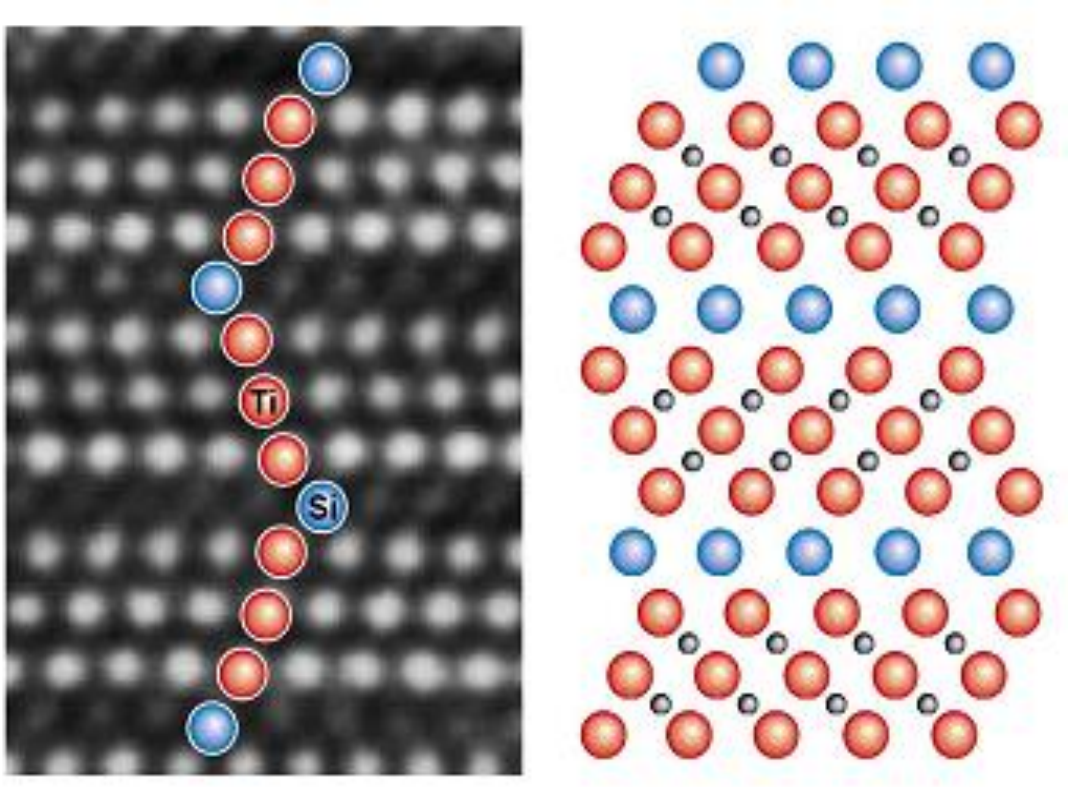

Fig I.3. The TEM image shows the cross section of the structure of Ti_3SiC_2. Small carbon atoms are not visible in the image (left). Diagram on the right is a micrograph of the same [5].

I.4. MAX Phases Properties

MAX phases have distinct properties of ceramic as well as certain properties of metals. The properties of the MAX phases compounds are generally similar to those of their binary carbide and nitride counterparts of formula MX.

I.4.1. Mechanical properties

Mechanical properties of some MAX phases were reported by Barsoum [5] and by Zhang et al [7]. In general, MAX phase are very stiffness with values of Young's modulus and shear modulus at room temperature ranging from 178 to 362 and 80 to 142 GPa, respectively [15,16]. This is especially true for the M_3AX_2 compounds where Young's modulus takes values greater than 300 GPa and shear modulus are close to 120 and 200 GPa. For example, Young's modulus value for Ti_3AlC_2 is 300 GPa while for Ti_2AlCit is only 200 GPa, since the number of M-X bonds is greater for 312 compounds compared to 211 compounds and therefore is stiffer than it. The Poisson's ratio for all MAX phases is approximately 0.2. This value is much lower than that of pure Ti (0.3) and closer to the TiC value (0.19) [15]. Although many of the physical

properties are similar between the MX and MAX phases, there are significant differences in mechanical properties. MX unlike MAX phases, are not machinable, do not tolerant damage, and are sensitive to thermal shock. The Debye temperature of MAX phases are relatively high and can be compared to ceramics instead of metals. The easy machinability of MAX phases at room temperature makes them candidates for many applications areas [14,15].

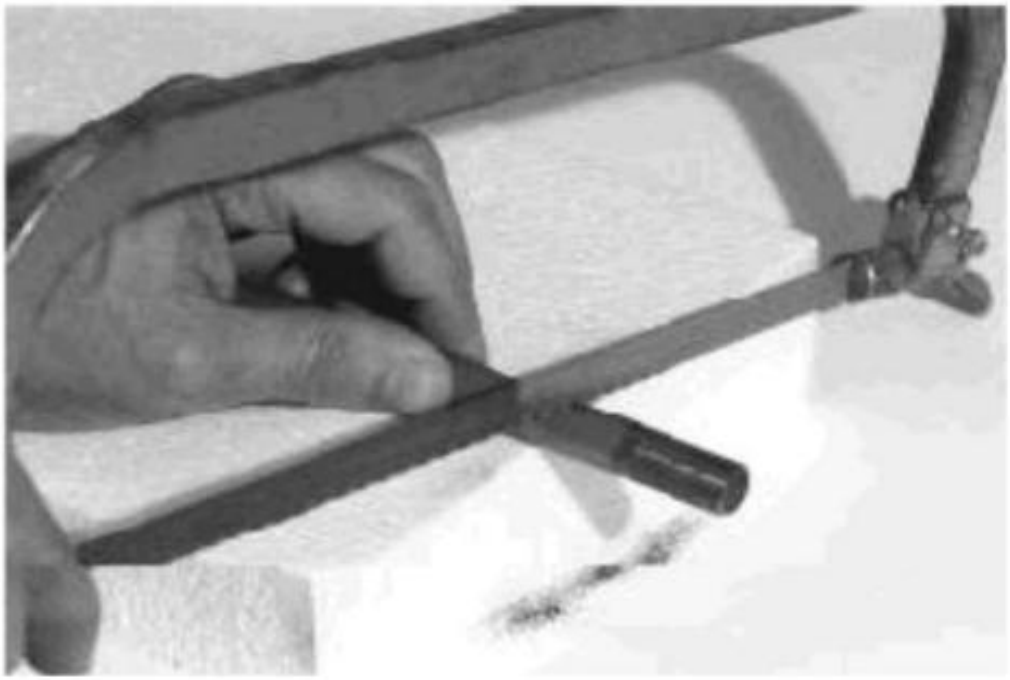

Fig I.4. Illustration of the machinability of the MAX phases Ti_3SiC_2 with the conventional tools [5].

I.4.2. Electrical properties

MAX phases are good metallic-type electrical conductors as their resistances are in a relatively narrow range of 0.2 to 0.7 $\mu\Omega$.m at room temperature [17]. It should be noted that the resistivity of MAX phases increases linearly with temperature as in the case of metals and its behavior can be described by:

$$\boldsymbol{\rho(T) = \rho_{300}\left(1 + \alpha(T - 300)\right)} \text{ ; T> } 100K \qquad \textbf{(I.1)}$$

where α is the temperature coefficient of resistivity. We note in the Fig I.5 that the Ti_3SiC_2 has better conductivity compared to Ti_3AlC_2, and even the latter is a good conductor compared to pure Ti. Exceptionally for Ti_4AlN_3, the resistivity of pure titanium and that of TiC are higher than those of compounds containing Ti.

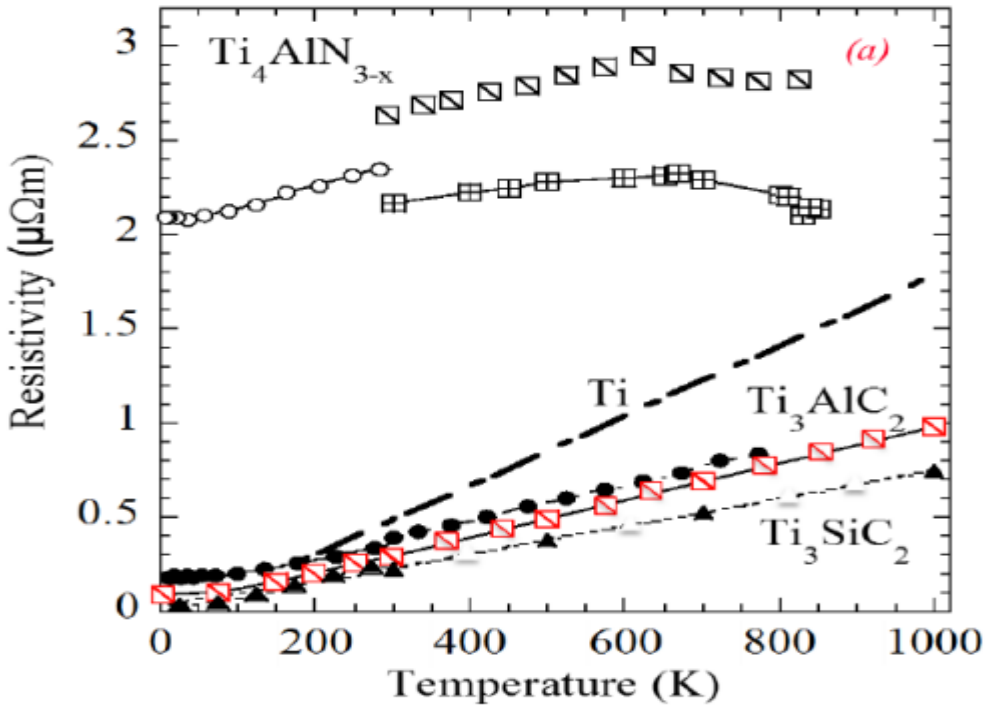

Fig I.5. Variation of the electrical resistivity with the temperature of some MAX phases [18,19].

I.4.3. Thermal properties

The MAX phases are good thermal conductors due to their good electrical conductivity, and their thermal conductivity ranges from 12 to 60 W/m.K at room temperature. Fig I.6 represents the variation in thermal conductivity of some MAX phases as a function of temperature.

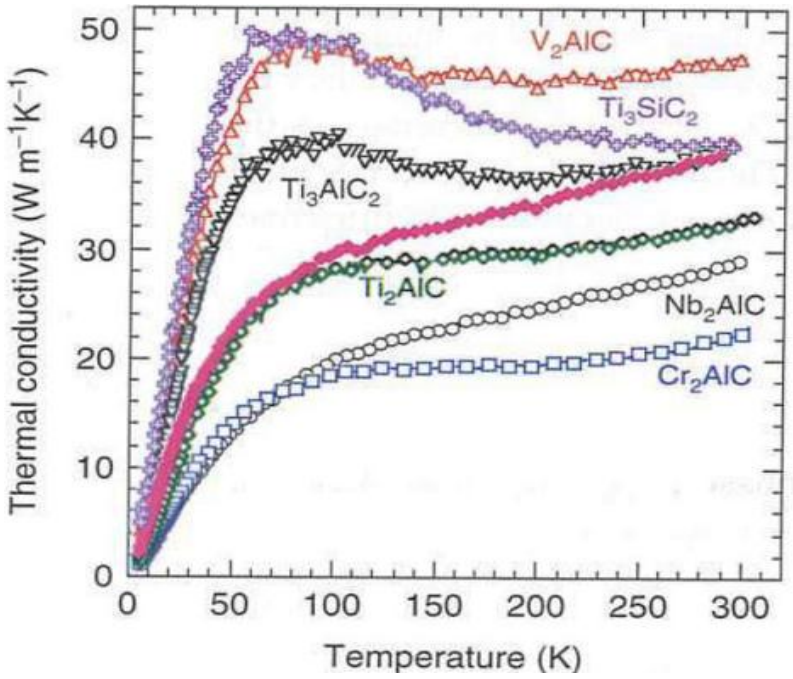

Fig I.6. The thermal conductivity of some MAX phases as a function of temperature [20].

MAX phases tend to have little anisotropy to thermal expansion, the coefficient of thermal expansion of the MAX phases is a little higher than that of the corresponding MX binary, which are in general between 5 and 10 μK^{-1} for the MAX phases [21]. More recently, it was discovered that Cr_2GeC has the highest thermal conductivity known to date, making it an excellent candidate for coating large areas on steels.

Also, Barsoum studied the evolution of the molar heat capacity C_p of the compounds: Nb_2SnC, Ti_3SiC_2 and Ti_4AlN_3 in the range 300-1300K under constant pressure [5]. The results of the experiment are shown in the Fig I.6 where the continuous lines created using the Debye model [5].

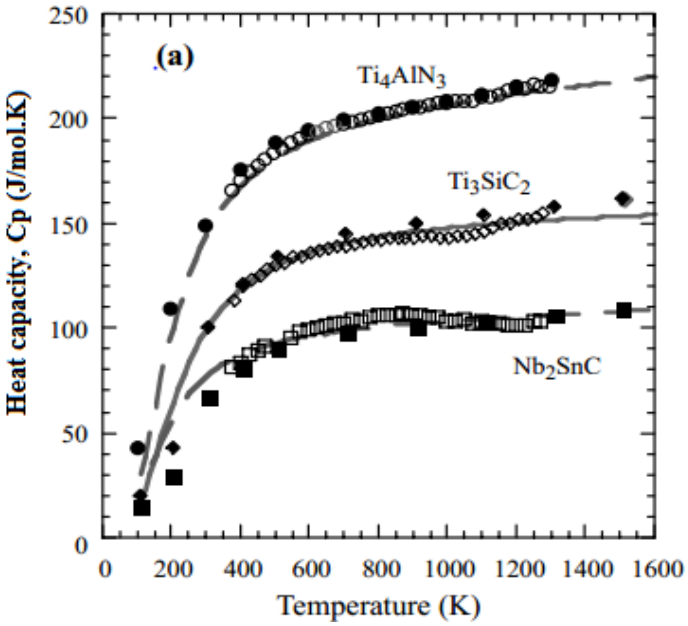

Fig I.7. The heat capacity C_P of Nb_2SnC, Ti_3SiC_2 and Ti_4AlN_3 compounds as a function of temperature [5].

The MAX phase don't melt, but decompose at high temperature producing transition metal carbide or nitride and the group A element depending on the reaction:

$$M_{n+1}AX_n \rightarrow M_{n+1}X_n + A \qquad \text{(I.2)}$$

This high temperature decomposition usually results in the evaporation of element A. The Ti_3SiC_2 compound is considered as a particularly heat resistant material because it only decomposes at more than 2300°C. Thermal shock resistance is a very important factor in thermal properties, and it can be defined as the thermal gradient that ceramic can undergo without affecting mechanical properties. Despite the brittleness of MAX phases, they have high

thermal shock resistance. For example, the Ti_3SiC_2 can withstand thermal shocks from 1400 °C to room temperature [5].

In the Table I.2, we present some of the physical properties of MAX phase compounds.

Metallic properties	***Ceramic properties***
➢ Excellent electrical and thermal conductivity ➢ Thermal shock resistance ➢ Resistance to damage ➢ Machinability at room temperature with traditional cutting tools ➢ Low hardness ➢ Relatively low thermoelectric power and Hall coefficient	➢ Very good resistance to acids and bases ➢ Refractory, decomposition at very high temperature ($> 1300℃$) ➢ Very good resistance to oxidation and corrosion ➢ Thermal stability of the crystal structure and retention of most of their properties at high temperature ➢ High stiffness and low density

Table I.2. Some physical properties of MAX phase compounds.

I.5. Synthesis of MAX phases

Herein, we briefly discuss the different methods of constructing MAX phases:

I.5.1. Synthesis of massive samples

The bulk MAX phases compounds are obtained from powder metallurgy. Two techniques are commonly used: Spark Plasma Sintering (SPS) [22] and Hot Isostatic Pressing (HIP) [4,23]. The modifications of the experimental conditions (temperature, pressure, duration) gives access to samples of different microstructures.

I.5.2. Synthesis of thin film

Growth of thin films from vapour phase can be divided into two two main groups: Physical vapour deposition (PVD) and chemical vapour deposition (CVD).

➢ ***P**hysical **v**apor **d**eposition **PVD**:* employs purely physical processes for generation vapour

which is condensed on substrate, for example thermal evaporation or sputtering.

- ***C**hemical **v**apor **d**eposition **CVD**:* the growth occurs through chemical reaction of species forming the desired material. This process takes place at thermodynamical equilibrium and thus requires high temperatures.

I.6. Potential applications

The MAX phases have distinct properties because they combine the mineral and ceramic properties, and they can be considered as good candidates for many applications. In addition to being good thermal and electrical conductors, they have good thermal and structural stability. Therefore, they are compounds that are used at high temperatures [5,24]. We will cite below some examples of the use of these materials:

- They can be used to build internal combustion engines that operate at higher temperatures than is currently possible, making them more efficient.
- Used as a structural material for aerospace applications.
- Protective coating in thermal barriers or as protective layers on various components.
- Automotive and vehicle applications.
- Defense, medical and nuclear reactors, … etc.

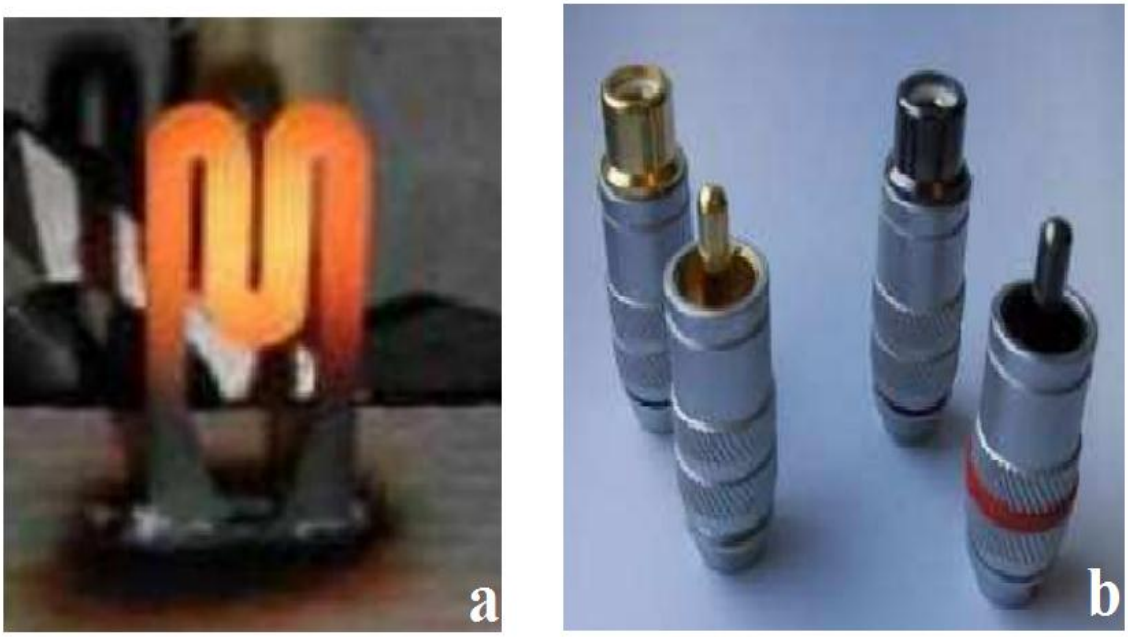

Fig I.8. (**a**): The Ti_2AlC is used as heating elements (~ 1400 ° C), (**b**): The replacement of the gold layer by Ti_3SiC_2 in the form of thin layers is carried out for electrical contacts coating [5,24].

References

[1] H. Nowotny, Prog. Solid State Chem. 2 (1970) 27.

[2] M.W. Barsoum, L. Farber, I. Levin, A. Procopio, T. El-Raghy, A. Berner, American Ceramic Society. 82 (1999) 2545-2547.

[3] C. Hu, F. Li, J. Zhang, J. Wang, J. Wang, Y. Zhou, Scripta Mater. 57 (2007) 893-896

[4] M. W. Barsoum and T. El-Raghy. Journal of the American Ceramic Society. 79 (1996) 1953–1956.

[5] M. W. Barsoum. Progress in Solid State Chemistry. 28 (2000) 201–281.

[6] P. Eklund, M. Beckers, U. Jansson, H. Högberg, and L. Hultman. Thin Solid Films 518 (2010) 1851–1878.

[7] H. B. Zhang, Y. W. Bao, and Y. C. Zhou. Journal of Materials Science and Technology 25 (2009) 1–38.

[8] X. H. Wang and Y.C. Zhou. Journal of Materials Science and Technology 26 (2010) 385 – 416.

[9] T. Lapauw, J. Halimc, J. Lu, T. Cabioc'h, L. Hultman, M.W. Barsoum, K. Lambrinou, J. Vleugels, Euro. Ceram. Soc. 36 (2016) 943.

[10] M.W.Barsoum, T. El-Raghy, A. Procopio, A 31 (2000) 333-337.

[11] H. Nowotny. Progress in Solid State Chemistry. 5 (1971) 27–70.

[12] J. Wang and Y. C. Zhou. Annual Review of Materials Research. 39 (2009) 415–443.

[13] M. W. Barsoum, T.El-Raghy. Am. Scientist. 89 (2001) 334-343.

[14] P. Eklund, M. beckers, U. Jansson, H. Hogberg, L.Hultman, Thin Solid Films. 518 (2010) 1851-1878.

[15] M.W. Barsoum, M. Radovic. Annu. Rev. Mater. Res. 41 (2011) 195-227.

[16] Z.M. Sun, Int. Mater. Rev. 56 (2011) 143-166.

[17] M.W. Barsoum. Encyclopedia of Materials Science and Technology, (2006) 1-1.

[18] P. Finkel, M.W. Barsoum, J.D. Hettinger, S.E. Lofland, H.I. Yoo. Phy. Rev. B 67 (2003) 235108.

[19] J.D. Hettinger, S.E. Lofland, P. Finkel, J. Palma, K. Harrell, S. Gupta, A. Ganguly, T. El-Raghy. B.W. Barsoum. Phy. Rev. B 72 115120 (2005) 235108.

[20] M. W. Barsoum. MAX Phases: Properties of Machinable Carbides and Nitrides. Wiley VCH-Verlag Gmb H&Co. KGaA, 2013.

[21] M. W. Barsoum, Edited by R. Riedel and I-W.Chen. Wiley-VCH Verlag. Ceramic Sience and Technology 2 (2010).

[22] M.A. El Saeed, F.A. Deorsola, R.M. Rashad, Int. Journal of Refractory Metals and Hard Materials 41 (2013) 48-53.

[23] L. Wang, J. Wang, J. Zhang, International Journal of Refractory Metals and Hard Materials. 39 (2013) 103-112.

[24] Z. M. Sun, Intern. Mat. Rev 56 (2011)143.

Chapter II. Density functional theory DFT

II.1- Introduction

The solid matters contain a large number of particles interacting with each other, which are represented by electrons, which are negatively charged particles, and in atomic nuclei, which are positively charged particles. They are usually arranged in a networked crystal system. If we had N nucleus, we would be faced with the issue of an electromagnetic reaction of $3(1+Z).N$ particles. Since the physical properties of a solid are closely related to the dynamics of these lightweight particles, the ground state of a system of atomic nuclei surrounded by electrons can be described by solving the time-independent Schrödinger equation, which is given by the following phrase [1,2]:

$$\boldsymbol{H\psi = E\psi} \qquad \textbf{(II.1)}$$

where :

ψ is the wave function of the crystal.

E is the energy of the basic state of the crystal.

H is the Hamiltonian that describes the electrostatic interaction between the particles (nuclei and electrons) inside the crystal.

The Hamiltonian H can be generalized:

$$\boldsymbol{H = T_e + T_N + V_{ee} + V_{eN} + V_{NN}} \qquad \textbf{(II.2)}$$

where:

$$\boldsymbol{T_e = -\frac{\hbar^2}{2m}\sum_i \nabla_i} \text{ (The kinetic energy of the electrons)} \qquad \textbf{(II.3)}$$

$$\boldsymbol{T_N = -\frac{\hbar^2}{2M}\sum_K \nabla_K} \text{ (The kinetic energy of the nuclei)} \qquad \textbf{(II.4)}$$

As well as the potential energies of the interaction:

$$\boldsymbol{V_{ee} = \frac{1}{2}\sum_{i,j\neq i} U_{ij} = \frac{1}{2}\sum_{i,j\neq i}\frac{e^2}{4\pi\varepsilon_0|\vec{r_i}-\vec{r_j}|}} \text{ (between the electrons)} \qquad \textbf{(II.5)}$$

$$\boldsymbol{V_{eN} = \frac{1}{2}\sum_{i,k} U_{ij} = \frac{1}{2}\sum_{i,j\neq i}\frac{e^2 Z_K}{4\pi\varepsilon_0|\vec{R_k}-\vec{r_l}|}} \text{ (between the electrons-nuclei)} \qquad \textbf{(II.6)}$$

$$\boldsymbol{V_{NN} = \frac{1}{2}\sum_{K,l\neq i} U_{ij} = \frac{1}{2}\sum_{K,l\neq i}\frac{e^2 Z_K Z_l}{4\pi\varepsilon_0|\vec{R_k}-\vec{R_l}|}} \text{ (between the nuclei)} \qquad \textbf{(II.7)}$$

where the indexes: k, l run on nuclei, i and j on electrons, R_k and M are positions and masses of the nuclei, r_i and m of the electrons, Z_k the atomic number of nucleus k.

The Schrödinger equation (1.1) contains $3(Z+1).N$ variable, N is the number of atoms in a crystal. If each one cm^3 of a solid crystal has about 5.10^{22} atoms and with $Z = 14$, then the number of variables will be equal to 2.10^{24} variables [3]. There is no general method in modern quantum mechanics that allows for a solution to this problem containing a large number of particles. Several approaches are presented at different levels to simplify equation (1.1) in order to be solvable. Generally, three approximations are entered at three different levels.

II.2. Born − Oppenheimer Approximation

Since nuclei are much heavier than electrons (the mass of a proton is about 1836 times the mass of an electron), so they move much slower than electrons, therefore, as a first approximation, the motion of the nucleus can be considered constant when studying the motion of electrons [4]. So, we can neglect the kinetic energy of the nucleus (T_N) and limit of the interaction of the nuclei with each other V_{NN} is taken as constant.

Accordingly, we have:

$$\boldsymbol{H_{tot} = H_e + V_{NN}} \qquad \textbf{(II.8)}$$

$$\boldsymbol{H_e = T_e + V_{Ne} + V_{ee}} \qquad \textbf{(II.9)}$$

where H_e is the electronic Hamilton.

Now, the problem is limited to searching for values and the intrinsic functions of electrons, that is searching for a solution to the following equation:

$$\boldsymbol{H_e\varphi = E_e\varphi} \qquad \textbf{(II.10)}$$

Thanks to the Born-Oppenheimer's Approximation, the problem has been simplified from $(Z + 1)\ N$ to the problem of ZN, but the solution of equation (1.10) is not possible analytical or numerical. Several methods have been developed to solve the multi-electron Schrödinger equation, among them the Hartree and Hartree-Fock method, and density functional theory.

Here we confine ourselves to giving the basic principles of the density functional theory used in the thesis topic.

II.3. Density Functional Theory

The basic idea of density functional theory (DFT) was introduced in 1927 by two scientists (Thomas and Fermi) [5,6] who proved that the homogeneous gas energy of electrons is a functional of the electronic density.

In fact, the use of electronic density as a functional variable to describe the properties of the system has existed since the earliest approaches to the electronic structure of matter, but it has obtained proof only by the demonstration of the two so-called Hohenberg and Kohn. DFT was developed in two phases:

- Theorems of Hohenberg and Kohn, in 1964 [7].
- Kohn − Sham equations, in 1965 [8]. Khon won the Nobel Prize in 1998 for his contribution to the development of the density functional theory DFT.

II.3.1. The Hohenberg and Kohn theorems

Density functional theory DFT was proven to be an accurate theory of multi-body systems by Hohenberg and Kohn [7] in 1964. It applies to any system of particles interacting in an external potential $V_{ext}(r)$. The theory is founded on two theorems:

II.3.1.1. First theorem

The first theorem of Hohenberg and Kohn states the following:

"The ground state density ρ (r) of a system of interacting electrons in an external potential $V_{ext}(r)$ uniquely defines this potential".

Hohenberg and Kohn have shown that the total energy E of a system with N electrons in its ground state in the presence of an external potential $V_{ext}(r)$ can only be determined by its electronic density $\rho(r)$ and can be written under the form:

$$\boldsymbol{E(\rho)=F(\rho)+\int \rho(r)V_{ext}(r)d^3r} \qquad \textbf{(II.11)}$$

where:

$$\boldsymbol{F(\rho)=T(\rho)+V_{ee}(\rho)} \qquad \textbf{(II.12)}$$

$F(\rho)$ is a universal function of the electron density ρ.

II.3.1.2. Second theorem

The second theorem of Hohenberg and Kohn is derectly related to the first and indicates that:

"There exists a universal functional $F(\rho)$ of the density, valid for any external potential V_{ext}, such that the global minimum value of the energy functional $E(\rho) = F_{HK}(\rho) + \int dr V_{ext}\rho(r)$ is the exact ground state energy of the system and the density that minimizes this functional is the exact ground state density ρ_0. Thus, the exact ground state energy and density are fully determined by the functional $E(\rho)$".

Here, Hohenberg and Kohn show that the real density of the ground state is only that which minimizes the energy E (ρ) and all the other properties are also a function of this density.

$$\boldsymbol{E(\rho_0) = \min E(\rho)} \qquad \textbf{(II.13)}$$

ρ_0 is the density of the ground state.

Unfortunately, the functional $F(\rho)$ is not known and the corresponding equations cannot be solved.

II.3.2. The Kohn −Sham equations

In 1965, Kohn and Sham (KS) [8] proposed a practical method for using the density functional theory. Kohn and Sham considered the equivalence between an electron system interacting in an external potential $V(r)$ and an electron system without interaction in an effective potential V_{eff}. Therefore, the functional of energy can be expressed by the following expression:

$$\boldsymbol{E[\rho(\vec{r})] = T_0[\rho(\vec{r})] + E_H[\rho(\vec{r})] + E_{xc}[\rho(\vec{r})] + \int V_{ext}(r)\rho(r)d^3r} \qquad \textbf{(II.14)}$$

where:

$T_0[\rho(\vec{r})]$: The kinetic energy of the electron gas without interaction.

$E_H[\rho(\vec{r})]$: The term of Hartree for electrons.

$E_{xc}[\rho(\vec{r})]$: The energy of exchange-correlation.

The difference between the real kinetic energy and that of electrons without interaction as well as the difference between the real interaction energy and that of Hartree are taken into account in the energy of exchange-correlation $E_{xc}[\rho(\vec{r})]$.

So the Schrödinger equation to be solved under the Kohn and Sham approach consistently is of the form:

$$\left(-\frac{1}{2}\nabla^2 + V_{eff}(r)\right)\varphi_i(r) = \varepsilon_i\varphi_i(r) \qquad \textbf{(II.15)}$$

where the effective potential is defined by:

$$V_{eff}[\rho(\vec{r})] = V_H[\rho(r)] + V_{ext}[\rho(r)] + V_{xc}[\rho(r)] \qquad \textbf{(II.16)}$$

where:

$V_H[\rho(r)] = \frac{1}{2}\int \frac{e^2}{4\pi\varepsilon_0}\frac{\rho(r')}{|r-r'|}dr'$ is the Hartree potential of the electrons.

$V_{xc}[\rho(r)] = \frac{\delta E_{xc}[\rho(r)]}{\delta\rho(r)}$ is the potential for exchange and correlation.

and $\varphi_i(r)$ are the states of a single particle and the electron density $\rho\ (r)$ is given by the sum of the orbitals occupied as follows:

$$\rho(r) = \sum\varphi_i^*(r)\varphi_i(r) \qquad \textbf{(II.17)}$$

To solve the system of equations (1.15) it is necessary to give an analytical form to the energy of exchange and correlation E_{xc}.

II.3.3. The exchange–correlation potential

Solving the Kohn and Sham equations which opened the way for practical applications of DFT, can only be achieved by giving an analytical form to the exchange and correlation energy. The most used approximations are: the local density approximation (LDA) and the generalized gradient approximation (GGA) and the Modified Becke–Johnson (MBJ) potential, …etc.

II.3.3.1. The local density approximation (LDA)

Kohn and Sham proposed the simplest way to approach the exchange-correlation energy, which is Local Density Approximation (LDA) [8].

The Local Density Approximation (LDA) consists in treating an inhomogeneous system, as locally homogeneous (uniform gas of interacting electrons where ρ is constant), therefore the exchange-correlation energy depends only on the electron density at a point r, neglecting any influence of the inhomogeneity of the system (the density is considered to vary very slowly). It is expressed as a function of the exchange-correlation energy per particle ε_{xc}:

$$E_{xc}^{LDA}[\rho] = \int \varepsilon_{xc}[\rho(r)]\rho(r)d^3r \quad \text{(II.18)}$$

The LDA approximation assumes that the functional of ε_{xc} is purely local. This energy can be divided into two negative terms:

$$\varepsilon_{xc}(\rho) = \varepsilon_x(\rho) + \varepsilon_c(\rho) \quad \text{(II.19)}$$

where ε_x is the exchange energy and ε_c is the correlation energy.

The LDA approximation is only strictly valid for interacting electron systems within the limits of a slowly varying density and high densities. In general, the LDA approximation is applicable for many systems close to the electronic gas model (electrons in solids), but it presents a serious defect for long distance interactions like molecules for example, it often leads to very poor energy data such as bond and low gap energy for semiconductors and insulating compounds.

Several approximate estimates of density have emerged to improve the exchange and correlation energy, and as a natural way to improve the LDA, is to make the exchange-correlation functional dependent on the local density and as well as density gradient. Generally, ε_{xc} is determined by the procedures like those of Kohn and Sham [8], Winger [9], Ceperly and Alder [10], Perdew and Wang [11].

II.3.3.2. The generalized gradient approximation (GGA)

In several cases, the LDA approximation has given reliable results with a slowly varying density, but in practical, it is rarely satisfied this condition**.** The generalized gradient approximation **(GGA)** was introduced to improve the accuracy of LDA results. The GGA proposed here retains correct features of LDA, and combines them with the most energetically important features of gradient-corrected nonlocality. It consists in writing the energy of exchange and correlation not only as a functional of the electronic density $\rho(r)$ but also of its gradient $\nabla\rho(r)$ to take into account the non-uniform character of the electron gas. It is written as follows:

$$E_{xc}^{GGA}(\rho) = \int f[\rho(r), \nabla\rho(r)]d^3r \quad \text{(II.20)}$$

The GGA approximation is given for different parametrizations, among them that of Perdew and its collaborators.

II.4. Solving the Kohn − Sham equations

In order to solve the Kohn - Sham equations numerically, it is necessary to choose a basis for the wave functions which can be taken as a linear combination of orbital, called the Kohn - Sham orbitals:

$$\boldsymbol{\varphi_i(r) = \sum C_{ij} \emptyset_j(r)} \quad \textbf{(II.21)}$$

where the $\emptyset_j(r)$ are the basic functions and the C_{ij} the development coefficients.

It is possible to determine the coefficients C_{ij} by solving the secular equation in a self-consistent manner for busy orbitals which minimize the total energy by keeping the orbitals orthogonal to each other.

$$\boldsymbol{(H - E_i S) C_i = 0} \quad \textbf{(II.22)}$$

where H represents the Hamiltonian and S the recovery matrix.

Then, the new charge density ρ_{out} is determined with the eigenvectors of this secular equation using the total charge density which can be obtained by summing over all the occupied orbitals (1.17). If the convergence of the calculations is not obtained, the charge densities ρ_{in} and ρ_{out} are mixed as follows:

$$\boldsymbol{\rho_{in}^{i+1} = (1 - \alpha)\rho_{in}^{i} + \alpha \rho_{out}^{i}} \quad \textbf{(II.23)}$$

with i represents the number of iterations and α the mixing parameter.

Thus, the iterative procedure can be continued until convergence is achieved.

Finally, in Fig II.1, a diagram illustrating the different steps in a self-consistent calculation performed by the density functional theory (DFT).

❖ For the resolution of the Kohn-Sham equations, several methods based on the density functional theory (DFT) are used:

- Methods based on a linear combination of atomic orbitals (LCAO) [12,13] which can be used, for example, for the d bands of transition metals.
- Methods derived from orthogonalized plane waves (OPW) [13,14] better suited to conduction bands of s-p character of simple metals.
- The augmented plane wave type (APW) [15].

- The linearized methods developed by Anderson [16]: Linearized augmented plane wave (LAPW) and linearized "Muffin-Tin" orbitals (LMTO), make it possible to gain several orders of magnitude in the computational times.

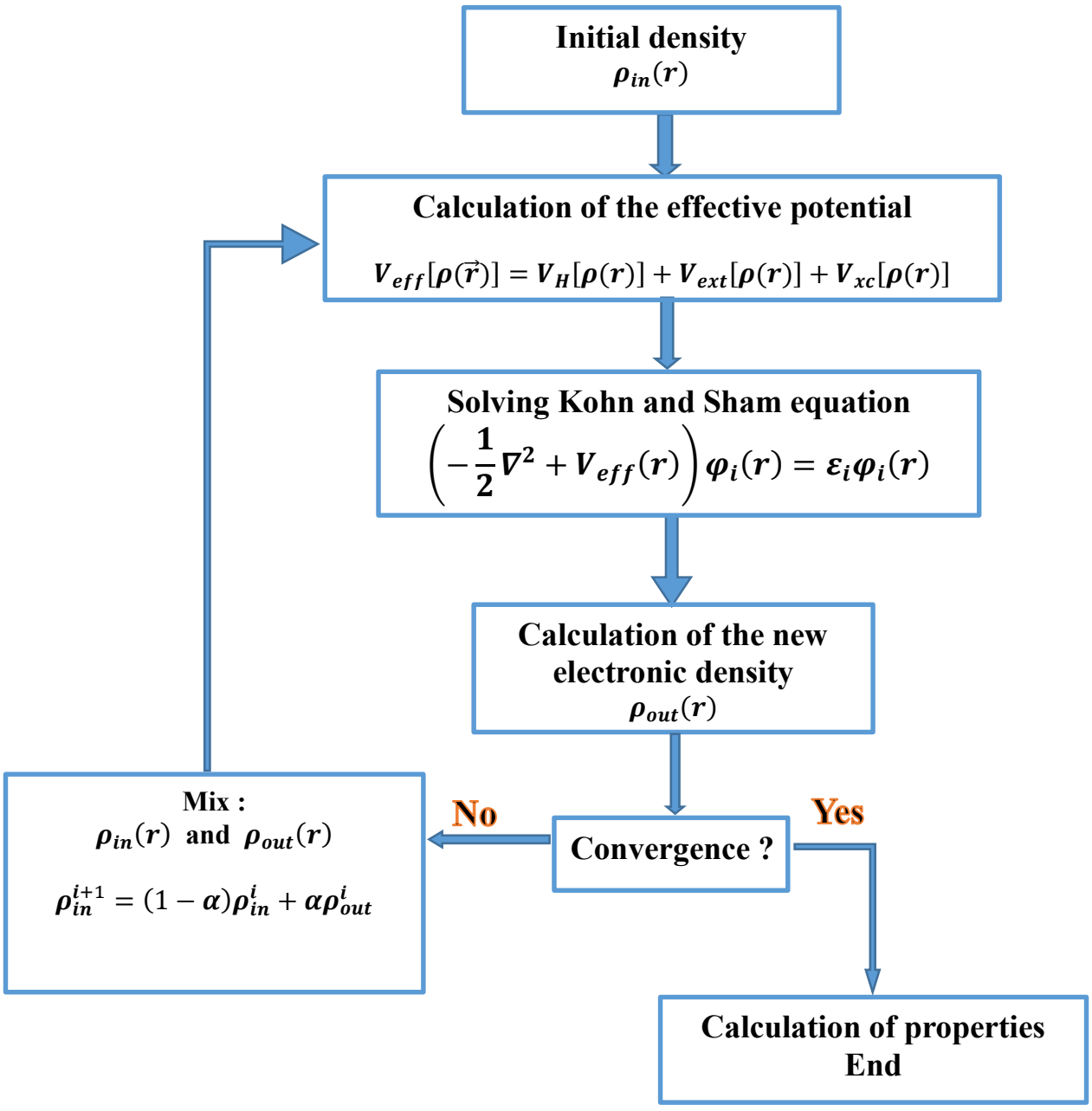

Fig II.1. The self-consistent field for solving KS and DFT equation.

References

[1] E. Schrödinger, Ann. Phys. 79 (1926) 361.

[2] E. Schrödinger, Ann. Phys. 79 (1926) 489.

[3] P. Kiréev, la physique des semi-conducteurs (Edition Mir, Moscou (1979)).

[4] M. Born, J.R. Oppenheimer, Ann. Phys. 87 (1927) 457.

[5] L.H. Thomas, Proc. Cambridge. Philos. Soc. 23 (1928) 542.

[6] E. Fermi, Z. Phys 48 (1928) 73.

[7] P. Hohenberg, W. Kohn, Phys. Rev. B 136 (1964) 864.

[8] W. Kohn, L.J. Sham, Phys. Rev. A 140 (1965) 1133.

[9] E. Winger, Phys. Rev. 46 (1934) 1001.

[10] D.M. Ceperly and B.J. Alder, Phys. Rev. Lett. 45 (1980) 566.

[11] J.P. Perdew and Y. Wang, Phys. Rev. B 45 (1992) 13244.

[12] F. Bloch, Z. Phys. 52 (1928) 555.

[13] J.C. Slater, Quantum Theory of Molecules and Solids, V2, Ch. 8 (1965).

[14] C. Herring, Phys. Rev. 57 (1940) 1169.

[15] J.C. Slater; Phys. Rev. 51 (1937) 846.

[16] O.K. Anderson, Phys. Rev. B12 (1975) 3060.

CHAPTER III.
Full-Potential Linearized Augmented Plane Wave Method

III.1. Introduction

The search for an effective way for solving the Kohn - Sham equations for solids, particles and materials (II.15) has led to the development of several more accurate and effective methods to calculating electronic structure, such as the Pseudo Potential Plane Wave and (PP-PW) and the Full Potential Linearized Plane Wave (FP-LAPW), which allow prediction of its structural, electronic, mechanical, optical and other properties. Often these methods replace experiment in which it is difficult or impossible to make experimental measurements. Among these more accurate computational methods for determining the electronic structure, constructed within framework of the functional density theory, the Full Potential Linearized Augmented Plane Wave (FP-LAPW) method, which we used in this study.

III.2. The augmented plane wave (APW)

In 1937, Slater proposed the augmented plane wave (APW) method in order to solve the Schrödinger equation for one electron [1-3]. Where the space surrounding the atoms is divided into two regions: the region near the nucleus, which is called a Muffin-Tin or atomic spheres, and the interstitial region, where it is further from the nucleus, as shown in Fig III.1.

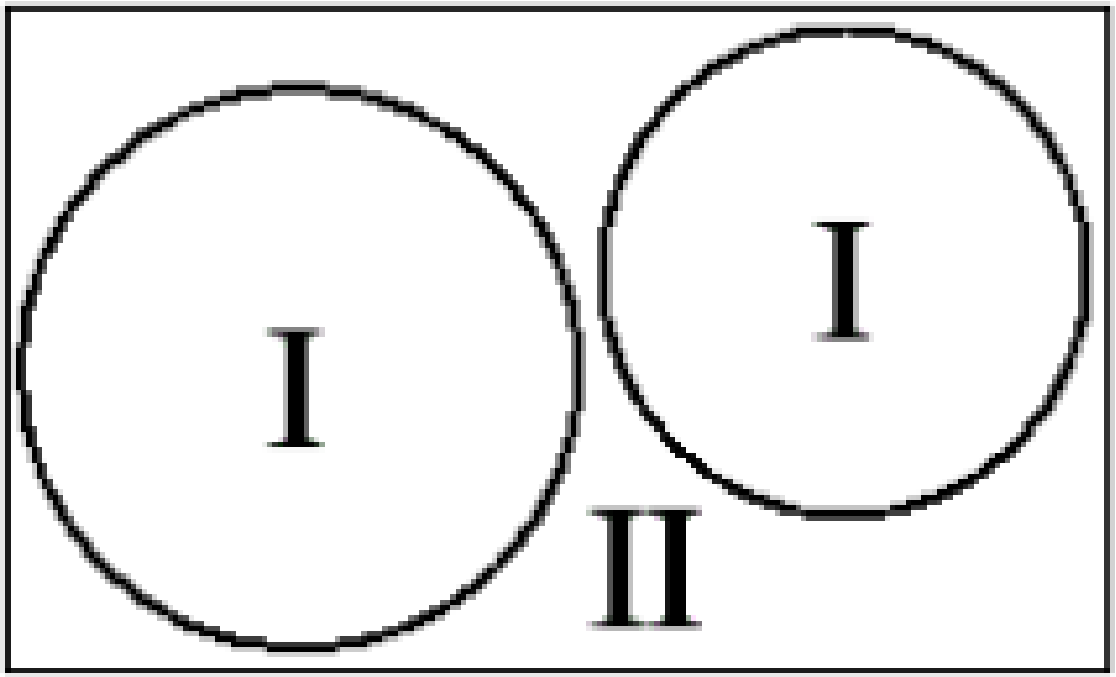

Fig III.1. Distribution of chemical unit cell spheres: Muffin-Tin region (I) and interstitial region (II).

The wave function for the wave vector K is written as the following:

$$\varphi(r) = \begin{cases} \sum_{lm} A_{lm} U_l(r) Y_{lm}(r) & r \in I \\ \frac{1}{\sqrt{\Omega}} \sum_G C_G e^{i(G+K)r} & r \in II \end{cases} \qquad \text{(III.1)}$$

where: K is Bloch vector, G is a reciprocal lattice vector, Ω is the unit cell volume, Y_{lm} are spherical harmonics, A_{lm} and C_G are expansion coefficients (l and m are quantum numbers) and the function $U_l(r)$ is the regular solution of the radial Schrödinger equation which is written in the form:

$$\left\{-\frac{d^2}{dr^2} + \frac{l(l+1)}{r^2} + V(r) - E_l\right\} r U_l(r) = 0 \qquad \text{(III.2)}$$

$V(r)$ represents the potential Muffin-Tin and E_l the linearization energy. The radial function $U_l(r)$ are the orthogonal to any eigenvalue of the heart. This orthogonality disappears in sphere limit [3] as shown by the following Schrödinger equation:

$$U_2 \frac{d^2 r U_1}{dr^2} - U_1 \frac{d^2 r U_2}{dr^2} = (E_2 - E_1) r U_1 U_2 \qquad \text{(III.3)}$$

where U_1 and U_2 are radial solutions for the E_1 and E_2 energies. Recovery being constructed using equation (3.2) and integrating it in parts.

Slater justifies the particular choice of these functions by noting that the plane wave are solutions of the Schrödinger equation when the potential is constant. As for the radial functions, they are solutions in the case of a spherical potential with E_1 as a proper value. This approximation is very good for face centered cubic materials, and less satisfactory with the decrease of symmetry of the material.

To ensure the continuity of the $\varphi(r)$ function on the surface of the MT sphere, the coefficients A_{lm} must be developed according to the C_G coefficients of the plane wave in the interstitial regions. After some algebraic calculations, these coefficients are expressed as the follows:

$$A_{lm} = \frac{4\pi i^l}{\sqrt{\Omega} U_l(R_\alpha)} \sum_G C_G j_l(|K+g|R_\alpha) Y_{lm}^*(K+G) \qquad \text{(III.4)}$$

The origin is taken at the center of the sphere, and the coefficients A_{lm} are determined from those of the plane waves C_G. The individual functions identified by G, thus become compatible with the radial functions in the M.T sphere, and one then obtains augmented plane waves (APWs).

The APWs functions are solutions to the Schrödinger equation in the spheres, but only for the energy E_l. Consequently, the energy E_l must be equal to that of the index band G. This means that the energy bands (for a point K) cannot be obtained by a simple diagonalization, and that it is necessary to treat the secular determinant as a function of energy.

There are some difficulties in the APW method related to the function $U_l(R_\alpha)$ which appears at the denominator of equation (III.4). Indeed, the value of $U_l(R_\alpha)$ can be equal zero at the surface of sphere M.T depending on the value of E_l, causing the radial functions to be separated with respect to the plane wave functions. To solve this problem, Koelling et al [4] and Anderson [3] made a series of changes to the APW method, mainly based on the representation of the radial function $\varphi(r)$ inside the spheres by a linear combination of the radial functions $U_l(r)$ and their derivatives with respect to the energy $U(r)$, thus giving birth the FP-LAPW method.

III.3. The linearized augmented plane wave (LAPW)

The LAPW approach solves the problems of APW method, that is, the basic functions and their first derivatives were parked at the Muffin-Tin boundary between core and interstitial region. To solve the problem, Anderson [3], Keolling et al [4] developed the linearized augmented plane wave (LAPW) method. Concerning this method, the basic functions in the MT spheres are combinations linear radial functions $U_l(r)Y_{lm}(r)$ and their derivatives $\dot{U}(r)Y_{lm}(r)$ with respect to energy. The $U_l(r)$ functions are defined as in the APW method (3.2) and the functions $\dot{U}(r)Y_{lm}(r)$ must satisfy the following condition:

$$\left\{-\frac{d^2}{dr^2}+\frac{l(l+1)}{r^2}+V(r)-E_l\right\}r\dot{U}(r)=rU_l(r) \qquad \textbf{(III.5)}$$

In the non-relativistic case, these radial functions $U_l(r)$ and $\dot{U}(r)$ ensure, on the surface of the MT spheres, continuity with the plane waves outside. And the augmented wave functions are used as basic functions of the FP-LAPW method, so we have:

$$\varphi(r)=\begin{cases}\sum_{lm}[A_{lm}U_l(r)+B_{lm}\dot{U}(r)]Y_{lm}(r) & r\in I\\ \frac{1}{\sqrt{\Omega}}\sum_G C_G e^{i(G+K)r} & r\in II\end{cases} \qquad \textbf{(III.6)}$$

where the coefficients B_{lm} corresponding to the function $\dot{U}(r)$ are the same nature as the coefficients A_{lm}.

The LAPW functions are flat waves only in the interstitial zones as in the APW method, but they are better suited within the spheres than the APW. In fact, if differs a bit from the E_l band energy, a linear combinations will better reproduce the radial function than the APW functions consisting of a single radial function. Therefore, the function, can be developed according to its derivative and the energy E.

$$\boldsymbol{U_l(E,r) = U_l(E_l,r) + (E - E_l)\dot{U}_l(E,r) + O[(E - E_l)^2]} \qquad \textbf{(III.7)}$$

where the $[(E - E_l)^2]$ represents the energetic quadratic error.

With this procedure the accuracy is less good than that of the APW method. The errors introduced into the calculation of the wave function and the energy are of the order $(E - E_l)^2$, $(E - E_l)^4$ respectively. The LAPW functions form a good basis which allowing one E_l to be used to obtain all the valence bands in a large energy region. When this is not possible, the energy window can generally be divided into two parts, which is a great simplification compared to the APW method. In general, if U_l is equal to zero on the surface of the sphere, its derivative will be different from zero. Consequently, the problem of continuity at the surface of the MT sphere will not arise in the LAPW method.

Takeda and Kubler [5] suggested popularizing the LAPW method using N radial functions and their derivatives (N-1). Each radial function has its own parameter E_{l_i} so that the linearization error is avoided. We find the standard LAPW method for $N = 2$ and E_{l_1} close to E_{l_2}, while for $N > 2$ the errors can be reduced. It should be noted, the use of high order derivatives to achieve convergence requires a much larger computation time than in the standard LAPW method. Singh [6] modified this approach by adding local orbitals at the base without increasing the cutoff energy of the plane waves.

III.4. The roles of linearization energies of E_l

We have already mentioned above that the errors in the wave function are on the order of $(E - E_l)^2$ and in the energy bands of the order $(E - E_l)^4$, indicates that the parameter E_l must be chosen in the center of the energy bands in order to obtain good results, and we can optimize the choice of the parameter E_l by calculation the total energy of the system for several values of E_l and selecting the set which gives the lowest energy.

Unfortunately, when these strategies work well in many cases, they can fail miserably in many others. The reason for this failure is described in the presence of high layer and extent of core state (only known as semi-core state) in several elements in particular: alkali metal, rare earths, recently metals of transition and actinides.

As mentioned, the augmented functions $U(r)Y_{lm}(r)$ and $\dot{U}(r)Y_{lm}(r)$ are orthogonal to each state of the core, this condition is never satisfied exactly accepted for the case where the states of the core would not have the same l. The effects of this inaccurate orthogonality to the core states in the FP-LAPW method are sensitive to the choices of E_l.

The most critical case, where there is an overlap between the bases FP-LAPW and the states of the core, which has presented false states of the core into the energy spectrum. To eliminate the ghost bands from the spectrum, we can set the energy parameter E_l equal to the energy of the state of the core.

III.5. Development in local orbitals

The aim of the LAPW method is to obtain precise band energies in the vicinity of the linearization energies E_l [3]. In most materials, just choose these energies from the center of the bands. However, this is not always possible and there are materials for which the choice of a single value of E_l is not sufficient for calculate all energy bands, it is for materials with $4f$ orbitals [7] and transition metals [8,9]. This is the fundamental problem of the state of semi-core which is intermediate between the state of valence and that of the core. To be able to remedy this situation, we either resort to using multiple energy windows, or by using development in local orbitals.

III.6. The LAPW + LO method

This method is based on treating all energy states with a single energy window. A linear combination of two radial functions are proposed [6,10]; the derivatives of these functions with respect energy are equal and their corresponding linearization energies are different.

The proper function is written as follows:

$$\boldsymbol{\varphi_{lm}^{LO}} = \left[\boldsymbol{A_{lm}U_l(r,E_{1,l}) + B_{lm}\dot{U}_l(r,E_{1,l}) + C_{lm}U_l(r,E_{2,l})}\right]\boldsymbol{Y_{lm}(r)}\ ; \quad \boldsymbol{r < R_\alpha} \qquad \textbf{(III.8)}$$

The A_{lm}, B_{lm} and C_{lm} coefficients are determined by the requirements that φ_{lm}^{LO} must be normalized and has zero value and slope at the sphere boundary.

III.7. The concept of the method FP-LAPW

Hamann and Wimmer [11,12] developed the accuracy of the LAPW + LO method by using the full potential (FP). In the FP-LAPW, no approximation is made in the interstitial region and inside the Muffin-tines which means that all the charge inside the solid is taken into account not only that of the valence states. In the FP-LAPW approach, the potential and the charge density are developed into radial functions times spherical harmonics inside each atomic spheres, and into Fourrier series in the interstitial region, with is the origin of the name "Full Potential". For this method, the potential and the charge density are expanded as:

$$V(\boldsymbol{r}) = \begin{cases} \sum_{lm} \boldsymbol{V_{lm} Y_{lm}(r)} & \boldsymbol{r < R} \\ \sum_{G} \boldsymbol{V_G\, e^{iG.R}} & \boldsymbol{r > R} \end{cases} \qquad \textbf{(III.9)}$$

and:

$$\boldsymbol{\rho(r)} = \begin{cases} \sum_{lm} \boldsymbol{\rho_{lm} Y_{lm}(r)} & \boldsymbol{r < R} \\ \sum_{G} \boldsymbol{V_G\, e^{iG.R}} & \boldsymbol{r > R} \end{cases} \qquad \textbf{(III.10)}$$

III.8. The WIEN2k code

WIEN2k is one of the fastest and most reliable simulation codes among the calculation methods. The FP-LAPW method has been implemented in the WIEN code, a set of independent F90 programs developed by Blaha, Schwarz and their collaborators [13] which are linked by C. Shell Script. There are several versions of WIEN including WIEN97 [14], which was later improved to give WIEN2k [13]. The main programs necessary to make the self-coherent calculation are:

NN: a program which gives the distance between the nearest neighbors, which helps to determine the atomic radius of the sphere MT and also check the overlap of the atoms.

LSTART: generate free atomic electronic densities, and determines the treatment of different orbitals in the band structure calculation, like states of the heart with or without local orbitals.

Symmetry: generates the space group symmetry operations and determines the point group of individual atomic sites in order to reduce the period of calculation.

KGEN: generates a k-mesh in the Brillouin zone.

DSTART: computes the initial starting density for the auto-coherent cycle from the superposition of free atomic densities generated in LSTART. Then a self-coherent cycle is initialized and repeated until the convergence criterion is verified.

This cycle is part of the following stages:

LAPW0: generates the potential from density.

LAPW1: calculates the eigenvalues and eigenvectors of valence bands.

LAPW2: calculates valence densities from eigenvectors and fermi's energy.

LCORE: calculates the energy and density of the core states.

MIXER: combine the initial density and the final density and uses the total resulting density as an initial one for the next iteration.

Once the self-consistent calculation is completed, the properties of the ground state (charge density, band structure, elastic properties, …etc.) are then determined.

The different calculation processes are illustrated in the diagram presented in Fig III.2.

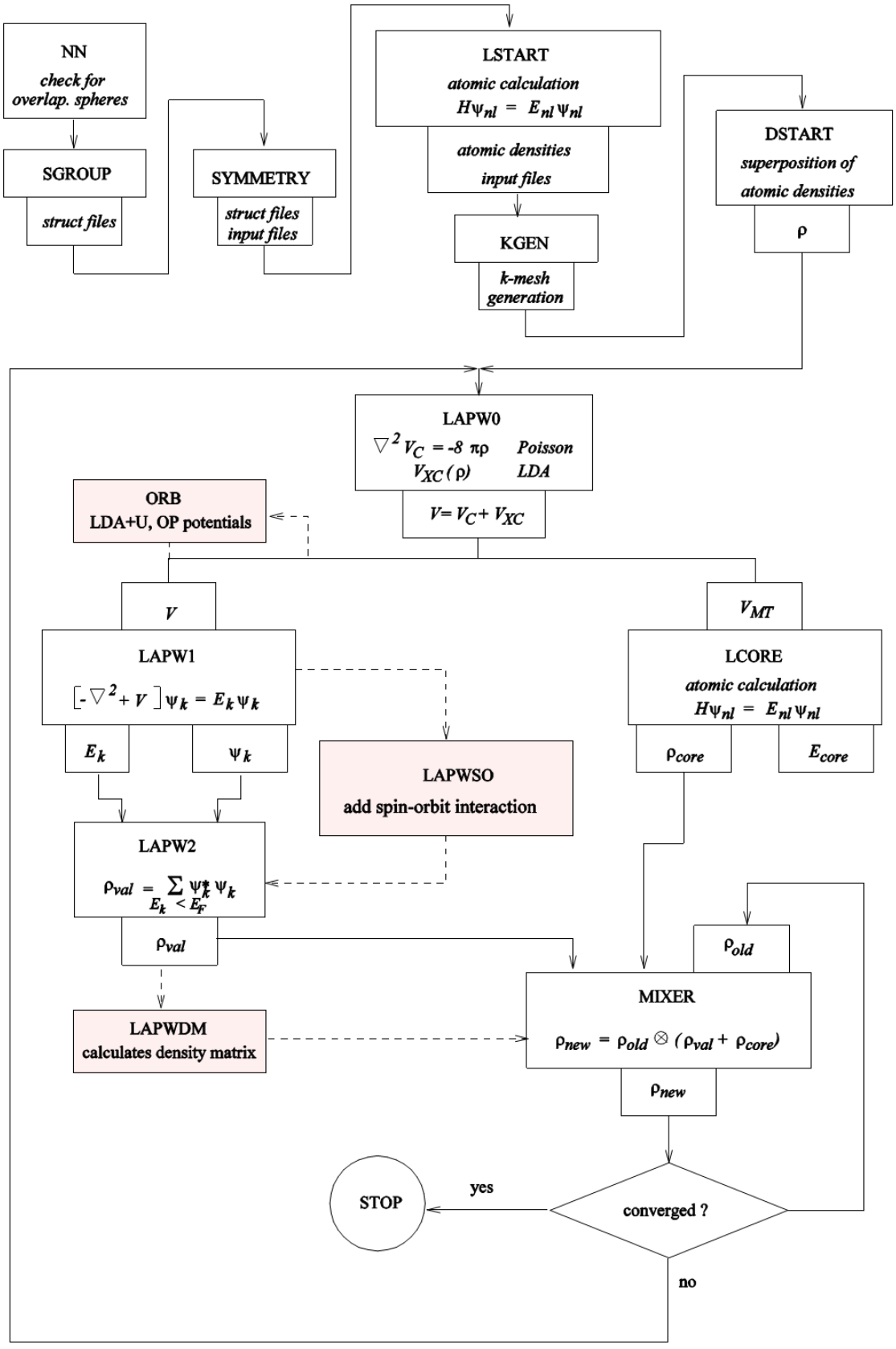

Fig III.2. Program flow in WIEN2K [13].

References

[1] J.C. Slater, Phys. Rev. 51 (1937) 846.

[2] J.C. Slater, Advances in Quantum Chemistry 1 (1964) 35.

[3] O. Andersen, Phys. Rev. B 12 (1975) 3060.

[4] D.D. Koelling, G.O. Arbman, J. Phys. F: Metal Phys. 5 (1975) 2041.

[5] T. Takeda, J. kubler, F 5, (1979) 661.

[6] D. Singh, Phys. Rev. B 43 (1991) 6388.

[7] S. Goedecker and K. Maschke, Phys. B 42 (1990) 8858.

[8] D.J. Singh, H. Krakauer, Phys. Rev B 43 (1991) 1441.

[9] D.J. Singh, H. Krakauer, P. Blaha, Phys. Rev B 46 (1992) 5849.

[10] J. Petru, L. Smrcka, Czech. J. Phys. B 35 (1985) 62-71.

[11] D. R. Hamann, Phys. 212 (1979) 662.

[12] E. Wimmer, H. Krakauer, M. Weinert, A.J. Freeman, Phys. B 24 (1981) 864.

[13] P. Blaha, K. Schwarz, G.k.H. Madsen, D. Kvasnicka, J. Luitz, WIEN2k, an Augmented Plane Wave+Local Orbitals Program for Calculating Crystal Properties, 2001, ISBN 3-9501031-1-2.

[14] A. WIEN "Improving the efficiency of FP-LAPW calculations. M. Petersen, F. Wagner, L. Hufnagel, M. Schwars, P. Blaha, K. Schwarz".

CHAPTER IV.

Results and Discussion

VI.1. Computational method

In this thesis and in order to do our calculation, we have employed full potential linearized augmented plane wave (FP-LAPW) method [1] implemented in the WIEN2k code [2] and based on the density functional theory (DFT) which has proven to be one of the most accurate theory for the calculation of the electronic and structural properties of solids [3-18].

In the FP-LAPW method, the space is divided into two regions: the first is a non-overlapping Muffin-Tin (MT) spheres where the basis set inside this region is described by radial solutions of the one-particle Schrodinger equation and their energy derivatives multiplied by spherical harmonics and the second one which is interstitial region (IR) the basis set consists of plane waves [19].

For the exchange-correlation functional we have adopted the generalized gradient approximation (GGA) parametrized by Perdew-Burke-Ernzerhof (PBE) [20]. The convergence tests allow us to choose the parameter $R_{mt}*K_{max} = 8$ where R_{mt} is the smallest atomic sphere radius and K_{max} is the plane wave cutoff [21]. The chosen R_{MT} values of Zr, Ti, Al and C are 1.96, 1.96, 2.38 and 1.74 Bohr, respectively. The G_{max} was chosen to equal the 14 value where G_{max} is defined as the magnitude of the largest vector in the charge density Fourier expansion. The MT sphere were considered up to $l_{max} = 10$. The Monkorst-Pack method in the first Brillouin zone (IBZ) was performed using 1500 kpoints. The charge convergence was set to 10^{-4}.

The M_3AlC_2 compounds crystallize in a hexagonal structure with the $P6_3/mmc$ space group (#194) [22,23] as shown in Fig IV. 1. The atoms Zr occupy the Wyckoff positions 2a and 4f with Z_M ~0.12. The Al atoms occupy 2b atomic positions while the C atoms reside in 4f with Z_C ~0.07 (see Table IV. 1).

Compound	Atom	Site	Coordinates
M_3AlC_2 M= Zr, Ti $P6_3/mmc$ (#194)	M	2a	(0, 0, 0)
		4f	(2/3, 1/3, z_M)
	Al	2b	(0, 0, 1/4)
	C	4f	(1/3, 2/3, z_C)

Table IV. 1. The Wyckoff positions for M_3AlC_2 compounds [24].

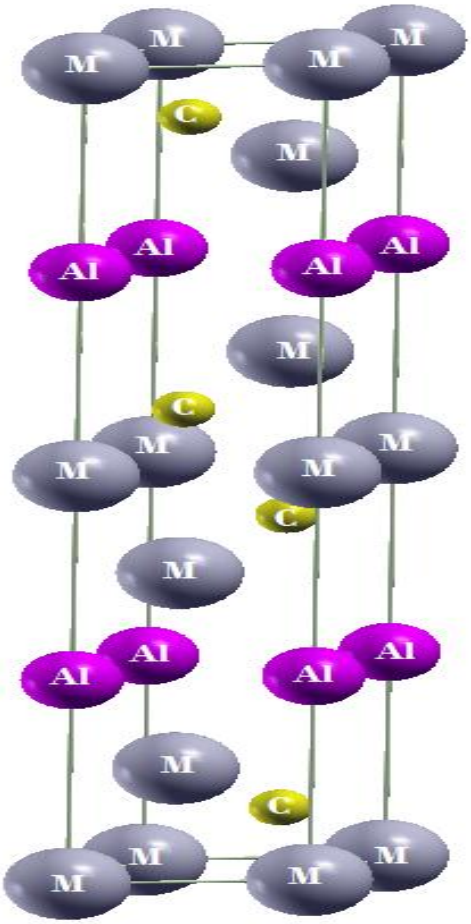

Fig IV.1. A view of the crystal structure of the MAX Phase M_3AlC_2 compound where (M=Zr and/or Ti) [24].

IV.2. Structural properties

The structural properties of $(Zr_{1-x}Tix)_3AlC_2$ compounds were studied for x=0, 1/3, 1/2, 2/3 and 1). The behavior of a solid under pressure is described by the equation of state. We initialize by calculating the total energy as a function of the unit volume using the Perdew-Burke-Ernzerhof (PBE), in order to determine the equilibrium unit-cell parameters (lattice parameter a and c), the bulk modulus B(GPa), the resulting data were fitted by the Birch-Maranghan state equation (EOS) [25,26].

$$E(V) = E_0 + \frac{9V_0B_0}{16}\left\{\left[\left(\frac{V_0}{V}\right)^{\frac{2}{3}} - 1\right]^3 B_0' + \left[\left(\frac{V_0}{V}\right)^{\frac{2}{3}} - 1\right]^2 \left[6 - 4\left(\frac{V_0}{V}\right)^{\frac{2}{3}}\right]\right\} \qquad \text{(IV.1)}$$

where:

V_0 is the equilibrium volume of the unit cell.

E_0 is the corresponding total energy (the minimum of the total energy).

B_0 is the compressibility modulus and B' is its pressure derivative; where:

$$B_0 = V\left(\frac{\partial^2 E}{\partial V^2}\right)_{P=0} \qquad \text{(IV.2)}$$

We have used the 2D-optimize package developed by J. Morteza [27] which is implemented in the WIEN2K code to determine the structural lattice parameters of our compounds.

The Fig IV.2 shows the change of the total energy as a function of the volume of unit cell of our compounds.

In Table IV.2, we presented our results and some other experimental and theoretical results recently obtained for comparison. We can see that our results are in good agreement with corresponding experimental and theoretical results. We also see that when the x concentration increases, all the lattice parameters a and c and the volume of the unit cell decrease while the hexagonal ration c/a increases in general. We can interpret this by decreasing the atomic radius because the atomic radius of Ti atom is less than the one of the Zr atom. The values of the bulk modulus B increase when the x concentration increases. This result is consistent with the fact that B is inversely proportional with the unit cell volume. Thus, it achieves the inverse relationship between the volume and pressure.

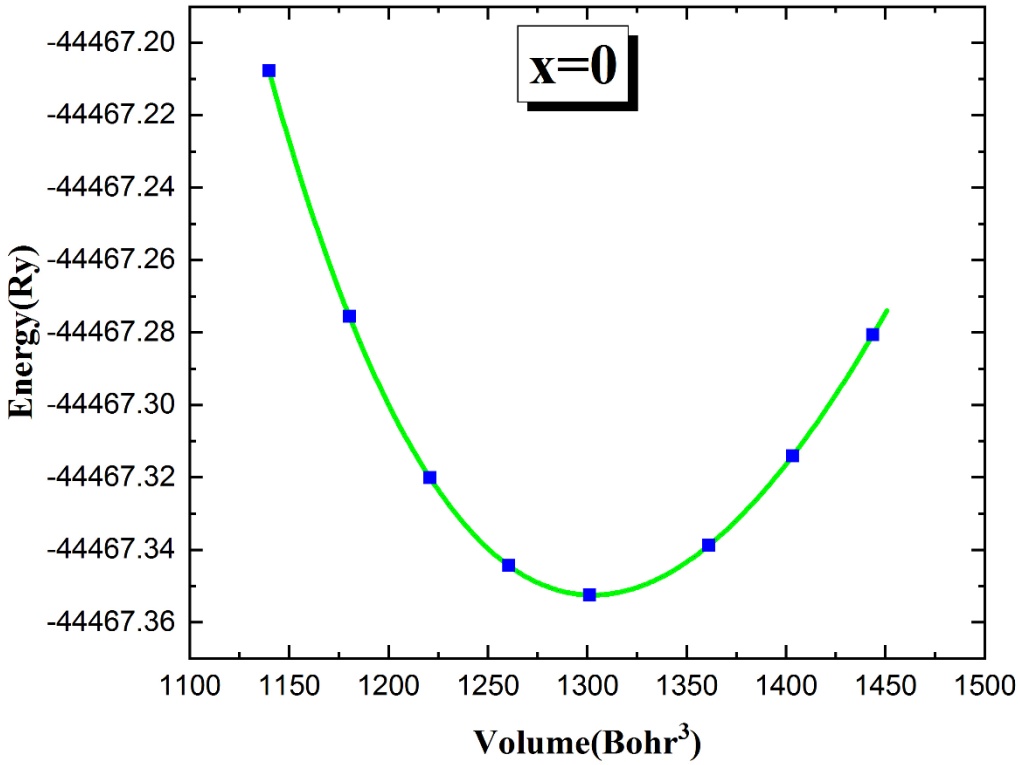
x=0
-44467.20
-44467.22
-44467.24
-44467.26
-44467.28
-44467.30
-44467.32
-44467.34
-44467.36
Energy(Ry)
1100
1150
1200
1250
1300
1350
1400
1450
1500
Volume(Bohr3)

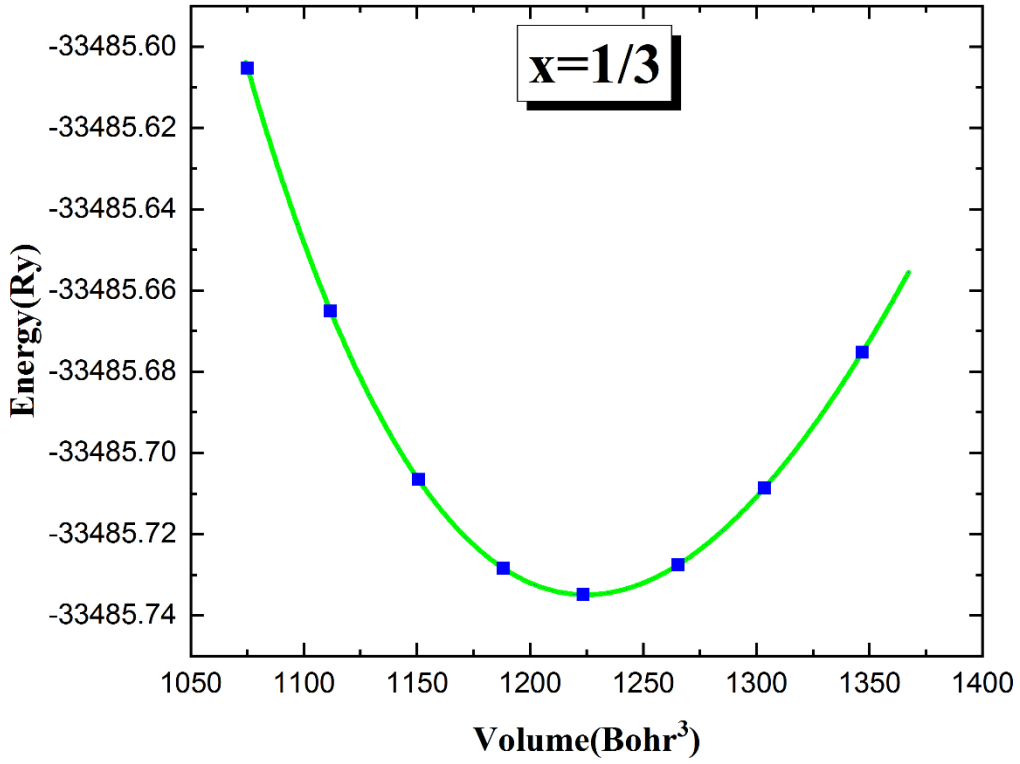
x=1/3
-33485.60
-33485.62
-33485.64
-33485.66
-33485.68
-33485.70
-33485.72
-33485.74
Energy(Ry)
1050
1100
1150
1200
1250
1300
1350
1400
Volume(Bohr3)

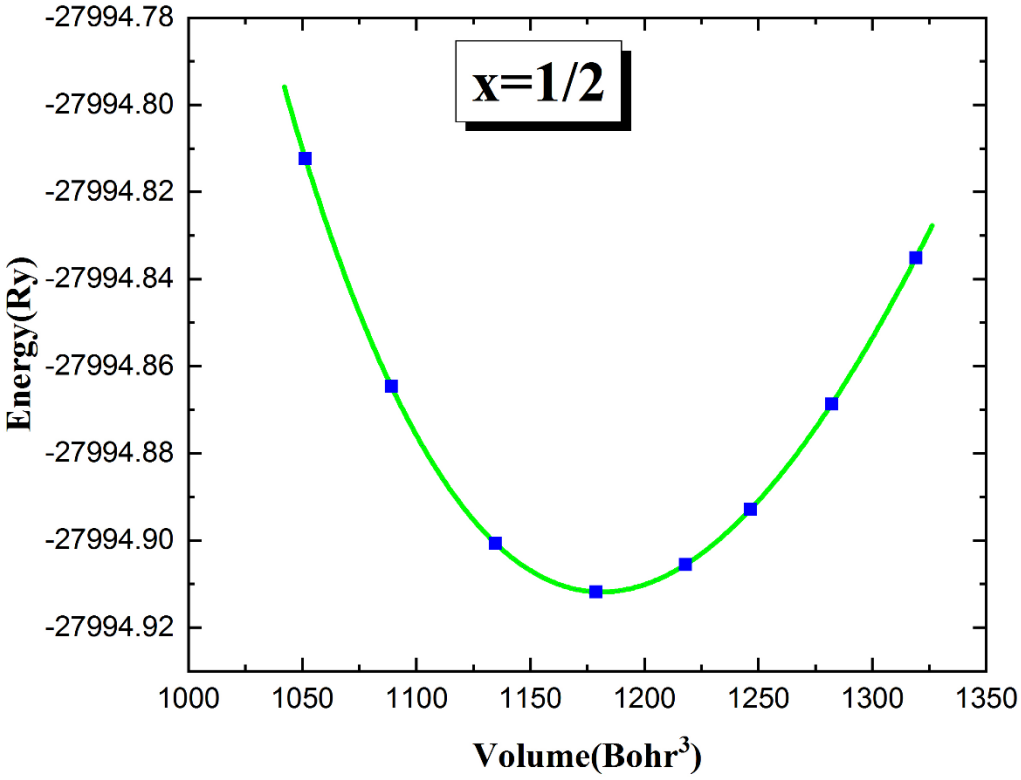
x=1/2
Energy(Ry)
-27994.78
-27994.80
-27994.82
-27994.84
-27994.86
-27994.88
-27994.90
-27994.92
1000
1050
1100
1150
1200
1250
1300
1350
Volume(Bohr3)

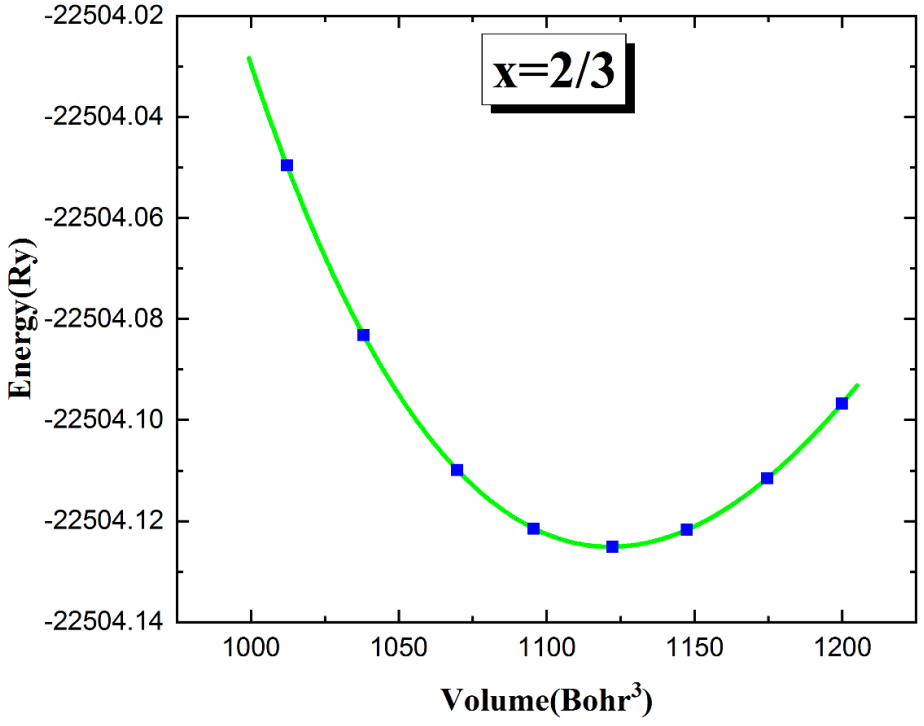
x=2/3
Energy(Ry)
-22504.02
-22504.04
-22504.06
-22504.08
-22504.10
-22504.12
-22504.14
1000
1050
1100
1150
1200
Volume(Bohr3)

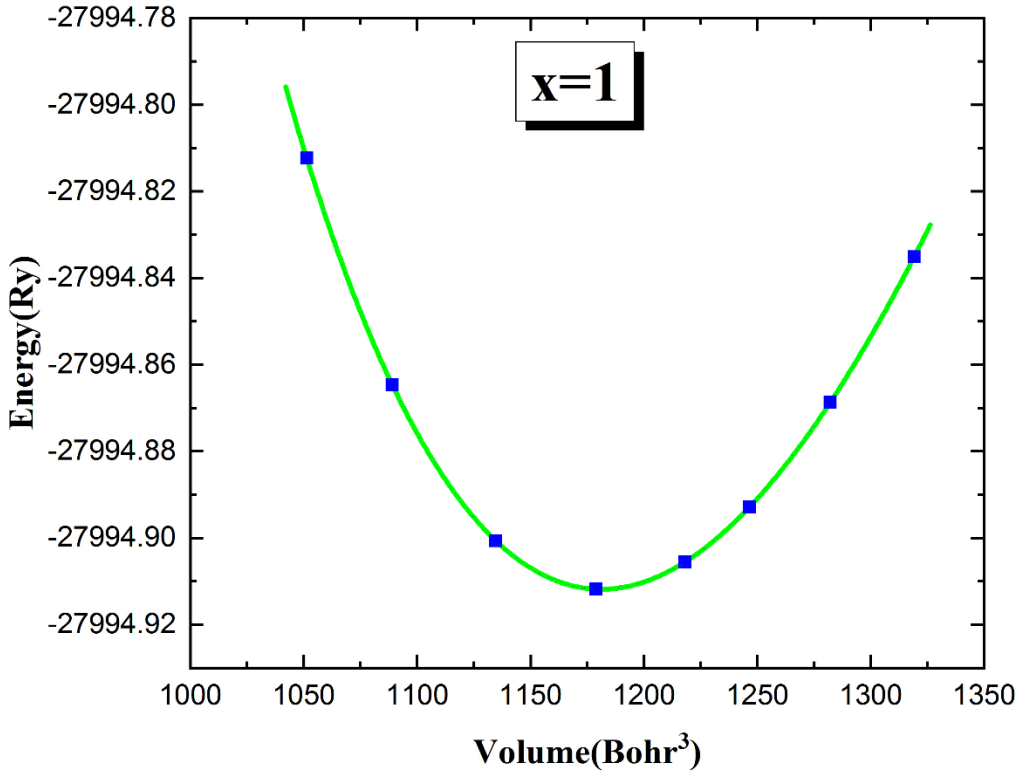

Fig IV.2. The variation of the energy as a function of the volume for the $(Zr_{1-x}T_x)_3AlC_2$ compounds, where x=0, 1/3, 1/2, 2/3 and 1 using GGA-PBE approximation [24].

In attempt to identify the effect of pressure on the structural properties, we have investigate the parameters constants a and c under pressure effect in the range from 0 to 25 GPa.

The Fig IV.3 illustrate the lattice parameters a and c as a function of the pressure. We can note that when the pressure increases, the lattice parameters a and c of our compounds $(Zr_{1-x}T_x)_3AlC_2$ decrease.

Also, we have investigate the parameters constants a and c as a function of x concentration.

The Fig IV.4 represents the relation between lattice parameters a and c and the x concentration under constant pressure, where all the lattice parameters a and c decrease with increasing value of x.

Ti content; x	a (Å)	c (Å)	c/a	V $(Å^3)$	B *(GPa)*	B'	Remarks
0	**3.341**	**19.960**	**5.974**	**193.02**	**165.77**	**4.26**	**Calc**[a]
	3.333	19.951	5.986	191.95	-	-	Expt[b]
	3.335	19.961	5.985	192.27	147.29	-	Calc[c]
1/3	**3.269**	**19.513**	**5.969**	**181.45**	**168.55**	**3.96**	**Calc**[a]
	3.267	19.572	5.991	180.97	-	-	**Calc**[d]
	3.240	19.439	5.999	176.75	156.67	-	**Calc**[c]
1/2	**3.230**	**19.366**	**5.995**	**175.02**	**168.93**	4.05	**Calc**[a]
	3.232	19.397	6.002	175.45	-	-	Expt[d]
	3.197	19.220	6.012	170.11	160.42	-	Calc[c]
2/3	**3.184**	**19.062**	**5.987**	**166.16**	**172.39**	**4.59**	**Calc**[a]
	3.128	18.816	6.015	159.41	-	-	**Calc**[d]
	3.156	19.026	6.029	164.11	159.06	-	**Calc**[c]
1	**3.077**	**18.638**	**6.057**	**152.78**	**185.26**	**4.06**	**Calc**[a]
	3.075	18.578	6.042	152.16	-	-	Expt[e]
	3.078	18.670	6.065	153.19	158.23	-	Calc[c]

[a] **Present work** [24]. [b] Ref [22]. [c] Ref [30]. [d] Ref [31]. [e] Ref [23].

Table IV. 2. The calculated lattice parameters, Hexagonal ration c/a and the unit cell volume of $(Zr_{1-x}Ti_x)_3AlC_2$ for different values of x concentration.

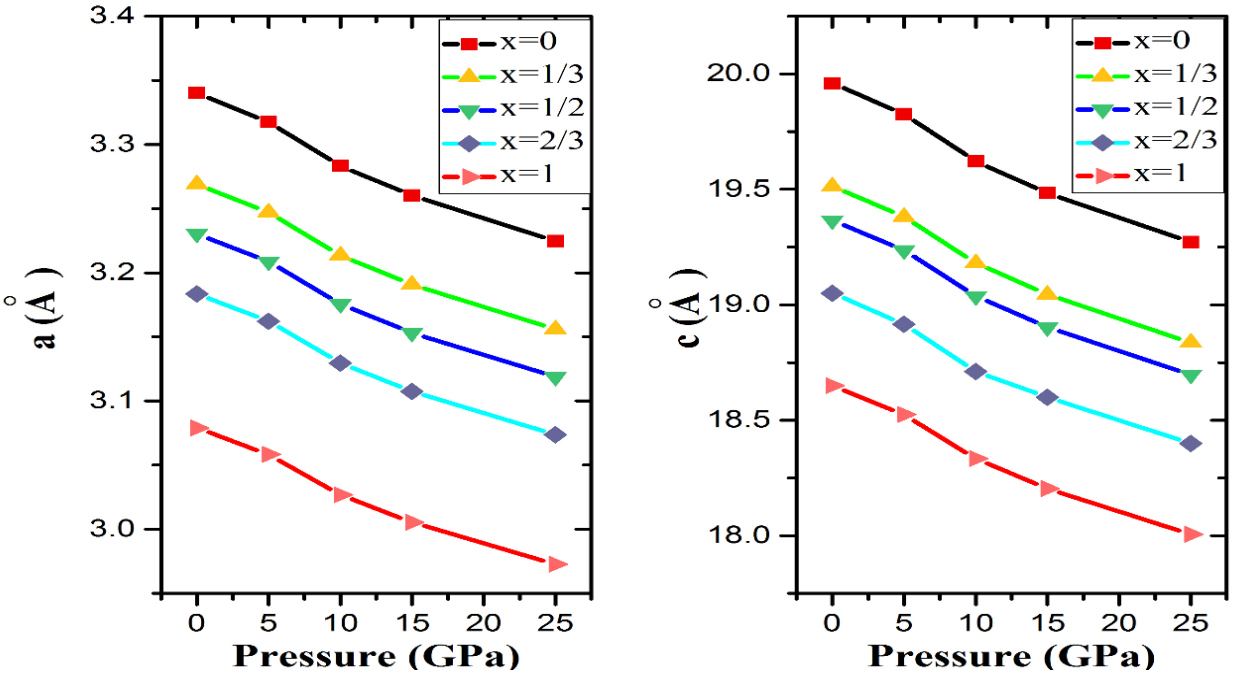

Fig IV. 3. The lattice parameters a and c of $(Zr_{1-x}Ti_x)_3AlC_2$ compounds, where x=0, 1/3, 1/2, 2/3 and 1 of as a function of the pressure [24].

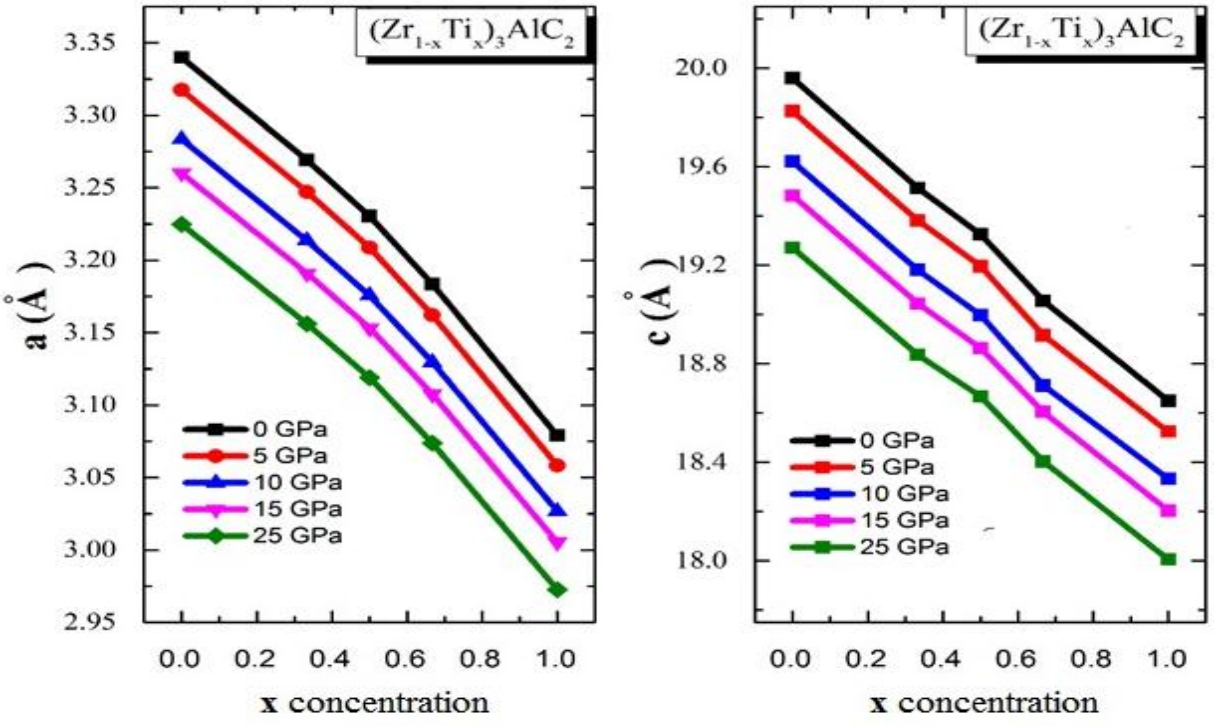

Fig IV.4. The variation of the lattice parameters a and c of $(Zr_{1-x}Ti_x)_3AlC_2$ compounds, as a function of x concentration [24].

.

➢ To calculate the stability of our compounds, the best indicator is their formation energy. The formation energy is calculated using the following equation [28,29]:

$$\Delta H_{f(Zr_{1-x}Ti_x)_3AlC_2} = (E_{tot(Zr_{1-x}Ti_x)_3AlC_2} - (3(1-x)E_{Zr} + 3xE_{Ti} + E_{Al} + 2E_C) \quad \textbf{(IV.1)}$$

where $\Delta H_{f(Zr_{1-x}Ti_x)_3AlC_2}$ is the formation energy of $(Zr_{1-x}Ti_x)_3AlC_2$, with (x = 0, 1/3,1/2, 2/3, 1), E_{tot} is the total energy per unit cell of the our compounds, E $(X = Zr, Ti, Al\ and\ C)$, it represents the total energy per atom of the element in pure solid state. The calculated formation energies of our compounds are regrouped in Table IV. 3. From these results, it is obvious that the calculated formation energies are negative, which indicates that the examined compounds are quite stable.

Compounds $(Zr_{1-x}Ti_x)_3AlC_2$	**Ti** content; ***x***				
	0	**1/3**	**1/2**	**2/3**	**1**
ΔH_f $(eV/f.u.)$	-0.817	-0.753	-0.776	-0.729	-0.826

Table IV. 3. The formation energy of $(Zr_{1-x}Ti_x)_3AlC_2$ for different values of x concentration [24].

IV.3. Mechanical properties

The study of the mechanical properties depends on the determination of the elastic parameters. These parameters allow us to get knowledge about the structural stability and the anisotropic character of a material. Furthermore, when a stress is applied on a material, these parameters are able to provide information about the mechanical stability, and strength under stress.

All solid objects are susceptible to deformation under the influence of applied external forces. The resistance against this deformation in crystals is greater than that of amorphous materials due to internal forces.

Elasticity is the physical property of a material that returns the material to its original form and dimensions after removing the external forces that affect the material and lead to its deformation and consequently the material has a preferred natural state. The behavior of the solid under the applied force F which stretches the solid elastically from L_0 to $L_0 + \delta L$ can be

illustrated through the Fig IV. 5. The force is divided between the chains of atoms that make up the solid, with each chain carrying a force δF.

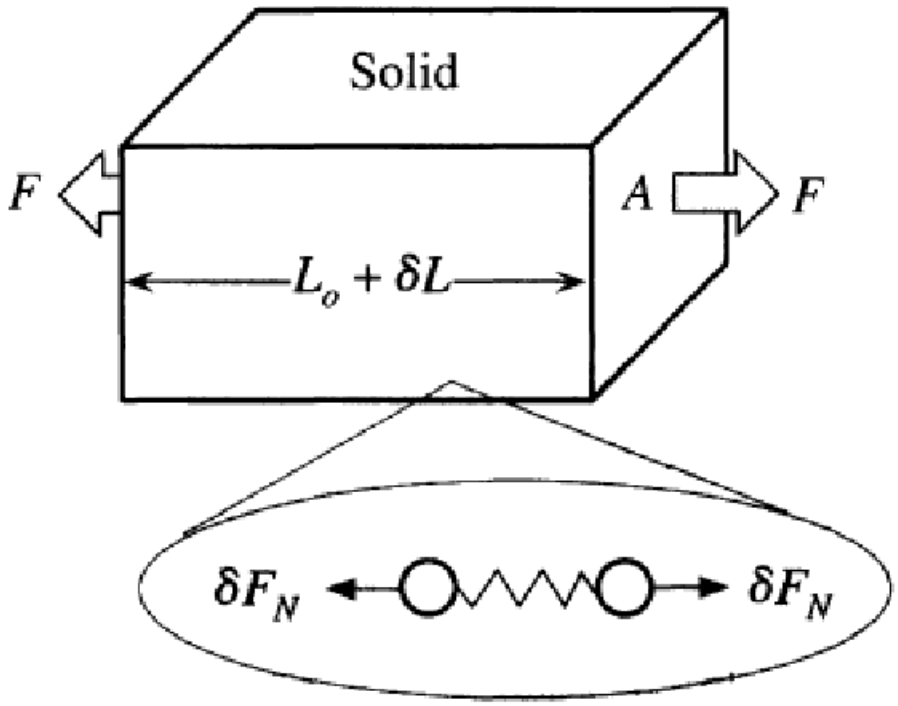

Fig IV.5. The behavior of a solid material under an applied force *F* [32].

The elastic constants of a material describe its response to an applied stress or, conversely, the stress required to maintain a given deformation. Both stress and strain have three tensile and three shear components, giving six components in total. The linear elastic constants form a 6 × 6 symmetric matrix, having 27 different components, such that $\sigma_j = C_{ij}\ \varepsilon_j$ for small stresses, σ, and strains, ε [33]. Any symmetry present in the structure may make some of these components equal and others may be fixed at zero.

In our hexagonal system of $(Zr_{1-x}Ti_x)_3AlC_2$ MAX phases, there are six different elastic constants C_{11}, C_{12}, C_{13}, C_{33}, C_{44} and C_{66} , where $C_{66} = \frac{(C_{11}-C_{12})}{2}$. We have used the Hex-elastic package of Jamal Morteza to determine the elastic constants of our compounds at their equilibrium lattice constants [34]. The elastic constants are derived by means of a Taylor expansion of the total energy *E(V, εi)* of the system with respect to the strain tensor ε_i:

$$\boldsymbol{E(V,\varepsilon_i) = E_0(V_0,0) + V_0\left(\sum_i \tau_i \xi_i\, \varepsilon_i + \frac{1}{2}\sum_{ij} c_{ij}\varepsilon_i\xi_i\,\varepsilon_j\xi_j\right) + O(\varepsilon^3)} \qquad \textbf{(IV. 2)}$$

where; E_0 and V_0 are the energy and the volume of unstrained hexagonal system respectively. The factor ξ_i takes the value 1 if the index *i* is equal to 1, 2 or 3 and the value 2 if it is equal to

4, 5 or 6. In the above equation τ_i are related to the strain on the crystal. For our compounds, the total energy from equation (IV.3) is modified by applying six distortions described as follows [24].:

$$D_1 = \begin{pmatrix} 1+\varepsilon & 0 & 0 \\ 0 & 1+\varepsilon & 0 \\ 0 & 0 & 1 \end{pmatrix} \quad (\mathbf{IV.3})$$

$$D_2 = \begin{pmatrix} 1+\varepsilon & 0 & 0 \\ 0 & 1+\varepsilon & 0 \\ 0 & 0 & \frac{1}{(1+\varepsilon)^2} \end{pmatrix} \quad (\mathbf{IV.4})$$

$$D_3 = \begin{pmatrix} 1 & 0 & 0 \\ 0 & 1 & 0 \\ 0 & 0 & 1+\varepsilon \end{pmatrix} \quad (\mathbf{IV.5})$$

$$D_4 = \begin{pmatrix} \left(\frac{1+\varepsilon}{1-\varepsilon}\right)^{\frac{1}{2}} & 0 & 0 \\ 0 & \left(\frac{1-\varepsilon}{1+\varepsilon}\right)^{\frac{1}{2}} & 0 \\ 0 & 0 & 1 \end{pmatrix} \quad (\mathbf{IV.6}$$

$$D_5 = \begin{pmatrix} 1 & 0 & \varepsilon \\ 0 & 1 & \varepsilon \\ \varepsilon & \varepsilon & 1+\varepsilon^2 \end{pmatrix} \quad (\mathbf{IV.7})$$

$$D_6 = \begin{pmatrix} (1+\varepsilon^2)^{\frac{1}{2}} & \varepsilon & 0 \\ \varepsilon & (1+\varepsilon^2)^{\frac{1}{2}} & 0 \\ 0 & 0 & 1 \end{pmatrix} \quad (\mathbf{IV.8})$$

The energy for these distortions can be obtained as:

$$E(V,\varepsilon) = E(V_0,0) + V_0\left((C_{11}+C_{12})\varepsilon^2 + O(\varepsilon^3)\right) \quad (\mathbf{IV.9})$$

$$E(V,\varepsilon) = E(V_0,0) + V_0\left(\frac{C_{33}}{2}\varepsilon^2 + O(\varepsilon^3)\right) \quad (\mathbf{IV.10})$$

$$E(V,\varepsilon) = E(V_0,0) + V_0\left((C_{zz})\varepsilon^2 + O(\varepsilon^3)\right) \quad (\mathbf{IV.11})$$

with:

$$C_{zz} = C_{11} + C_{12} + 2C_{33} - 4C_{13} \quad (\mathbf{IV.12})$$

$$E(V, \varepsilon) = E(V_0, 0) + V_0\left((C_{11} - C_{12})\varepsilon^2 + O(\varepsilon^4)\right) \quad (\mathbf{IV.13})$$

$$E(V, \varepsilon) = E(V_0, 0) + V_0\left(4(C_{44})\varepsilon^2 + O(\varepsilon^3)\right) \quad (\mathbf{IV.14})$$

and :

$$E(V, \varepsilon) = E(V_0, 0) + V_0\left(2(C_{66})\varepsilon^2 + O(\varepsilon^3)\right) \quad (\mathbf{IV.15})$$

respectively.

To date, there is no experimental report in the elastic constants for the compounds examined here. Our results of these elastic constants are illustrated in Table IV.4

Compounds $(Zr_{1-x}Ti_x)_3AlC_2$	Ti content; ***x***				
	0	**1/3**	**1/2**	**2/3**	**1**
C_{11} (GPa)	308.59	308.58	313.41	340.01	358.86
C_{12} (GPa)	89.33	89.35	90.86	90.62	99.95
C_{13} (GPa)	97.37	102.70	97.20	93.85	92.33
C_{33} (GPa)	318.24	328.91	331.38	355.97	366.22
C_{44} (GPa)	82.27	90.86	89.09	98.55	102.19
C_{66} (GPa)	109.63	109.62	111.28	124.69	129.45

Table IV.4. Calculated elastic constants C_{ij} (GPa) of $(Zr_{1-x}Ti_x)_3AlC_2$ compounds [24].

We can observe obviously that all these elastic constants C_{ij} are positive and completely satisfy the conditions of mechanic stability of compounds for hexagonal structure [35]:

$$C_{11} > 0, \quad C_{33} > 0, \quad C_{44} > 0, \quad C_{11} - C_{12} > 0,$$
$$(C_{11} + C_{12})C_{33} > 2C_{13}^2 \qquad (IV.16)$$

These results confirm the stability of the $(Zr_{1-x}Ti_x)_3AlC_2$ MAX phases against elastic deformation. Meanwhile, the present results of the elastic constants show that C_{33} is larger than C_{11} for all our compounds, which reveals that the *a* and *b*-axes are more compressible than the *c*-axis. These results can be explained in terms of the existence of strong covalent bonding in the [001] direction for the studied compounds. Also, we can note that the C_{11} and C_{33} are considerably higher than other elastic constants, which divulge an elastic anisotropy in these compounds.

The bulk modulus B, which describes volumetric elasticity, or the tendency of an object to deform in all directions when uniformly loaded in all directions, is defined as volumetric stress over volumetric strain, and is the inverse of compressibility and in other words, B measures the resistance of a material to volume change and provides us an estimate of its response to a hydrostatic pressure [36], where:

$$B = -V\frac{dV}{dP} \qquad (IV.17)$$

where *P* is pressure, *V* is volume, and denotes the derivative of volume with respect to pressure.

The shear modulus G, which describes an object's tendency to shear (the deformation of shape at constant volume) when acted upon by opposing forces, is defined as shear stress over shear strain [36].

From the elastic constants, we have calculated the elastic modulus (the bulk modulus B and the shear modulus G), which allow us to determine all the mechanical properties. From the Hill approximation which based on the Reuss and Voigt approaches, the bulk modulus B and the shear modulus G are given by these following expressions [37-39]:

$$B_V = \frac{2(C_{11} + C_{12}) + C_{33} + 4C_{13}}{9} \qquad (IV.18)$$

$$B_R = \frac{(C_{11} + C_{12})C_{33} - 2C_{13}^2}{C_{11} + C_{12} + 2C_{33} - 4C_{13}} \qquad (IV.19)$$

$$B_H = \frac{B_V + B_R}{2} \qquad (IV.20)$$

$$G_V = \frac{C_{11} + C_{12} + 2C_{33} - 4C_{13} + 12(C_{55} + C_{66})}{30} \qquad (VI.21)$$

$$G_R = \frac{5}{2} \frac{[(C_{11} + C_{12})C_{33} - 2C_{13}^2]C_{55}C_{66}}{3B_V C_{55}C_{66} + [(C_{11} + C_{12})C_{33} - 2C_{13}^2](C_{55}+C_{66})} \qquad (VI.22)$$

$$G_H = \frac{G_V + G_R}{2} \qquad (VI.23)$$

where B = B_H (the Hill bulk modulus) and G = G_H (the Hill shear).

Young's modulus *E*, which describes the tensile elasticity or the tendency of an object to deform along an axis when opposing applied forces along that axis, is defined as the ratio of tensile stress to tensile strain and is considered a measure of the material's ability to resist stress and pressure in the elastic deformation range [40], where when it is Young's modulus is bigger, the deformation of the material is more difficult.

$$E = \frac{\sigma}{\varepsilon} \qquad (VI.24)$$

Poison's ratio ν is the ratio of transverse contraction strain to longitudinal extension strain in the direction of stretching force.

$$\nu = -\frac{\varepsilon_{transverse}}{\varepsilon_{longitudinal}} \qquad (VI.25)$$

In engineering science, calculating the Poisson ratio allow us to classify materials as brittle or ductile. If the Poisson ratio of the material is greater than the value 0.26, it is considered as ductile, otherwise if it is considered as brittle [41].

The Young's modulus E and Poisson's ratio ν of a hexagonal structure are also calculated by using the following expressions [42]:

$$E = \frac{9BG}{3B + G} \qquad (VI.26)$$

$$\nu = \frac{3B - E}{6B} \qquad (VI.27)$$

The values of the B, G, E and ν for our compounds $(Zr_{1-x}Ti_x)_3AlC_2$ with different values of x are represented in the Table IV.5. We can see that:

- When the x concentration increases, the values of B, G and E increase, indicating that the hardness of these compounds increases with x.
- For each considered compound, the calculated B value from the single-crystal elastic constants through the Voigt-Reuss-Hill average is in good agreement with the corresponding one derived from the EOS fit.
- Therefore, this good agreement between the B values obtained via two different computational methods constitutes another proof of the reliability and accuracy of the computed elastic modulus.
- For all the compounds examined, the shear modulus G is smaller than the volume modulus B and thus the parameter that can limit the mechanical stability of these materials is the shear modulus.
- We have found that all Poisson ratio values are less than 0.26, which means that they are all classified as brittle.
- The compound Ti_3AlC_2 present a higher ability to resist deformation, while it's the inverse in the case of the compound Zr_3AlC_2.

Another criterion called Pugh criterion can also make classification of ductile and brittle materials. When B/G is greater than 1.75, the material will be ductile, and if not, it will be considered brittle [43]. From our results of B/G ratio in the Table IV.5, we obtained that all the B/G values are less than 1.75 which confirms that these compounds exhibit a brittle nature.

The Poisson's ratio *v* is frequently used to deduce the type of the chemical bonding. When its value is less than 0.25, the chemical bonding has a covalent, while if its value is more than 0.25, the bonding will be a typical ionic [44].

The calculated values of the Poisson's ratio *v* are 0.255, 0.252, 0.249, 0.234 and 0.233 for x=0, 1/3, 1/2, 2/3 and 1 respectively, which indicate that the chemical bonding nature is more ionic for Zr_3AlC_2 and $(Zr_{2/3}Ti_{1/3})_3AlC_2$, a mixed ionic-covalent nature for $(Zr_{1/2}Ti_{1/2})_3AlC_2$ and more covalent for $(Zr_{1/3}Ti_{2/3})_3AlC_2$ and Ti_3AlC_2. It's also possible to study the nature of the chemical bonding using the Cauchy pressure. When the value of Cauchy pressure is positive, then the ionic bonding is dominant, while the covalent bonding is dominant when its value is negative [45].

In the hexagonal system, the Cauchy pressure is estimated in different directions as follows:

$$\mathbf{P_x^{Cauchy} = C_{13} - C_{44}} \qquad \mathbf{(IV.28)}$$

$$\mathbf{P_y^{Cauchy} = C_{12} - C_{66}} \qquad \mathbf{(IV.29)}$$

From the Table IV. 5, it clear that for the $(Zr_{2/3}Ti_{1/3})_3AlC_2$ and Ti_3AlC_2 compounds, all the values of Cauchy pressure P_x^{Cauchy} or P_y^{Cauchy} are negative, which confirm the more covalent character for this compound, while the compounds Zr_3AlC_2, $(Zr_{1/3}Ti_{2/3})_3AlC_2$ and $(Zr_{1/2}Ti_{1/2})_3AlC_2$ have positive values of P_x^{Cauchy} and negative values of P_y^{Cauchy} which indicate the mixed nature for these compounds, especially in for the compound Zr_3AlC_2 where the ionic character is clear.

The calculation of the shear anisotropic factors of materials is extremely important to study the degree of durability related mainly to micro-cracks in crystals. In our hexagonal system, we have calculated three elastic anisotropy factors A_1, A_2 and A_3 [46], where A_1 for {100} planes between the [011] and [010] directions, A_2 for {010} shear planes between the [101] and [001] directions and A_3 for {001} shear planes between the [110] and [010] directions, where:

$$\mathbf{A_1 = \frac{C_{11} + C_{12} + 2C_{33} - 4C_{13}}{6C_{44}}} \qquad \mathbf{(IV.30)}$$

$$\mathbf{A_2 = \frac{2C_{44}}{C_{11} + C_{12}}} \qquad \mathbf{(IV.31)}$$

$$\mathbf{A_3 = \frac{C_{11} + C_{12} + 2C_{33} - 4C_{13}}{3(C_{11} - C_{12})}} \qquad \mathbf{(IV.32)}$$

All the values of A_1, A_2 and A_3 must be equal to 1 for an isotropic crystal while they differ from 1 for anisotropic crystal [47]. According to our results reported in Table IV. 5, all the anisotropy factors are greater or smaller than 1, which indicates that the $(Zr_{1-x}Ti_x)_3AlC_2$ MAX phase compounds exhibit an anisotropy behavior.

Hardness is another mechanical property of a material related to the elastic and plastic response of a material. In general, hardness is an important indicator of corrosion resistance of materials, so the most corrosion-resistant materials are those with the greater hardness [48]. We have used the formula of Chen of Vickers's Hardness [24,49]:

$$H_V = 2\left(\frac{G^3}{B^2}\right)^{0.585} - 3 \qquad (IV.33)$$

The calculated results are found to equal 12.48 GPa, 13.20 GPa, 13.52 GPa, 16.11 GPa and 16.74 GPa for $(Zr_{1-x}Ti_x)_3AlC_2$ when x=0, 1/3, 1/2, 2/3 and 1 respectively. The hardness of Zr_3AlC_2 is the smallest among of the three compounds, and the hardness of Ti_3AlC_2 is the greatest among of them.

Compounds $(Zr_{1-x}Ti_x)_3AlC_2$	Ti contient, ***x***				
	0	**1/3**	**1/2**	**2/3**	**1**
B (GPa)	167.01	170.42	169.76	176.91	183.68
G (GPa)	97.33	101.27	102.11	114.05	119.10
E (GPa)	244.50	253.52	255.16	281.63	293.80
B/G	1.72	1.68	1.66	1.55	1.54
ν	0.255	0.252	0.249	0.234	0.233
P_x^{Cauchy}	15.10	11.84	8.11	-4.70	−9.86
P_y^{Cauchy}	−20.30	-20.27	−20.42	-34.07	−29.50
A_1	1.30	1.18	1.27	1.29	1.24
A_2	0.75	0.45	0.80	0.45	0.79
A_3	0.98	0.98	1.01	1.02	1.06
H_V (Gpa)	12.48	13.20	13.52	16.11	16.74

Table IV.5. Calculated elastic moduli (B , G and E) (GPa), Poisson's ratio *ν*, B/G ratio, shear anisotropic factor for the three different shear planes (A_1, A_2 and A_3), Cauchy pressure and Vickers hardness H_V (GPa) for $(Zr_{1-x}Ti_x)_3AlC_2$ compounds [24].

IV.4. Electronic properties

The electronic properties of a crystalline material are generally determined by its electronic band structure as the calculation of the electronic properties of the material is very important, it tells us about the electronic conductivity, and the nature of the contacts that are formed between the various elements of this material, and these properties include band structure band, state density, and charge density**.** The electrical conductivity of a material is determined by the distribution of electrons in the conduction and valence bands.

In the Fig IV.6, we illustrate the band structures for $(Zr_{1-x}Ti_x)_3AlC_2$ compounds, where x=0, 1/3, 1/2, 2/3 and 1 along the high-symmetry axes of the first Brillouin zone. We can note from this figure that the band structures are topologically identical and we can easily observe the overlap between the valence and conduction bands at the Fermi level of all these diagrams. Consequently, no band gap is found at the Fermi level and as a result, all these compounds show metallic nature. We can also observe a great dispersion at both the valence and conduction bands.

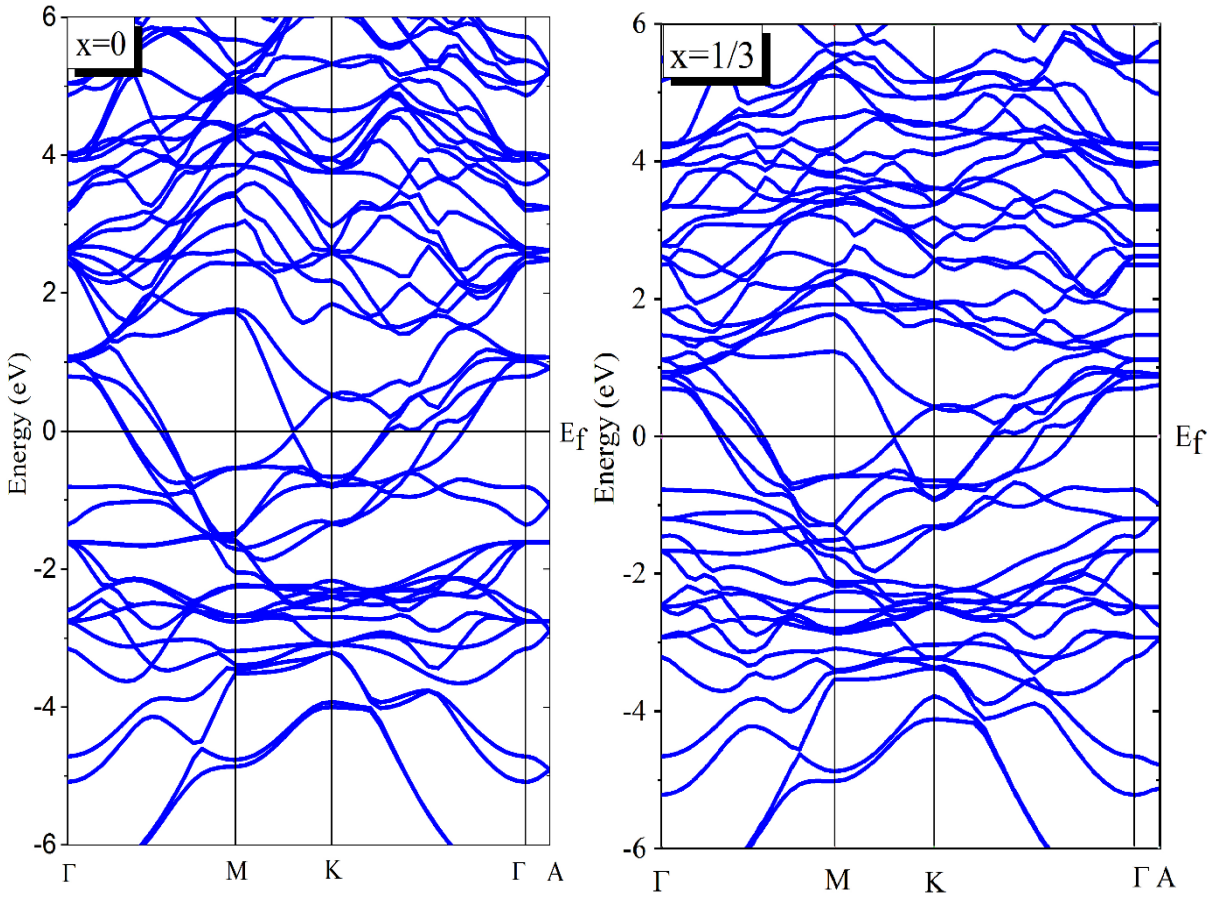

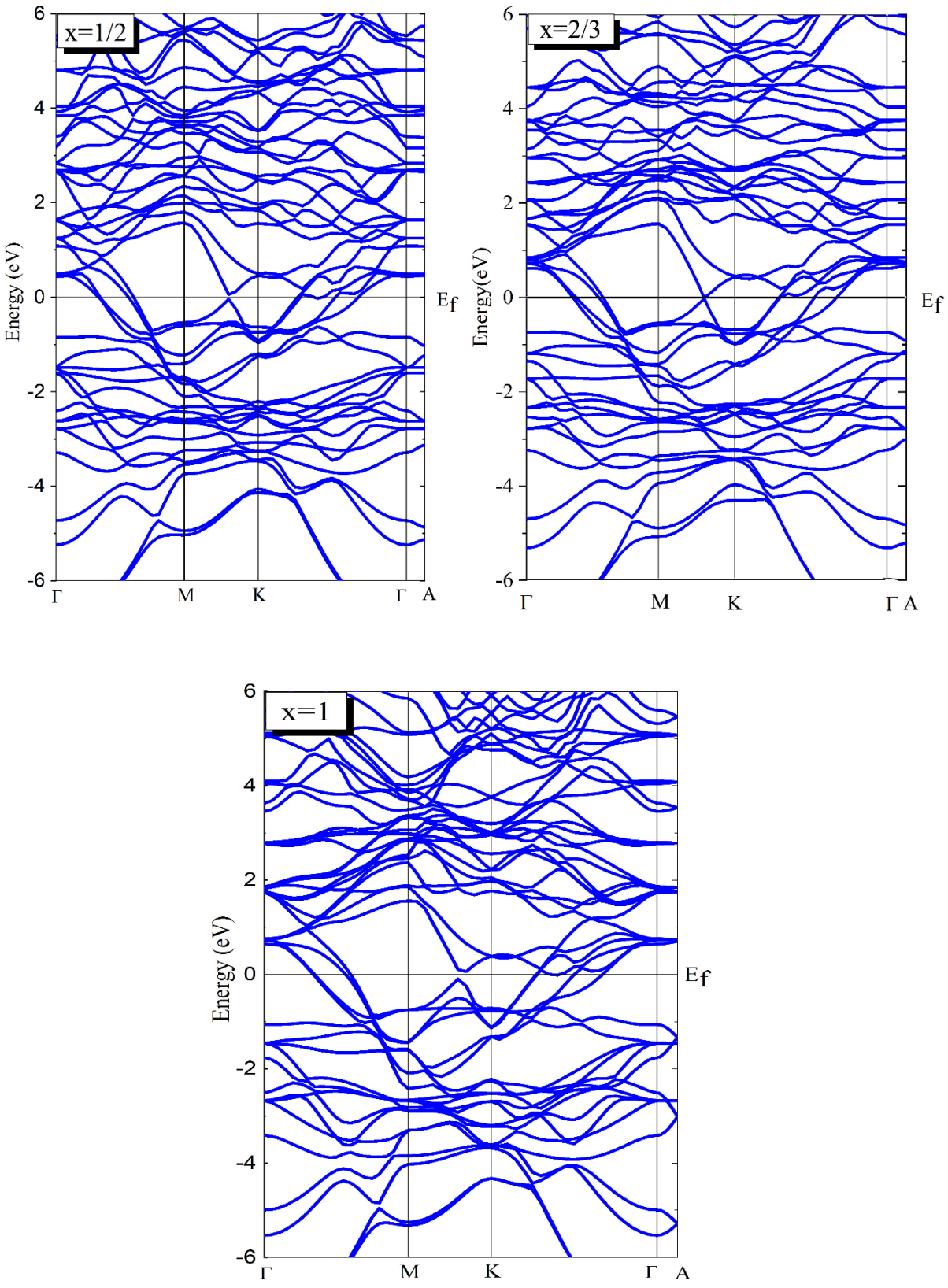

Fig. IV.6. The band structures for $(Zr_{1-x}Ti_x)_3AlC_2$ compounds, where x=0, 1/3, 1/2, 2/3 and 1 along the high-symmetry axes of the first Brillouin zone [24].

In order to further understanding the nature of the calculated band structures, we have also calculated the total density of states (TDOS) and partial density of states (PDOS) for the studied compounds in a wide energy interval [-6 eV, 6 eV] symmetric around the Fermi level. We illustrate in Fig IV. 7 the TDOS and PDOS of our compounds.

The Fermi level is taken as the origin of the energies.

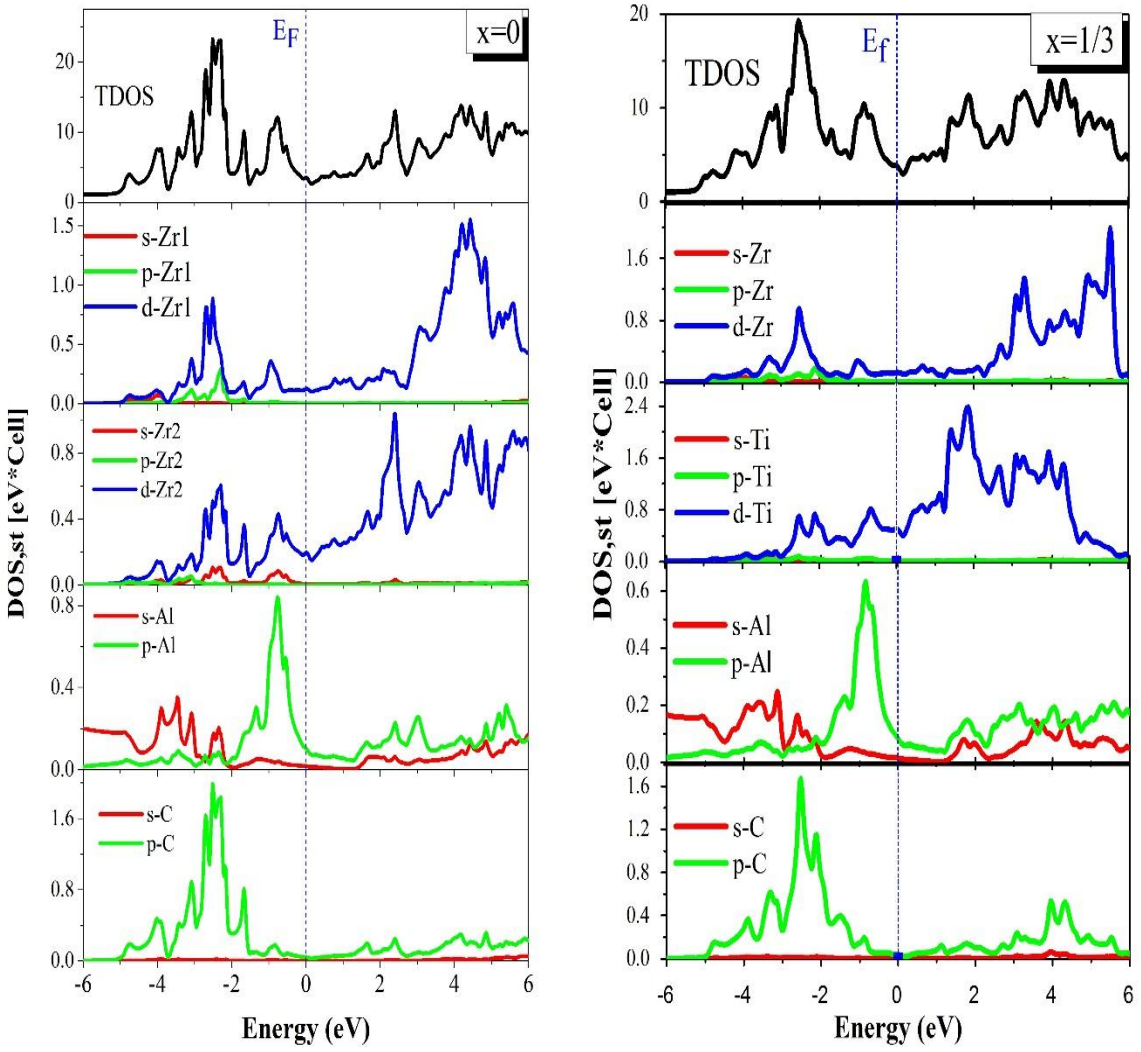

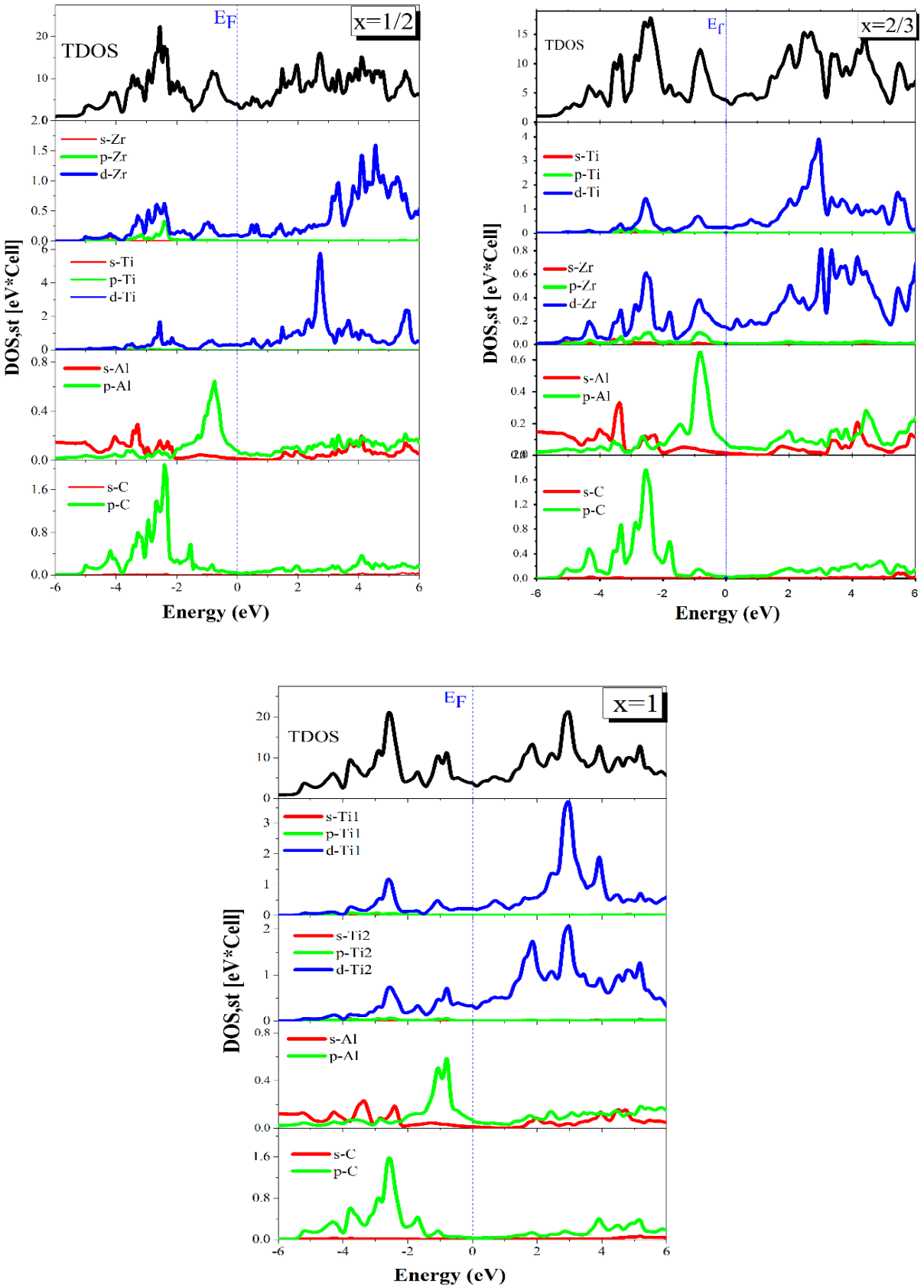

Fig IV.7. The Total and Partial densities of states (TDOS, PDOS) of $(Zr_{1-x}Ti_x)_3AlC_2$ compounds, where x=0, 1/3, 1/2, 2/3 and 1 [24].

The TDOS results confirming the metallic nature for our compounds. We can divide the valence region into two parts:

- ❖ The first part where the valence band between -5.0 eV to -1.5 eV.
- ❖ The second part where the valence band between -1.5 eV to 0.0 eV.

- ➢ The first part is mostly dominated by the *p*-*d* states of the transition elements (Zr and Ti), *s*-Al and *p*-C for all the five investigated compounds.
- ➢ The second part presents a *p*-*d* states hybridization between the *d* orbital of transition metal elements (Ti and Zr) and *p* orbital of Al.
- ➢ The conduction band is originated mainly to the *d*-Zr and or Ti contributions with a minor contribution of *s*-*p* states of Al and p states of C.

IV.5. Thermodynamic properties

Thermodynamics is a branch of physics concerned with pressure and temperature and their relationship to energy and work [50]. The laws of thermodynamics are explained in terms of macroscopic constituents by statistical mechanics.

In solid states physics, the Debye temperature θ_D and the sound velocity v play a very important role to study the thermodynamic properties. The determination of both values is calculated as follows [51,52]:

$$\theta_D = \frac{h}{k_B}\left[\left(\frac{3n}{4\pi}\right)\frac{N_A\rho}{M}\right]^{\frac{1}{3}} \qquad (\mathbf{IV.31})$$

$$v_m = \left[\frac{1}{3}\left(\frac{2}{v_t^3}+\frac{1}{v_l^3}\right)\right]^{-\frac{1}{3}} \qquad (\mathbf{IV.32})$$

Where :

$$v_l = \left(\frac{3B+4G}{3\rho}\right)^{\frac{1}{2}} \qquad (\mathbf{IV.33})$$

$$v_t = \left(\frac{G}{\rho}\right)^{\frac{1}{2}} \qquad (\mathbf{IV.34})$$

where h is Plank's constant, k_B is Boltzmann's constant, n is the number of atoms per formula unit, N_A is Avogadro's number, ρ is the density, M is the molecular weight, v_m is the average sound velocity, v_l and v_t are the longitudinal and transverse sound velocities, respectively.

The values of ρ, v_t, v_l, v_m and θ_D are shown in the Table IV.5.

Ti content; ***x***	$\boldsymbol{\rho}(g/cm^3)$	$\boldsymbol{v_l}(Km/s)$	$\boldsymbol{v_t}(Km/s)$	$\boldsymbol{v_m}(Km/s)$	$\boldsymbol{\theta_D}$ *(K)*	**Remarks**
0	**5.95**	**7.29**	**4.17**	**4.64**	**546.8**	Calc [a]
	5.61	12.74	4.57	5.19	613.0	Calc [b]
1/3	**5.15**	**7.94**	**4.57**	**5.07**	**599.0**	Calc [a]
	5.28	13.69	4.96	5.63	684.0	Calc [b]
1/2	**4.93**	**7.88**	**4.55**	**5.05**	**615.8**	Calc [a]
	5.07	14.16	5.14	5.83	718.0	Calc [b]
2/3	**4.76**	**8.35**	**5.00**	**5.53**	**685.9**	Calc [a]
	4.81	14.54	5.30	6.02	750.0	Calc [b]
1	**4.22**	**9.01**	**5.31**	**5.89**	**749.9**	Calc [a]
	4.22	15.48	5.64	6.40	815.0	Calc [b]

[a] Present work [24], [b] Ref [53].

Table IV. 6. Density ρ , longitudinal, transverse and average sound velocity v_l, v_t and v_m as well as Debye temperature θ_D for $(Zr_{1-x}Ti_x)_3AlC_2$ compounds.

We can note that:

- All the values of velocity v_l, v_t, v_m and θ_D of $(Zr_{1-x}Ti_x)_3AlC_2$ are increase with x, while the density ρ is decreases with x.
- The longitudinal wave velocity is larger than the transverse one and both the longitudinal and transverse waves increase with increasing the value of x.
- The θ_D value increases with increasing x, which corresponds to an increase in stiffness in the same sequence. This may indicate an increase in thermal conductivity when x is increased.

Unfortunately, there is no experimental report in the literature about these quantities for our compounds up to now.

Many of the physical properties of an atomic crystal lattice can be successfully determined from the first principles within static approximation at zero temperature. However, the crystal lattice is in a dynamic, continuous state, as the atoms vibrate around their equilibrium sites and hence, the material gains or loses heat by gaining or losing phonons [54].

We have also evaluated the Debye temperature, bulk modulus and heat capacity under temperatures from 0 to 600 K and the pressure from 0 to 30 GPa by employing the quasi-harmonic Debye model as implemented in the Gibbs code [55], which is based on the estimation of the Debye temperature θ_D by using the following formulas [56]:

$$\boldsymbol{\theta_D = \frac{\hbar}{K_B}\left[6\pi^2 V^{\frac{1}{2}} r\right]^{\frac{1}{3}} f(\nu)\sqrt{\frac{B_s}{M}}} \qquad \textbf{(IV.35)}$$

where V is the molecular volume, M the molecular mass of the compound, k_B is the Boltzman constant and f (ν) the scaling function [57,58], that depends on the Poisson's ratio ν of the isotropic material [59]:

$$\boldsymbol{f(\nu) = \left\{3\left[2\left(\frac{2}{3}\,\frac{1+\nu}{1-2\nu}\right)^{\frac{3}{2}} + \left(\frac{1}{3}\frac{1+\nu}{1-\nu}\right)^{\frac{3}{2}}\right]^{-1}\right\}^{\frac{1}{3}}} \qquad \textbf{(IV.36)}$$

B_s the adiabatic bulk modulus given by the static compressibility:

$$B_s \cong B_{static} = V\left(\frac{d^2E(V)}{dV^2}\right) \qquad (IV.37)$$

where E (V) is the total energy per unit cell for our compounds.

The heat capacity C_V (the constant- volume heat capacity) and C_P (the constant- pressure heat capacity) are given by:

$$C_V = 3nk_B\left(4D\left(\frac{\theta_D}{T}\right)\frac{\frac{3\theta_D}{T}}{e^{\frac{\theta_D}{T}}-1}\right) \qquad (IV.38)$$

$$C_P = C_V(1+\alpha\gamma T) \qquad (IV.39)$$

where $D\left(\frac{\theta_D}{T}\right)$ denote the Debye integral and n is the number of atoms per unit cell.

$$D\left(\frac{\theta_D}{T}\right) = \frac{3}{(\theta_D/T)^3}\int_0^{\theta_D/T}\frac{x^3}{e^x-1}dx \qquad (IV.40)$$

and volumetric thermal expansion α can be derived as

$$\alpha = \frac{\gamma C_V}{B_T V} \qquad (IV.41)$$

where γ is the Gruneisen parameter, which is defined as

$$\gamma = -\frac{d\,ln\theta_D(V)}{d\,lnV} \qquad (IV.42)$$

The calculated bulk modulus of Zr_3AlC_2, $(Zr_{0.5}Ti_{0.5})_3AlC_2$ and Ti_3AlC_2 are show in Figs IV.8 (a, b and c), respectively.

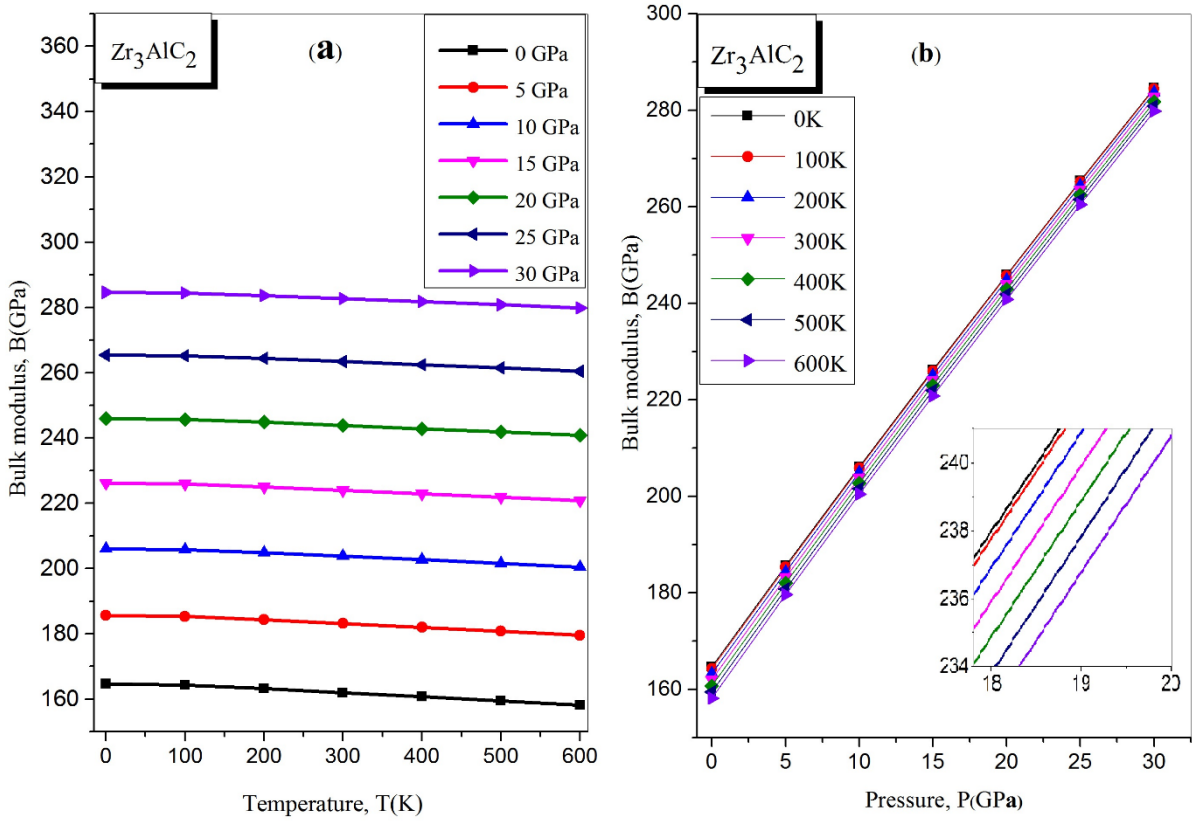

Fig IV.8a. The bulk modulus of Zr_3AlC_2 compound as a function of temperature and pressure [24].

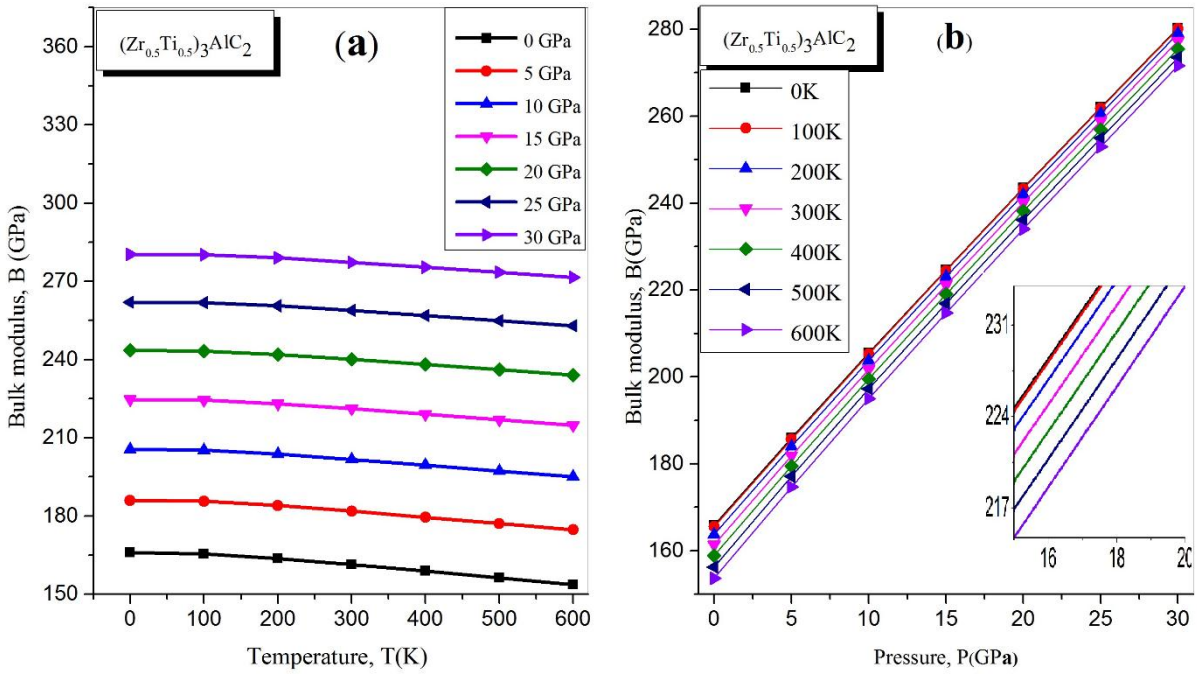

Fig IV.8b. The bulk modulus of $(Zr_{0.5}Ti_{0.5})_3AlC_2$ compound as a function of temperature and pressure [24].

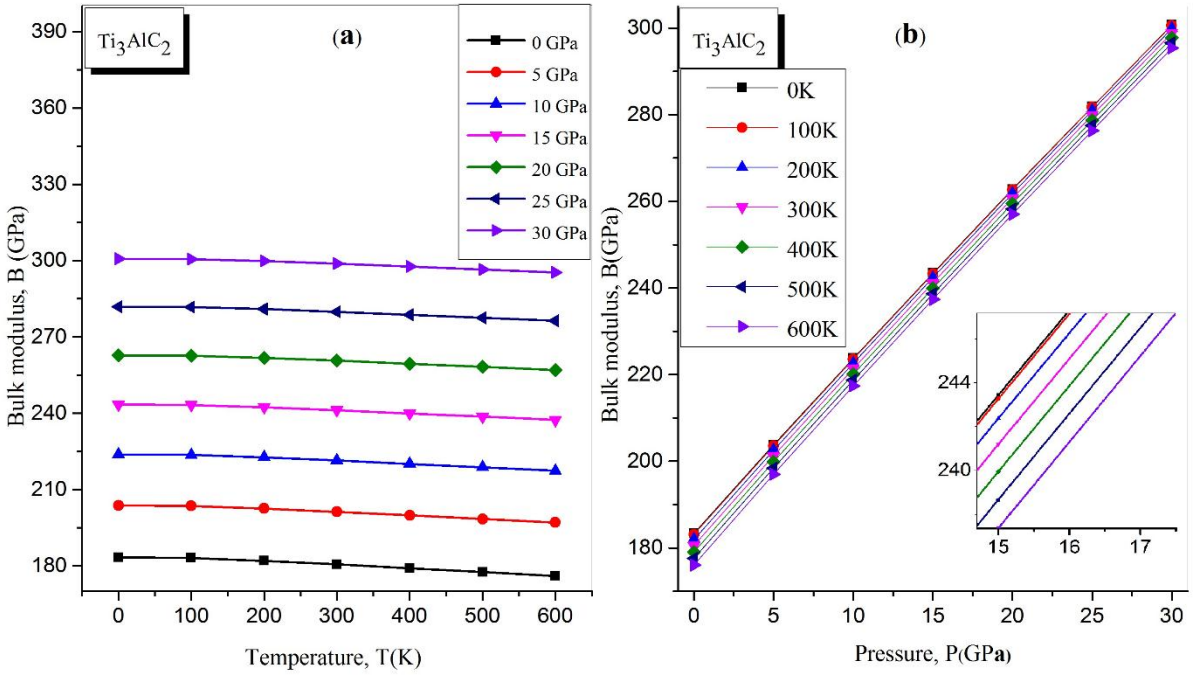

Fig. IV.8c. The bulk modulus of Ti_3AlC_2 compound as a function of temperature and pressure [24].

Fig. IV.8 **(** a**,** b and c**)** gives respectively the variation of the bulk modulus B with temperature and pressure for Zr_3AlC_2, $(Zr_{0.5}Ti_{0.5})_3AlC_2$ and Ti_3AlC_2. From these Figures, we can note the following:

- The value of bulk modulus B slowly decreases with increasing temperature under constant pressure, but increases rapidly as pressure increases under constant temperature for all our compounds.
- It is noted from the figure that the relationship between bulk modulus and pressure (temperature) is nearly linear at fixed temperature (pressure).

The calculated Debye temperature θ_D of Zr_3AlC_2, $(Zr_{0.5}Ti_{0.5})_3AlC_2$ and Ti_3AlC_2 are show in Figs IV.9 (a, b and c), respectively.

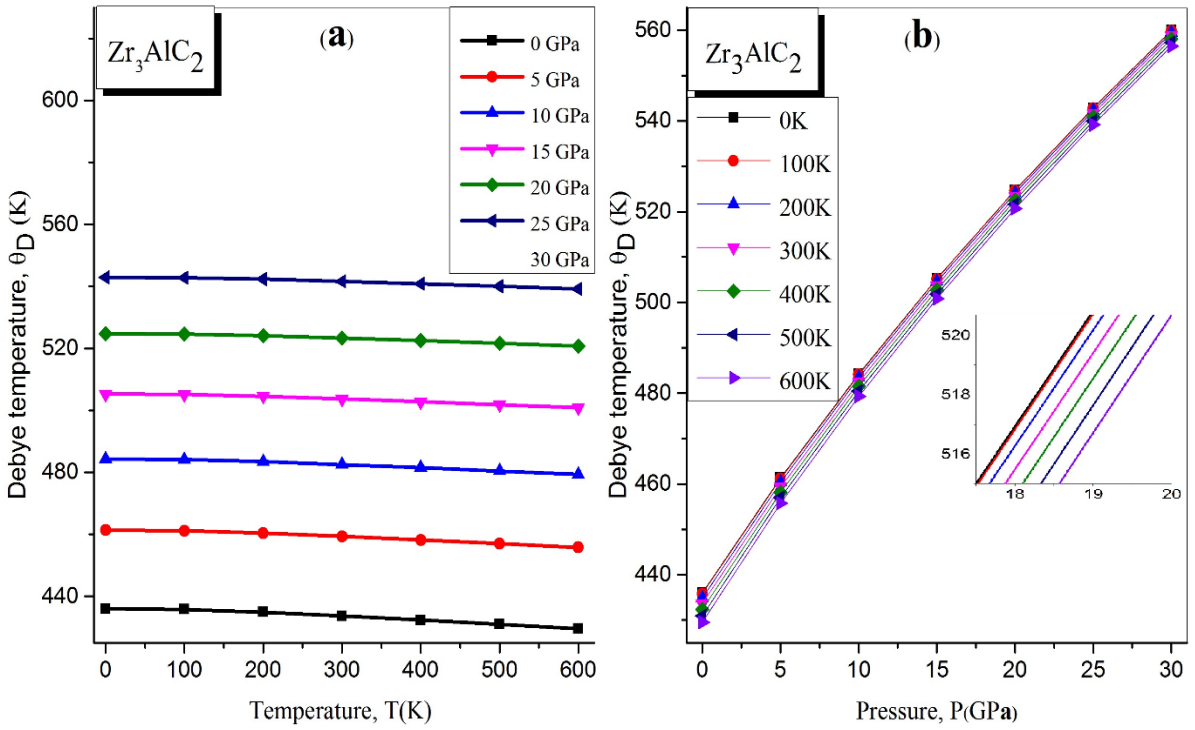

Fig. IV.9a. The Debye temperature of Zr_3AlC_2 compound as a function of temperature and pressure [24].

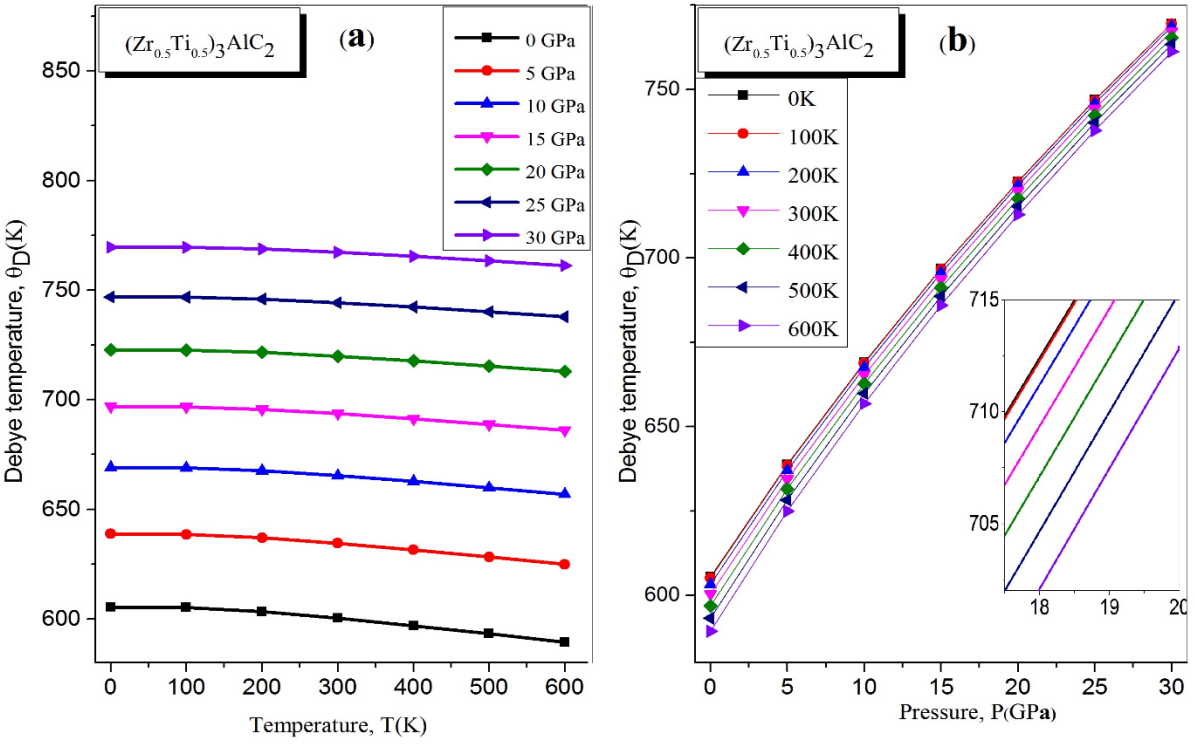

Fig. IV. 9b. The Debye temperature of $(Zr_{0.5}Ti_{0.5})_3AlC_2$ compound as a function of temperature and pressure [24].

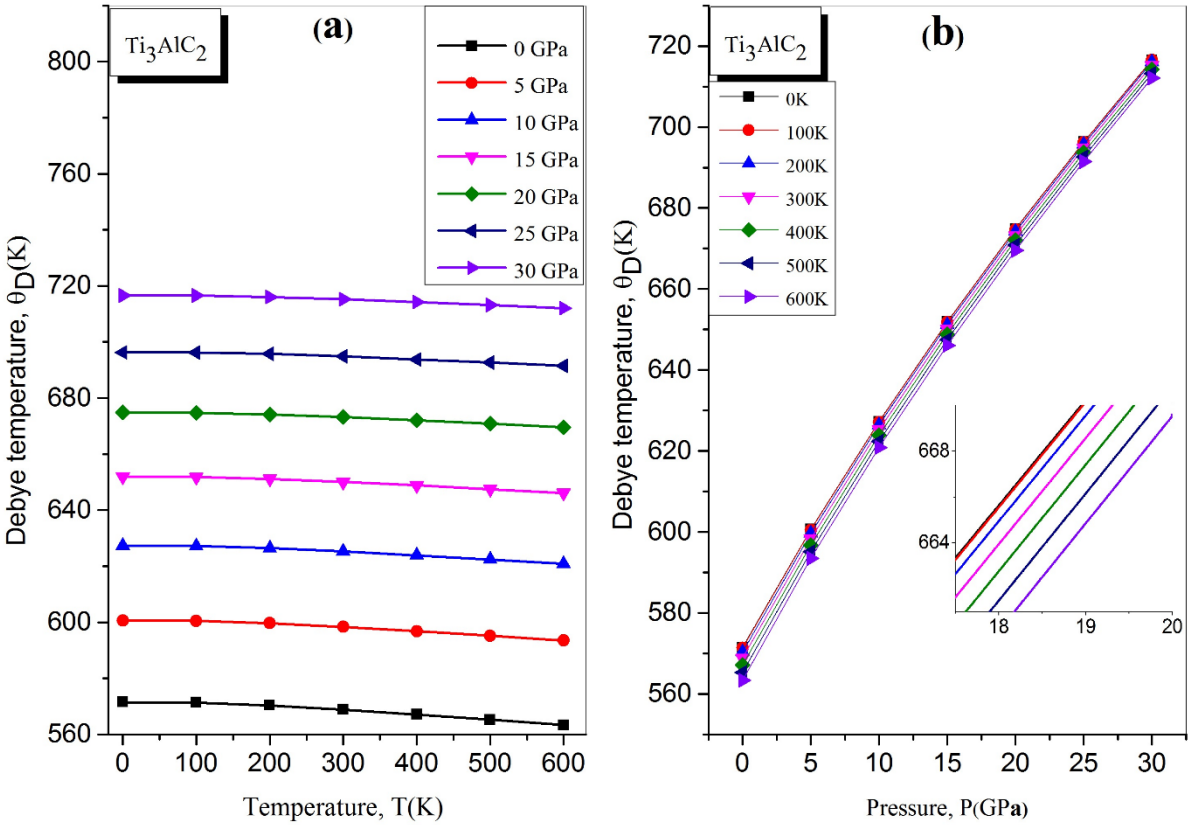

Fig. IV. 9c. The Debye temperature of Ti_3AlC_2 compound as a function of temperature and pressure [24].

Fig. IV.9 **(**a**,** b and c**)** give respectively the variation of the Debye temperature θ_D with temperature and pressure for Zr_3AlC_2, $(Zr_{0.5}Ti_{0.5})_3AlC_2$ and Ti_3AlC_2. From these Figures, we can note that:

- The value of the Debye temperature θ_D slowly decreases when the temperature increases at constant pressure, but it increases rapidly when the pressure increases at constant temperature for all our compounds.

From the Fig. IV.8 and Fig. IV.9, we point out that bulk modulus and Debye temperature θ_D change similarly for all our compounds.

The heat capacity C_P and C_V are also investigated under the pressure and temperature variations. The Fig. IV.10 (a, b and c) and Fig. IV.11 (a, b and c) show the variation of the heat capacity C_P and C_V of Zr_3AlC_2 $(Zr_{0.5}Ti_{0.5})_3AlC_2$ and Ti_3AlC_2 as a function of temperature and pressure, respectively.

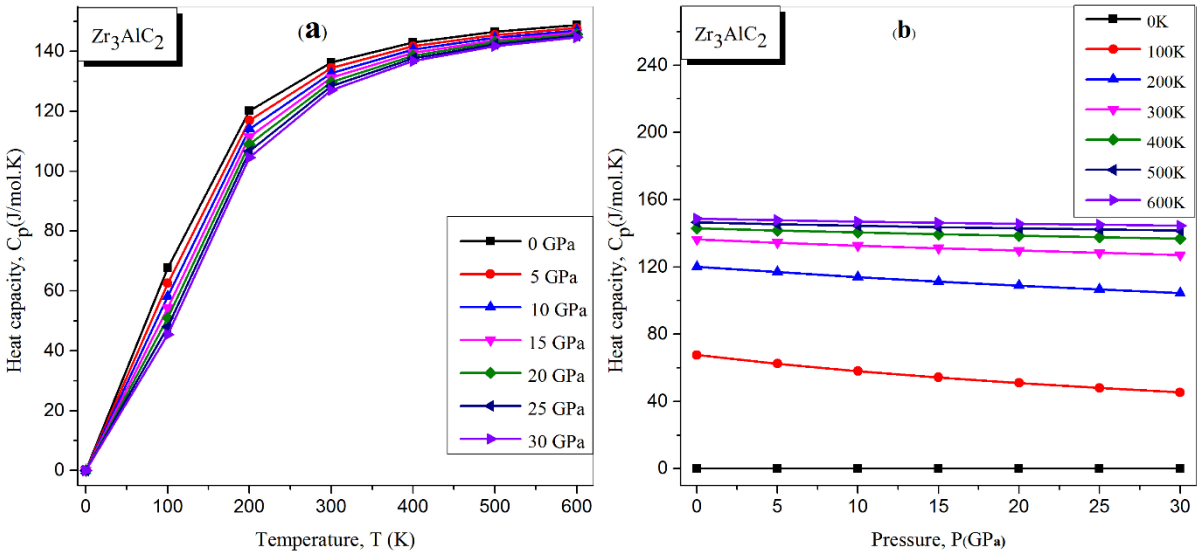

Fig. IV.10a. The heat capacity C_P of Zr_3AlC_2 compound as a function of temperature and pressure [24].

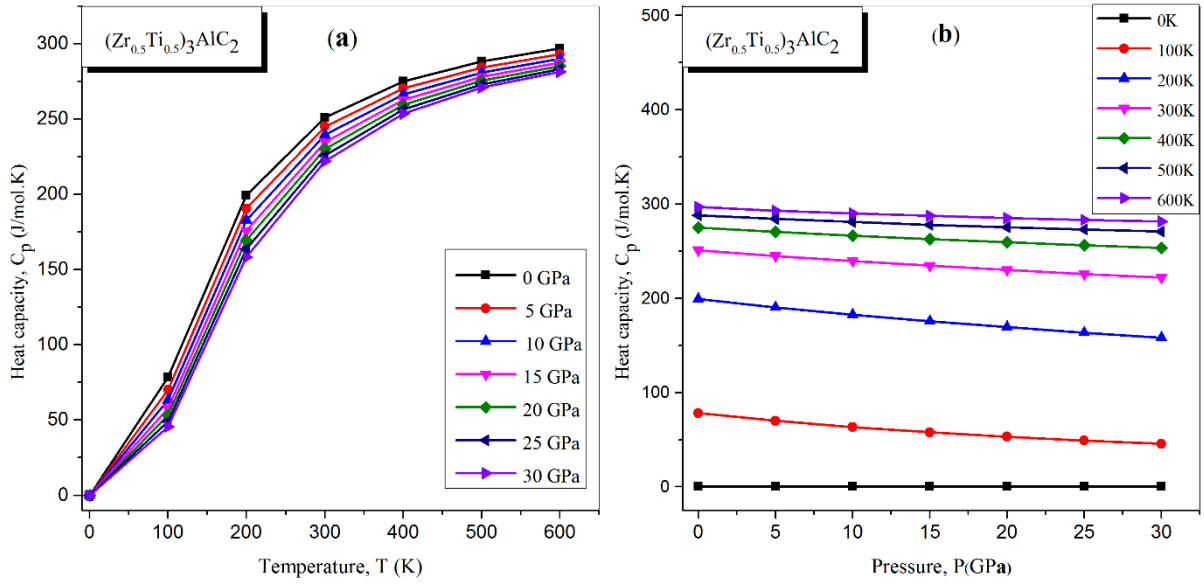

Fig. IV. 10b. The heat capacity C_P of $(Zr_{0.5}Ti_{0.5})_3AlC_2$ compound as a function of temperature and pressure [24].

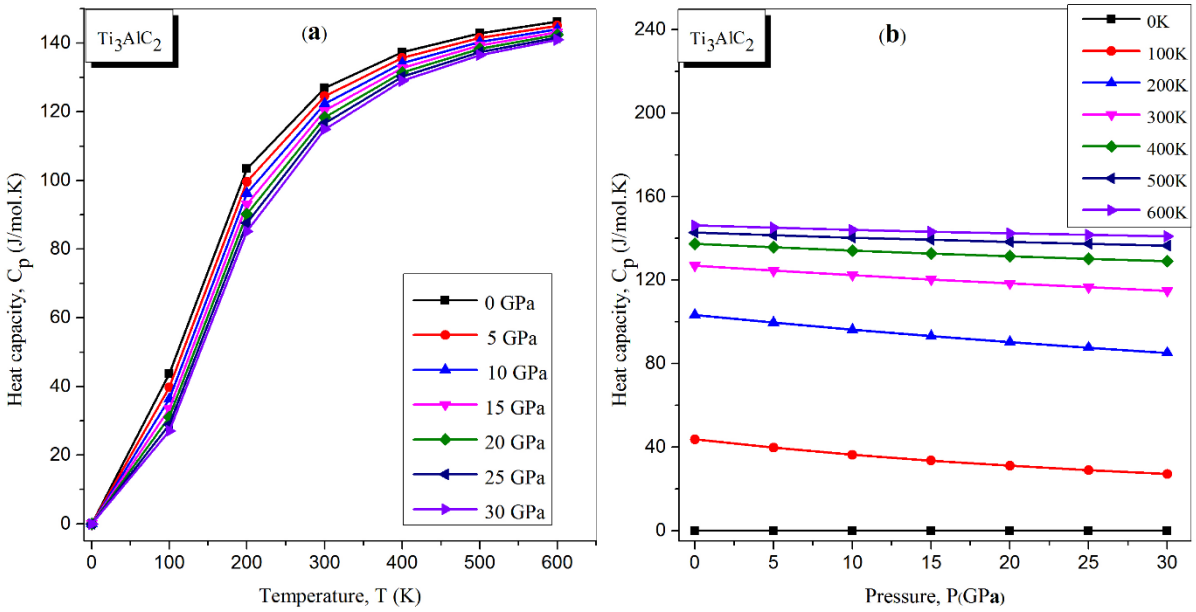

Fig. IV.10c. The heat capacity C_P of Ti_3AlC_2 compound as a function of temperature and pressure [24].

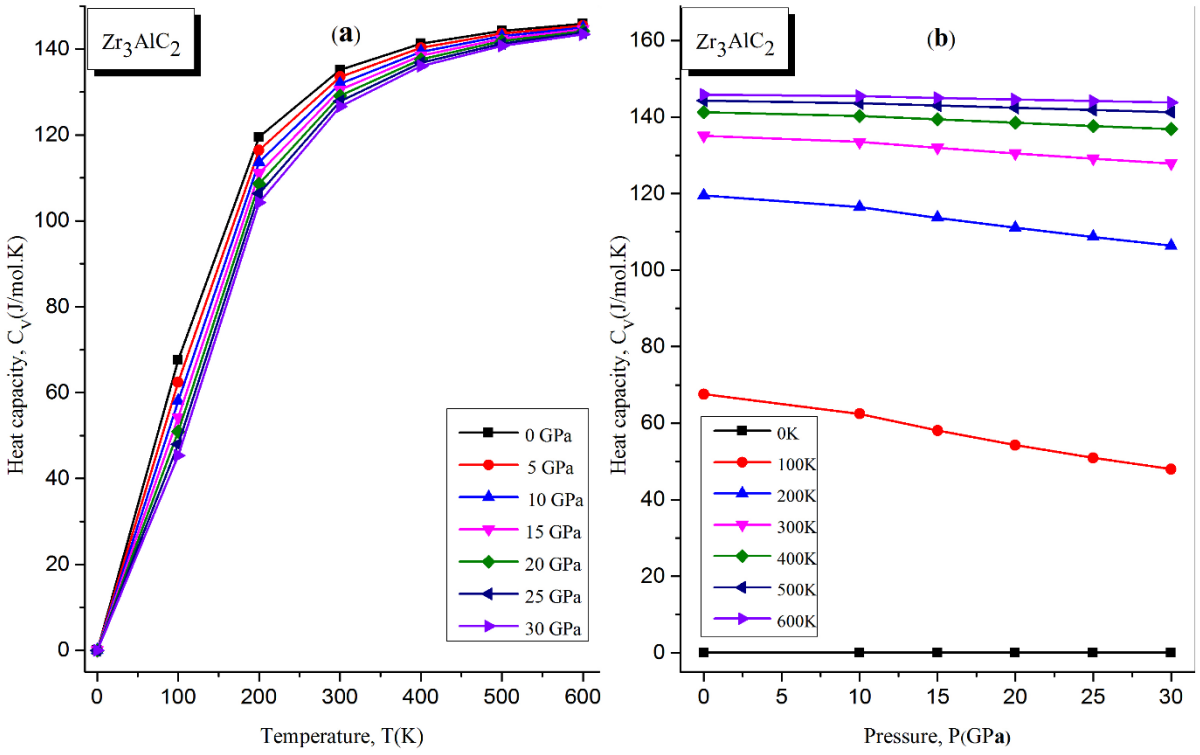

Fig. IV .11a. The heat capacity C_V of Zr_3AlC_2 compound as a function of temperature and pressure [24].

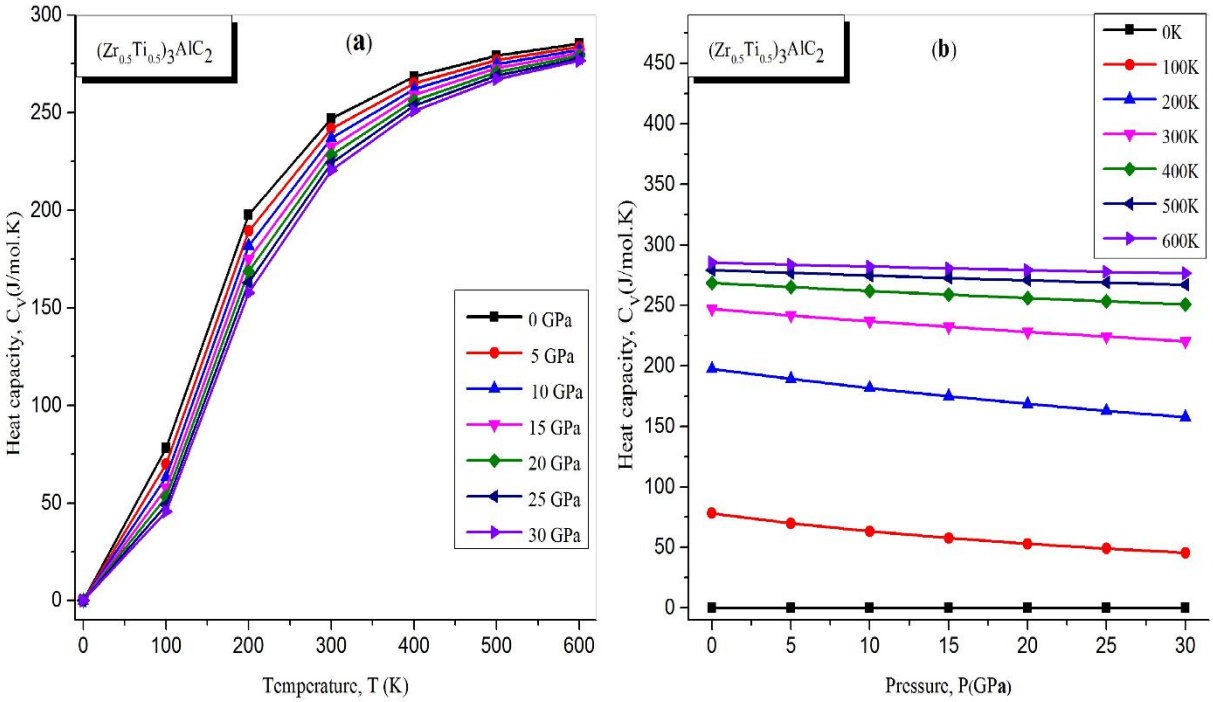

Fig. IV.11b. The heat capacity C_V of $(Zr_{0.5}Ti_{0.5})_3AlC_2$ compound as a function of temperature and pressure [24].

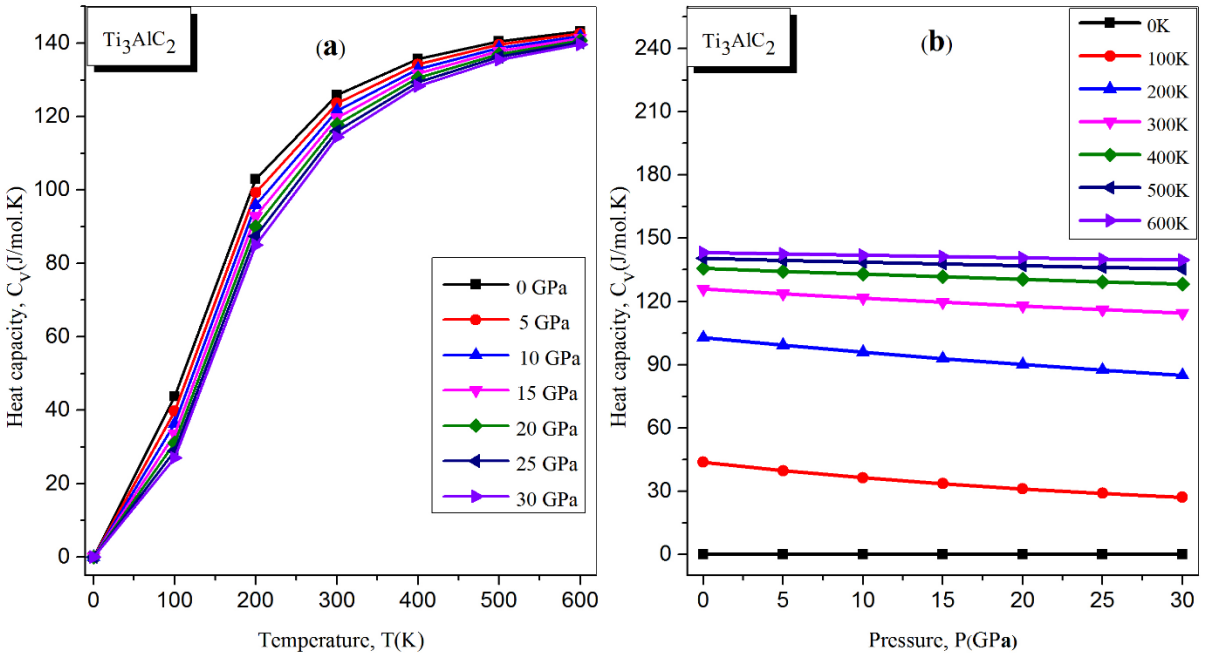

Fig. IV.11c. The heat capacity C_V of Ti_3AlC_2 compound as a function of temperature and pressure [24].

We can note from these figures that the C_P and C_V values change similarly for all our compounds, increasing rapidly with increasing temperature when the temperature is below 200K and continuing to increase weakly with increasing temperature.

The C_P and C_V values slowly decrease when the pressure increases under the constant temperature for all of our compounds except when the temperature is equal to zero where all the values of C_P and C_V remain zero.

References

[1] J.C. Slater, Adv. Quant. Chem. 1 (1994) 5564.

[2] P. Blaha, K. Schwarz, G.K.H. Madsen, D. Kvasnicka, J. Luitz, WIEN2K, an Augmented Plane Wave þLocal Orbitals Program for Calculating Crystal Properties, 2001, ISBN 3-9501031-1-2.

[3] S. Aouimer, M. Ameri, D. Bensaid, N.E. Moulay, A.Z. Bouyakoub, F.Z. Boufadi, I. Ameri, Y. Al-Douri, Acta Phys. Pol. 136 N1 (2019) 127-134.

[4] A. Bouhemadou, D. Allali, K. Boudiaf, B. Al Qarni, S. Bin-Omran, R. Khenata, Y. Al Douri, J. Alloys Compd. 774 (2019) 299-314.

[5] Friha Khelfaoui, Mohammed Ameri, Djillali Bensaid, Ibrahim Ameri, Yarub AlDouri, J. Supercond. Nov. Magnetism 31 (2018) 3183-3192.

[6] M.H. Benkabou, M. Harmel, A. Haddou, A. Yakoubi, N. Baki, R. Ahmed, Y. AlDouri, S.V. Syrotyuk, H. Khachai, R. Khenata, C.H. Voon, Mohd Rafie Johan, Chin. J. Phys. 56 (2018) 131-144.

[7] Z. Souadia, A. Bouhemadou, O. Boudrifa, S. Bin-Omran, R. Khenata, Y. Al Douri, High Pres. Res. 37 (Issue 4) (2017) 558-578.

[8] Kada Bidai, Mohammed Ameri, Slamani Amel, Ibrahim Ameri, Y. Al-Douri, Dinesh Varshney, C.H. Voon, Chin. J. Phys. 55 (Issue 5) (2017) 2144-2155.

[9] K. Bidai, M. Ameri, I. Ameri, D. Bensaid, A. Slamani, A. Zaoui, Y. Al-Douri, Arch. Metall. Mater. 62 (N 2) (2017) 865-871.

[10] Nadjia Tayebi, Kada Bidai, Mohammed Ameri, Slamani Amel, Ibrahim Ameri, Y. Al-Douri, Dinesh Varshney, Chin. J. Phys. 55 (2017) 769-779.

[11] A. Bennadji, M. Ameri, D. Hachemane, Y. Al-Douri, I. Ameri, D. Varshney, C.H. Voon, Chin. J. Phys. 55 (2017) 386-399.

[12] Kada Bidai, Mohammed Ameri, Zaoui Ali, Ibrahim Ameri, Yarub Al-Douri, Chin. J. Phys. 54 (2016) 678-694.

[13] Mohammed Ameri, Faiza Bennar, Slamani Amel, Ibrahim Ameri, Y. Al-Douri, Dinesh Varshney, Phase Transitions 89 (2016) 1236-1252.

[14] Samir Mustapha Laoufi, Amina Touia, Mohammed Ameri, Ibrahim Ameri, Fatima Boufadi, Keltouma Boudia, Amel Slamani, Fadila Belkharroubi, Y. AlDouri, Optik 127 (2016) 7382-7393.

[15] A. Benkabou, H. Bouafia, B. Sahli, B. Abidri, M. Ameri, S. Hiadsi, D. Rached, B. Bouhafs, N. Benkhettou, Y. Al-Douri, Chin. J. Phys. 54 (2016) 33-41.

[16] Kada Bidai, Mohammed Ameri, Djillali Bensaid, Slamani Amel, Ibrahim Ameri, Y. Al-Douri, Optik 127 (2016) 5155-5162.

[17] Nadhira Bioud, Optik 127 (2016) 4559-4573.

[18] S. Daho, M. Ameri, Y. Al Douri, D. Bensaid, D. Varshney, I. Ameri, Mater. Sci. Semicond. Process. 41 (2016) 102-108.

[19] A. Reggad, R. Lardjani, R. Baghdad, B. Bouhafs, Physica B 526 (2017) 89-95.

[20] J.P. Perdew, K. Burke, M. Ernzerhof, Phys. Rev. Lett. 77 (1996) 3865.

[21] S. Berri, D. Maouche, F. Zerarga, Y. Medkour, Physica B 407 (2012) 3328-3334.

[22] T. Lapauw, J. Halimc, J. Lu, T. Cabioc'h, L. Hultman, M.W. Barsoum, K. Lambrinou, J. Vleugels, Euro. Ceram. Soc 36 (2016) 943.

[23] M. Pietzka, J. Schuster, J. Phase Equil. 15 (1994) 392.

[24] I. Ouadha, H. Rached, A. Azzouz-Rached, A. Reggad, D. Rached, Computational Condensed Matter 23 (2020) e00468.

[25] C. Hu, F. Li, J. Zhang, J. Wang, J. Wang, Y. Zhou, Scripta Mater. 57 (2007) 893-896

[26] M. W. Barsoum and T. El-Raghy. Journal of the American Ceramic Society. 79 (1996) 1953–1956.

[27] 2Doptimize Package Is provided by M. Jamal as Part of the Commercial Code WIEN2K. http://www.wien2k.at/.

[28] Gokhan Surucu, Mater. Chem. Phys. 203 (2018) 106-117.

[29] Gokhan Surucu, Cagil Kaderoglu, Engin Deligoz, Haci Ozisik, Mater. Chem. Phys. 189 (2017) 90-95.

[30] M.A. Hadi, Y. Panayiotatos, A. Chroneos, J. Mater. Sci. Mater. Electron. 28 (2016) 3386-3393.

[31] E. Zapata, M.A. Hadi, D. Horlait, D.C. Parfitt, A. Thibaud, A. Chroneos, W.E. Lee, J. Am. Ceram. Soc. 100 (2017) 3393-3401.

[32] S. O. Kasap, *Principles of electronic materials and devices*, 3rd Ed, The McGraw-Hill, (2006).

[33] N.W. Ashcroft, N.D. Mermin, "*Solid State Physics*", Saunders College: Philadelphia (1976).

[34] A.H. Reshak, Moreteza jamal, Int. J. Electrochem. Sci. 8 (2013) 12252-12263.

[35] H. Rached, D. Rached, S. Benalia, A.H. Reshak, M. Rabah, R. Khenata, S. Bin Omran, Mater. Chem. Phys. 143 (2013) 93-108.

[36] J. Wang, J. Wang, Y. Zhou, C. Hu, Acta Mater. 56 (2008) 1511-1518.

[37] R. Hill, Proc. Phys. Soc. 65 (1952) 349-354.

[38] W. Voigt, Leipzig: Teubner, 1928, pp. 95-100.

[39] A. Reuss, Z. Angew. Math. Mech. 9 (1929) 49-58.

[40] Y. Tu, Y. Wang, Solid State Commun. 151 (2011) 238-241.

[41] G. Vaitheeswaran, V. Kanchana, A. Svane, A. Delin, J. Phys. Condens. Matter 19 (2007), 326214.

[42] X. TaO, J. Yang, L. Xi, Y. Ouyang, J. Solid State Chem. 194 (2012) 179-187.

[43] S.F. Pugh, Phil. Mag. 45 (1954) 823.

[44] A. Yildirim, H. Koc, E. Deligoz, Chin. Phys. B 21 (2012), 037101.

[45] M. Jamal, N. Kamali Sarvestani, A. Yazdani, A.H. Reshak, RSC Adv. 4 (2014) 57903-57915.

[46] H.M. Ledbetter, J. Phys. Chem. 6 (1977) 1181.

[47] Z.E. Biskri, H. Rached, M. Bouchear, D. Rached, J. Mech, Behav. Biomed. Mater 32 (2014) 345-350.

[48] A.L. Ding, C.M. Li, J. Wang, J. Ao, Z.-Q. Chen, Chin. Phys. B 23 (2014), 096201.

[49] X.Q. Chen, H. Niu, D. Li, Y. Li, Intermetallics 19 (2011) 1275-1281.

[50] M. Kaufman, *Principles of Thermodynamics*, Marcel Dekker, Inc, New York, (2002).

[51] M.H. Elahmar, H. Rached, D. Rached, R. Khenata, G. Murtaza, S. Bin Omran, W.K. Ahmed, J. Magn. Magn Mater. 393 (2015) 165-174.

[52] M. Benkabou, H. Rached, A. Abdellaoui, D. Rached, R. Khenata, M.H. Elahmar, B. Abidri, N. Benkhettou, S. Bin-Omran, J. Alloys Compd. 647 (2015) 276-286.

[53] M.A. Hadi, M. Roknuzzaman, A. Chroneos, S.H. Naqib, A.K.M.A. Islam, R.V. Vovk, K. Ostrikov, Comput. Mater. Sci. 137 (2017) 318.

[54] K. Haddadi, *Etude des propriétés structurales, élastiques et électroniques des composes antiperovskites de type XNCa3*, doctoral thesis, Faculty of Science, University of Setif 1, Algeria, (2013).

[55] M.A. Blanco, E. Francisco, V. Luana, Comput. Phys. Commun. 158 (2004) 57.

[56] A.G. McLellan, The Classical Thermodynamics of Deformable Materials, vol. 165, Cambridge University Press, Cambridge, 1980.

[57] E. Francisco, J.M. Recio, M.A. Blanco, A. Martín Pend as, J. Phys. Chem. 102 (1998) 1595.

[58] E. Francisco, G. Sanjurjo, M.A. Blanco, Phys. Rev. B 63 (2001), 094107.

[59] J.P. Poirier, Introduction to the Physics of the Earth's Interior, Cambridge University Press, 1991.

V. Summary and Conclusion

In summary, we have presented a report on the structural, electronic, mechanical and the thermodynamic properties of the MAX phases $(Zr_{1-x}Ti_x)_3AlC_2$ compounds by means of the *ab-initio* plane-wave (FP-LAPW) method. The equilibrium properties were calculated and compared with other work. The lattice constants *a* and *c* as function of pressure were evaluated. We have found that the compression along the (a,c)-axis decreases with linear dependence when the pressure increases. The formation energy shows that the compounds examined are quite stable and can be synthesized experimentally. The independent elastic constants obtained confirm the stability of the $(Zr_{1-x}Ti_x)_3AlC_2$ compounds against elastic deformation. Elastic moduli such as bulk modulus, shear modulus, Young's modulus E, Poisson's ratio, Cauchy pressure and Vickers hardness are calculated. The chemical bonding between the nearest neighbor atoms which is dominant is the ionic for Zr_3AlC_2 and $(Zr_{2/3}Ti_{1/3})_3AlC_2$, mixed ionic-covalent for $(Zr_{0.5}Ti_{0.5})_3AlC_2$ and covalent for $(Zr_{1/3}Ti_{2/3})_3AlC_2$ and Ti_3AlC_2. Also, all these compounds present a brittle nature and anisotropy behavior. Calculation of the Hardness shows that hardness increases with increasing concentration x. For example, the Ti_3AlC_2 compound is harder than $(Zr_{0.5}Ti_{0.5})_3AlC_2$ and Zr_3AlC_2 compounds. Since all the electronic structures don't have band gap at the Fermi level, so the studied compounds exhibit metallic behavior. The TDOS and PDOS curves reveal the existence of *p-d* hybridization. Finally, by the quasi-harmonic Debye model we have calculated the variation of the bulk modulus, Debye temperature and heat capacity as function of temperature and pressure. The bulk modulus and the Debye temperature in each compound increase significantly with increasing pressure and slowly decrease with increasing temperature. Conversely, the heat capacity increases with increasing temperature and slightly decreasing with increasing pressure.

Abstract

The structural, electronic, mechanical and the thermodynamic properties of the MAX phases $(Zr_{1-x}Tix)_3AlC_2$ compounds have been investigated by using the full-potential plane-wave FP-LAPW method as implemented in the Wien2k code. The exchange-correlation (XC) energy of electrons was treated using the Perdew-Burke-Ernzerhof parametrization. The ground-state properties for the studied compounds were calculated and compared with available experimental and theoretical data. The calculated lattice parameters are reasonably comparable with experimental and theoretical results. The formation energy has been evaluated in order to determinate the stability of our compounds. The calculation of the electronic structure was predicted for the first time for the present MAX phase compounds. These results indicate that, all our compounds exhibit metallic behavior and this metallicity is due to the *p-d* hybridization. The elastic constants have also evaluated by the Hex-elastic package. The mechanical stability reveal that, all our compounds are stable mechanically. The bulk modulus (B), shear modulus (G), Young's modulus (E), Poisson's ratio (ν), Debye temperature (θ_D) , Cauchy pressure (P^{Cauchy}) as well as the Vickers's hardness (H_v) were calculated and discussed in detail. Furthermore, the temperature and pressure effect on: Bulk modulus, Debye temperature and heat capacity at constant volume and constant pressure (C_V) and (C_P) respectively, have been investigated by the quasi-harmonic Debye model.

Keywords:

New MAX phases, Mechanical properties, Thermodynamic properties, Bonding nature.

Résumé

Les propriétés structurales, électroniques, mécaniques et thermodynamiques des composés de phases MAX $(Zr_{1-x}Tix)_3AlC_2$ ont été étudiées en utilisant la méthode FP-LAPW des ondes planes à potentiel total mise en œuvre dans le code Wien2k. L'énergie de corrélation d'échange (XC) des électrons a été traitée à l'aide du paramétrage Perdew-Burke-Ernzerhof. Les propriétés de l'état fondamental des composés étudiés ont été calculées et comparées aux données expérimentales et théoriques disponibles. Les paramètres de réseau calculés sont raisonnablement comparables aux résultats expérimentaux et théoriques. L'énergie de formation a été évaluée afin de déterminer la stabilité de nos composés. Le calcul de la structure électronique a été prédit pour la première fois pour les présents composés en phase MAX. Ces résultats indiquent que tous nos composés présentent un comportement métallique et que cette métallicité est due à l'hybridation *p-d*. Les constants élastiques ont également été évalués par le sous-programme Hex-elastic. La stabilité mécanique révèle que tous nos composés sont stables mécaniquement. Le module de compressibilité (B), le module de cisaillement (G), le module de Young (E), le coefficient de Poisson (v), la pression de Cauchy (P^{Cauchy}) et dureté (Hv) ont été calculés et discutés en détail. En outre, l'effet de la température et de la pression sur : le module de compressibilité, la température de Debye et la capacité thermique à volume constant et pression constante (C_V) et (C_P), respectivement, ont été étudiés par le modèle quasi-harmonique de Debye.

Mots clés :

Nouvelles phases Max, Propriétés mécaniques, Propriétés thermodynamiques, Nature de liaison

ملـــــخص

في دراستنا هذه تم فحص الخصائص الهيكلية والإلكترونية والميكانيكية والديناميكية الحرارية لمركبات $(Zr_{1-x}Ti_x)_3AlC_2$ MAX phases باستخدام طريقة الموجة المستوية المتزايدة خطيا FP-LAPW المدمجة في برنامج Wien2k.

لـقد تمت معالجة طاقة التبادل و الارتباط (XC) للإلكترونات باستخدام المعايير والثوابت Perdew-Burke-Ernzerhof.

كما تم حساب خصائص الحالة الأساسية للمركبات المدروسة ومقارنتها مع البيانات التجريبية والنظرية المتوفرة.

تمت دراسة ثوابت الشبكة لجميع مركباتنا وكانت متوافقة مع النتائج التجريبية والنظرية المتوفرة، كما تم تقييم طاقة التكوين من أجل تحديد ثبات مركباتنا. قمنا أيضا بدراسة البنية اللكترونية للمركبات المدروسة ولأول مرة. تشير النتائج إلي أن جميع هذه المركبات تظهر سلوكا معدنيا بسبب التهجين *p-d* .

تم الحصول على الثوابت المرنة المستقلة باستخدام برنامج Hexa-elastic ، والتي برهنت على الاستقرار الميكانيكي للمركبات. كما تم حساب و مناقشة قيم المعاملات التالية: معامل الإنضغاطية (B)، معامل القص (G) ، معامل يونغ (E)، نسبة بواسون (ν) ، ضغط Cauchy (P^{Cauchy}) و الصلابة (H_V).

قمنا أيضا بدراسة تأثير درجة الحرارة والضغط على معامل الإنضغاطية ودرجة حرارة Debye والسعة الحرارية بثبوت الحجم C_V و والسعة الحرارية بثبوت الضغط C_P بواسطة نموذج quasi-harmonic Debye.

الكلمات المفتاحية: مركبات MAX phases الجديدة، الخواص الميكانيكية، الحرارية، طبيعة الروابط.

International Publications:

1. Ismail Ouadha, Habib Rached, Ahmed Azzouz-Rached, Abderrahmane Reggad, Djamel Rached, « Study of the structural, mechanical and thermodynamic properties of the new MAX phase compounds $(Zr_{1-x}Ti_x)_3AlC_2$ », Computational Condensed Matter **23**, (2020) e00468. https://doi.org/10.1016/j.cocom.2020.e00468.
2. Ahmed Azzouz-Rached, Habib Rached, Ismail Ouadha, Djamel Rached, Abderrahmane Reggad, « The Vanadium-doping effect on physical properties of the Zr_2AlC MAX phase compound. », Materials Chemistry and Physics **260**, (2021) 124189. https://doi.org/10.1016/j.matchemphys.2020.124189.

National and international Communications :

1. Ismail Ouadha, Habib RACHED, Ahmed AZZOUZ-RACHED, Nabil BELOUFA, Samir BEKHEIRA, « Study of the structural and electronic properties of the new MAX phase compound Zr3AlC2 », 1ère Conférence Nationale Virtuelle (Webinaire) , Les Objectifs de Développement Durable après la Pandémie du COVID-19, Organisée les journées de 13 et 14 Mai 2020, par l'Association nationale, Eco-conception , Analyse de Cycle de Vie et Développement Durable (ANEADD) affiliée au Réseau des Clubs UNESCO en Algérie en partenariat avec le Laboratoire de recherche en technologie alimentaire (LRTA), université de Boumerdes, le Centre National des Technologies de Production plus Propre et le Conservatoire national des formations à l'environnement (CNFE).
2. Ahmed AZZOUZ-RACHED, Habib RACHED, Ismail OUADHA, Tariq HADJI, « Phase stability and physical properties of MAX phases», 1ère Conférence Nationale Virtuelle (Webinaire) , Les Objectifs de Développement Durable après la Pandémie du COVID-19, Organisée les journées de 13 et 14 Mai 2020, par l'Association nationale, Eco-conception , Analyse de Cycle de Vie et Développement Durable (ANEADD) affiliée au Réseau des Clubs UNESCO en Algérie en partenariat avec le Laboratoire de recherche en technologie alimentaire (LRTA), université de Boumerdes, le Centre National des Technologies de Production plus Propre et le Conservatoire national des formations à l'environnement (CNFE).
3. Ismail OUADHA, Ahmed AZZOUZ-RACHED, Habib RACHED, « Study of the structural, mechanical and thermodynamic properties of the new MAX phase compound Ti3AlC2 », in the first National Conference on Materials Sciences: From research to Teaching" MSRT", held virtually at Oran, in February 23-24, 2021.
4. Ahmed AZZOUZ-RACHED, Habib RACHED, Tariq HADJI, Ismail OUADHA, « First-principle study of magnetic, mechanical and thermodynamic properties of MAX phase Fe2AlC », in the first National Conference on Materials Sciences: From research to Teaching" MSRT", held virtually at Oran, in February 23-24, 2021.

5. Ismail OUADHA, Habib RACHED, Ahmed AZZOUZ-RACHED, « The physical properties of the new MAX phase compounds M3AlC2 », N°: TAM436/2021, 1st International Conference on Sustainable Energy and Advanced Materials, IC-SEAM'21 April 21-22,2021, Ouargla, ALGERIA (Virtual conference).
6. Ahmed AZZOUZ RACHED, Tariq HADJI, Habib RACHED, Ismail OUADHA, « Discovery of the Novel Ferromagnetic MAX Phase Compound: Case Study on MnFeSiN from ab-initio », N°: TAM426/2021, 1st International Conference on Sustainable Energy and Advanced Materials, IC-SEAM'21 April 21-22,2021, Ouargla, ALGERIA (Virtual conference).

Computational Condensed Matter 23 (2020) e00468

Contents lists available at ScienceDirect

Computational Condensed Matter

journal homepage: http://ees.elsevier.com/cocom/default.asp

Study of the structural, mechanical and thermodynamic properties of the new MAX phase compounds $(Zr_{1-x}Ti_x)_3AlC_2$

Ismail Ouadha [a], Habib Rached [a, b, *], Ahmed Azzouz-Rached [b], Abderrahmane Reggad [c], Djamel Rached [a]

[a] Magnetic Materials Laboratory, Faculty of Exact Sciences, Djillali Liabes University of Sidi Bel-Abbes, Algeria
[b] Department of Physics, Faculty of Exact Sciences and Informatics, Hassiba Benbouali University of Chlef, Algeria
[c] C2MO, Engineering Physics Laboratory, Matter Sciences Faculty, Ibn Khaldoun University, Tiaret, Algeria

ARTICLE INFO

Article history:
Received 10 February 2020
Received in revised form
22 March 2020
Accepted 23 March 2020

Keywords:
New MAX phases
Mechanical properties
Thermodynamic properties
Bonding nature

ABSTRACT

The structural, electronic, mechanical and the thermodynamic properties of the MAX phases $(Zr_{1-x}Ti_x)_3AlC_2$ compounds have been investigated by using the full-potential plane-wave FP-LAPW method as implemented in the Wien2k code. The exchange-correlation (XC) energy of electrons was treated using the Perdew–Burke–Ernzerhof parametrization. The ground-state properties for the studied compounds were calculated and compared with available experimental and theoretical data. The calculated lattice parameters are reasonably comparable with experimental and theoretical results. The formation energy has been evaluated in order to determinate the stability of our compounds. The calculation of the electronic structure was predicted for the first time for the present MAX phase compounds. These results indicate that, all our compounds exhibit metallic behavior and this metallicity is due to the p-d hybridization. The elastic constants have also evaluated by the Hex-elastic package. The mechanical stability reveal that, all our compounds are stable mechanically. The bulk modulus, shear modulus, Young's modulus, Poisson's ratio and Cauchy pressure were calculated and discussed in detail. Furthermore, the temperature and pressure effect on: Bulk modulus, Debye temperature and heat capacity at constant volume and constant pressure C_V and C_P, respectively have been investigated by the quasi-harmonic Debye model.

1. Introduction

The MAX phases $M_{n+1}AX_n$ are compounds with specific composition where M is an early transition metal, A is an A-group element and X is C and/or N, knows as 211, 312, 413 MAX phases for n = 1, 2 and 3, respectively. They have attracted an intensive interest at the community of science for nearly two decades. This group of compounds crystallizes with the hexagonal $P6_3/mmc$ space group (#194) [1–3]. The first study of this type of compounds was done on the Ti_3SiC_2 powder to determine its specific properties [3]. The interest on the MAX phases increased since mid- 1990s after the intrinsic properties of the compounds became known [4,5]. By combining the properties of metals and ceramics, MAX phases have an exceptional properties: high elastic stiffness, high melting temperature, high thermal shock resistance and high electrical conductivity [6,7].

In 2016, T. Laupauw et al. were the first to succeed to synthesize experimentally a new compound Zr_3AlC_2 of MAX family (312) [8]. The MAX phase materials are known to enter into many industrial applications for their desirable property [9], such as in aerospace, automotive, defense, medical and nuclear reactors [10–12]. A lot of MAX phase compounds are studied in the recent years by Gokhan Surucu et al. [13–18]. The structural, mechanical, electronic and lattice dynamic properties of hypothetical $Sc_2AlB_{0.5}C_{0.5}$, $Sc_2AlB_{0.5}N_{0.5}$ and $Sc_2AlC_{0.5}N_{0.5}$ compounds are investigated by CASTEP plane-wave pseudo-potential code. These compounds have hexagonal crystal structure and show a metallic behavior. The same author Gokhan have also investigate the structural, electronic, dynamic, and thermo-elastic properties of M_2AlB (X = V, Nb, Ta) MAX phase borides by VASP code, which are found to be energetically, mechanically and dynamically stable. To get better properties of the MAX family compounds, Zapata-Solvas et al. synthesized

* Corresponding author. Magnetic Materials Laboratory, Faculty of exact Sciences, Djillali Liabes University of Sidi Bel-Abbes, Algeria.
E-mail address: habib_rached@yahoo.fr (H. Rached).

https://doi.org/10.1016/j.cocom.2020.e00468
2352-2143/

experimentally solid solutions $(Zr_{3-x}Ti_x)AlC_2$ by mixing Zr with Ti for different x concentration [9,19,20]. M.A. Hadi et al. have studied the structural and optical properties of these solutions $(Zr_{1-x}Ti_x)_3AlC_2$ [19]. The elastic and thermodynamic properties also were studied by M.A. Hadi et al. to understand their mechanical comportment under extreme conditions [20].

In order to widen previous works on Zr_3AlC_2 and Ti_3AlC_2 compounds and enriched literature by the as yet uninvestigated properties of the $(Zr_{3-x}Ti_x)AlC_2$, we have investigated the structural, mechanical electronic and thermodynamic properties of new quaternary MAX phases $(Zr_{1-x}Ti_x)_3AlC_2$ for different concentrations (x = 0, 0.5, 1) by using a first-principles density functional theory (DFT) [21,22].

2. Computational method

To doing our calculation, we have employed full potential linearized augmented plane wave (FP-LAPW) method [23] implemented in the Wien2k code [24] and based on the density functional theory (DFT) which has proven to be one of the most accurate theory for the calculation of the electronic and structural properties of solids [25–40]. In the FP-LAPW method, the space is divided into two regions: the first is a non-overlapping muffin-tin (MT) spheres where the basis set inside this region is described by radial solutions of the one-particle Schrodinger equation and their energy derivatives multiplied by spherical harmonics and the second one which is interstitial region (IR) the basis set consists of plane waves [41]. For the exchange-correlation functional we have adopted the generalized gradient approximation (GGA) parametrized by Perdew–Burke–Ernzerhof (PBE) [42]. The convergence tests allow us to choose the parameter $R_{mt}*K_{max} = 8$ where R_{mt} is the smallest atomic sphere radius and Kmax is the plane wave cutoff [43]. The chosen R_{MT} values of Zr, Ti, Al and C are 1.96, 1.96, 2.38 and 1.74 Bohr, respectively. The G_{max} was chosen to equal the 14 value where G_{max} is defined as the magnitude of the largest vector in the charge density Fourier expansion. The MT sphere were considered up to $l_{max} = 10$. The Monkorst-Pack method in the first Brillouin zone (IBZ) was performed using 1500 kpoints. The charge convergence was set to 10^{-4}.

The M_3AlC_2 compounds crystallize in a hexagonal structure with the $P6_3/mmc$ space group (#194) [8,44] as shown in Fig. 1. The atoms Zr occupy the Wyckoff positions 2a and 4f with Z_M ~0.12. The Al atoms occupy 2b atomic positions while the C atoms reside in 4f with Z_C ~0.07 (Table 1).

3. Results and discussions

3.1. Structural properties

We have used the 2D-optimize package developed by J. Morteza [45] to determine the structural lattice parameters of our compounds. In Table 2, we presented our results and some other experimental and theoretical results recently obtained for comparison. We can see that our results are in good agreement with corresponding experimental and theoretical results. We can see also that when the x concentration increase, all the lattice parameters a and c and the volume of unit cell decrease while the hexagonal ration c/a increase. We can interpret that by the decrease of the atomic radius because the atomic radius of Ti atom is less than the one of the Zr atom. In attempt to identify the effect of pressure on the structural properties, we have investigate the parameters constants a and c under pressure effect in the range from 0 to 25 GPa. Fig. 2 illustrate the Lattice parameters a and c as function of pressure. We can note that when the pressure is enhanced the compression along the (a,c)-axis decreases.

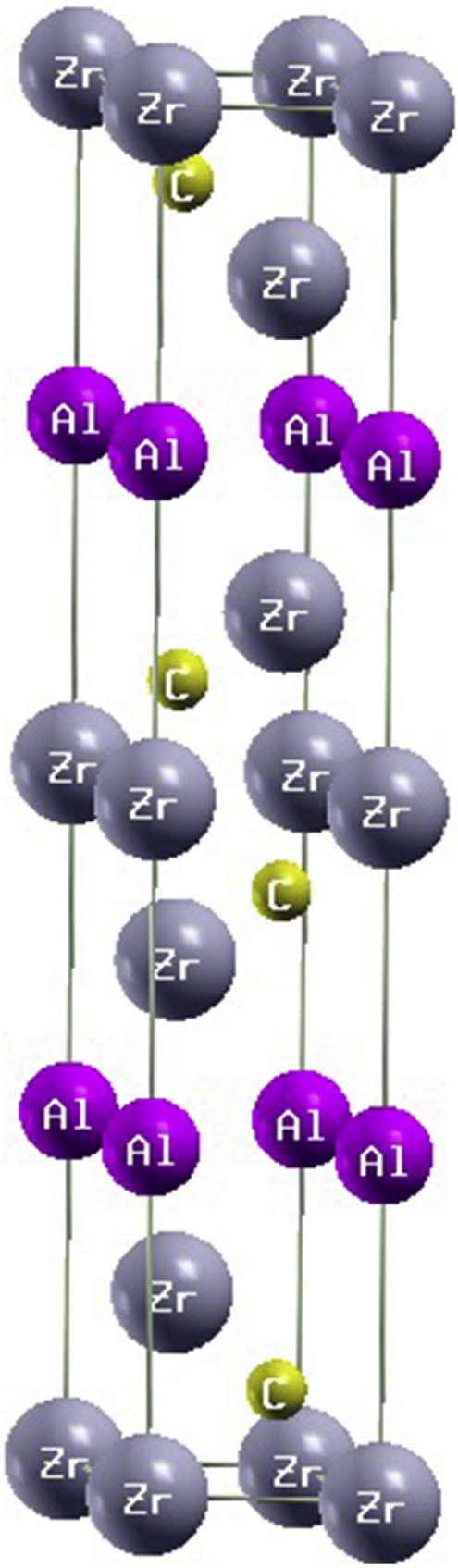

Fig. 1. A view of the crystal structure of the MAX Phase Zr_3AlC_2 compound.

Table 1
The Wyckoff positions for Zr_3AlC_2 compounds.

Compound	Atom	Site	Coordinates
M_3AlC_2 M = Zr, Ti $P6_3/mmc$ (#194)	M	2a	(0,0,0) $(0,0,\frac{1}{2})$
		4f	$(\frac{1}{3}, \frac{2}{3}, z_M)$ $(\frac{2}{3}, \frac{1}{3}, z_M+\frac{1}{2})$ $(\frac{2}{3}, \frac{1}{3}, -z_M)$ $(\frac{1}{3}, \frac{2}{3}, -z_M+\frac{1}{2})$
	Al	2b	$(0,0, \frac{1}{4})$ $(0,0, \frac{3}{4})$
	C	4f	$(\frac{1}{3}, \frac{2}{3}, z_C)$ $(\frac{2}{3}, \frac{1}{3}, z_C+\frac{1}{2})$ $(\frac{2}{3}, \frac{1}{3}, -z_C)$ $(\frac{1}{3}, \frac{2}{3}, -z_C+\frac{1}{2})$

To calculate the stability of our compounds, the best indicator is their formation energy. The formation energy is calculated using the following equation [18,46]:

$$\Delta E_{f\,(Zr_{1-x}Ti_x)_3AlC_2} = E_{tot\,(Zr_{1-x}Ti_x)_3AlC_2} - (3(1-x)E_{Zr} + 3xE_{Ti} + E_{Al} + 2E_C) \quad (1)$$

where $\Delta E_f(Zr_{1-x}Ti_x)_3AlC_2$ is the formation energy of $(Zr_{1-x}Ti_x)_3AlC_2$ with ((x = 0, 0.5, 1), E_{tot} is the total energy per unit cell of the bulk compounds, E (X = Zr, Ti, Al and C), it represents the total energy per atom of the element in pure solid state. The calculated formation energies of our compounds are regrouped in Table 2. To the best of our knowledge, the formation energy has not been measured or calculated yet for these compounds, hence our result maybe considered as a quantitative theoretical prediction. From these results, it is obvious that the calculated formation energies are negative, which indicates that the examined compounds are quite stable even at high temperatures.

3.2. Mechanical properties

The study of the mechanical properties is based upon the determination of the elastic parameters. These parameters allow us to get knowledge about the structural stability and anisotropic character of a material. Furthermore, when a pressure is applied on a material, these parameters are able to provide information about the mechanical stability, and strength under compression. In our hexagonal system of $(Zr_{1-x}Ti_x)_3AlC_2$ MAX phases, there are six different elastic constants C_{11}, C_{12}, C_{13}, C_{33}, C_{44} and C_{66} where $C_{66} = \frac{(C11-C12)}{2}$. We have used the Hex-elastic package of Jamal Morteza

Table 2
The calculated lattice parameters, Hexagonal ration c/a and unit cell volume of Zr_3AlC_2, $(Zr_{0.5}Ti_{0.5})_3AlC_2$ and Ti_3AlC_2.

Compounds	a (Å)	c (Å)	c/a	V(Å^3)	ΔH_f(eV/f.u.)	Remarks
Zr_3AlC_2	3.341 3.333 3.335	19.960 19.951 19.961	5.974 5.986 5.985	193.02 191.95 192.27	−0.8176	Calc[a]
					–	Expt[b]
					–	Calc[c]
$(Zr_{0.5}Ti_{0.5})_3AlC_2$	3.230 3.232 3.197	19.366 19.397 19.220	5.995 6.002 6.012	175.02 175.45 170.11	−0.7765	Calc[a]
					–	Expt[d]
					–	Calc[c]
Ti_3AlC_2	3.077 3.075 3.078	18.638 18.578 18.670	6.057 6.042 6.065	152.78 152.16 153.19	−0.8262	Calc[a]
					–	Expt[e]
					–	Calc[c]

[a] Present work.
[b] Ref [8].
[c] Ref [19].[d] Ref [48].
[e] Ref [44].

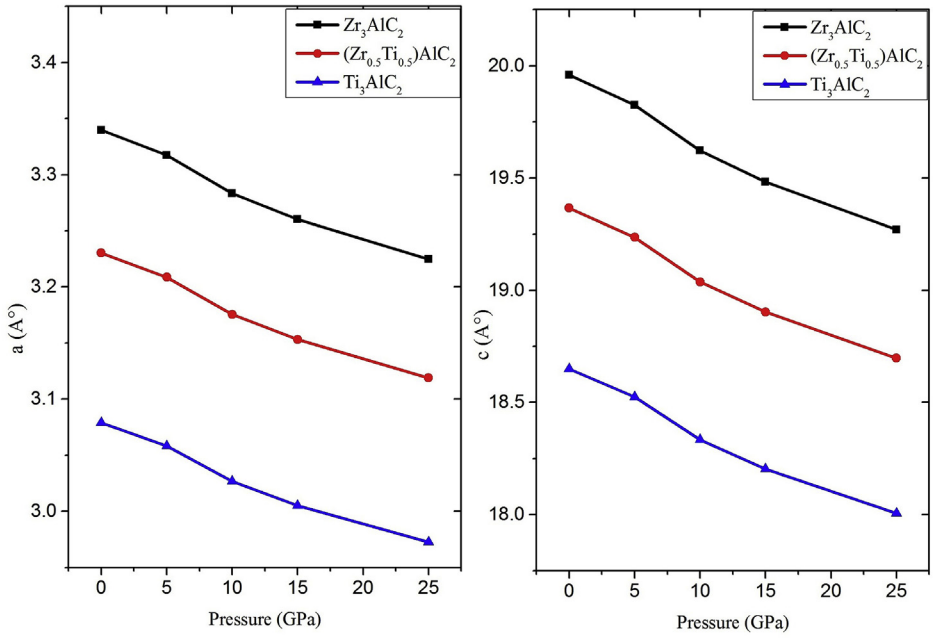

Fig. 2. The Lattice parameters a and c as function of pressure.

to determine the elastic constants of our compounds at their equilibrium lattice constants [47]. The elastic constants are derived by means of a Taylor expansion of the total energy E (V, ε_i) of the system with respect to the strain tensor ε_i:

$$E(V,\varepsilon_i) = E_0(V_0,0) + V_0\left(\sum_i \tau_i \xi_i \varepsilon_i + \frac{1}{2}\sum_{ij} c_{ij}\varepsilon_i\xi_i\varepsilon_j\xi_j\right) + O\left(\varepsilon^3\right) \tag{2a}$$

Where E_0 and V_0 are the energy and the volume of unstrained hexagonal system respectively. The factor ξ_i, takes the value 1 if the index i is equal to 1, 2 or 3 and the value 2 if it is equal to 4, 5 or 6. In the above equation τ_i are related to the strain on the crystal. For our compounds, the total energy from equation (2a) is modified by applying six distortions described as follows:

$$D_1 = \begin{pmatrix} 1+\varepsilon & 0 & 0 \\ 0 & 1+\varepsilon & 0 \\ 0 & 0 & 1 \end{pmatrix} \tag{2b}$$

$$D_2 = \begin{pmatrix} 1+\varepsilon & 0 & 0 \\ 0 & 1+\varepsilon & 0 \\ 0 & 0 & \dfrac{1}{(1+\varepsilon)^2} \end{pmatrix} \tag{3}$$

$$D_3 = \begin{pmatrix} 1 & 0 & 0 \\ 0 & 1 & 0 \\ 0 & 0 & 1+\varepsilon \end{pmatrix} \tag{4}$$

$$D_4 = \begin{pmatrix} \left(\dfrac{1+\varepsilon}{1-\varepsilon}\right)^{\frac{1}{2}} & 0 & 0 \\ 0 & \left(\dfrac{1-\varepsilon}{1+\varepsilon}\right)^{\frac{1}{2}} & 0 \\ 0 & 0 & 1 \end{pmatrix} \tag{5}$$

$$D_5 = \begin{pmatrix} 1 & 0 & \varepsilon \\ 0 & 1 & \varepsilon \\ \varepsilon & \varepsilon & 1+\varepsilon^2 \end{pmatrix} \tag{6}$$

$$D_6 = \begin{pmatrix} \left(1+\varepsilon^2\right)^{\frac{1}{2}} & \varepsilon & 0 \\ \varepsilon & \left(1+\varepsilon^2\right)^{\frac{1}{2}} & 0 \\ 0 & 0 & 1 \end{pmatrix} \tag{7}$$

The energy for these distortions can be obtained as:

$$E(V,\varepsilon) = E(V_0,0) + V_0\left((C_{11}+C_{12})\varepsilon^2 + O\left(\varepsilon^3\right)\right) \tag{8}$$

$$E(V,\varepsilon) = E(V_0,0) + V_0\left(\frac{C_{33}}{2}\varepsilon^2 + O\left(\varepsilon^3\right)\right) \tag{9}$$

$$E(V,\varepsilon) = E(V_0,0) + V_0\left((C_{zz})\varepsilon^2 + O\left(\varepsilon^3\right)\right) \tag{10}$$

with $$C_{zz} = C_{11} + C_{12} + 2C_{33} - 4C_{13} \tag{11}$$

$$E(V,\varepsilon) = E(V_0,0) + V_0\left((C_{11}-C_{12})\varepsilon^2 + O\left(\varepsilon^4\right)\right) \tag{12}$$

$$E(V,\varepsilon) = E(V_0,0) + V_0\left(4(C_{44})\varepsilon^2 + O\left(\varepsilon^3\right)\right) \tag{13}$$

and

$$E(V,\varepsilon) = E(V_0,0) + V_0\left(2(C_{66})\varepsilon^2 + O\left(\varepsilon^3\right)\right) \tag{14}$$

respectively.

Our results of these elastic constants are illustrated in Table 3. To date, there is no experimental report in the elastic constants for the herein investigated compounds. We can observe obviously that all these elastic constants C_{ij} are positive and completely satisfy the conditions of mechanic stability of compounds for hexagonal structure [49]:

$$C_{11} > 0,\quad C_{33} > 0,\quad C_{44} > 0,\quad C_{11} - C_{12} > 0,\quad (C_{11}+C_{12})C_{33} > 2C_{13}^2 \tag{15}$$

These results confirm the stability of the $(Zr_{1-x}Ti_x)_3AlC_2$ MAX phases against any elastic deformation. Meanwhile, the present results of the elastic constants shows that C_{33} is larger than C_{11} for all our compounds, which reveals that the *a* and *b*-axes are more compressible than the *c*-axis. These results can be explained in terms of the existence of strong covalent bonding in the [001] direction for the studied compounds. Also, we can note that the C_{11} and C_{33} are considerably higher than other elastic constants, which divulge an elastic anisotropy in these compounds.

From the elastic constants we have calculate the elastic modulus which allow us to determine all the mechanical properties. These modulus are the bulk modulus B and the shear modulus G. The B measures the resistance of a material to volume change and provides us an estimate of its response to a hydrostatic pressure, while G describes the resistance of a material to shape change [50]. From the Hill approximation which based on the Reuss and Voigt approaches, the compressibility modulus B and the shear modulus G are given by these following expressions [51–53]:

Table 3
Calculated elastic constants C_{ij} (GPa), elastic modulus (B, G and E) (GPa), Poisson's ratio ν, B/G ratio, shear anisotropic factor for the three different shear planes (A_1, A_2 and A_3), Cauchy pressure and Vickers hardness H_V (GPa) for Zr_3AlC_2, $(Zr_{0.5}Ti_{0.5})_3AlC_2$ and Ti_3AlC_2 compounds.

Compound	Zr_3AlC_2	$(Zr_{0.5}Ti_{0.5})_3AlC_2$	Ti_3AlC_2
C_{11} (GPa)	308.59	313.41	358.86
C_{12} (GPa)	89.33	90.86	99.95
C_{13} (GPa)	97.37	97.20	92.33
C_{33} (GPa)	318.24	331.38	366.22
C_{44} (GPa)	82.27	89.09	102.19
C_{66} (GPa)	109.63	111.28	129.45
B (GPa)	167.01	169.76	183.68
G (GPa)	97.33	102.11	119.10
E (GPa)	244.50	255.16	293.80
B/G	1.72	1.66	1.54
ν	0.255	0.249	0.233
P_x^{Cauchy}	15.1	8.1	−9.86
P_y^{Cauchy}	−20.30	−20.42	−29.5
A_1	1.30	1.27	1.24
A_2	0.75	0.80	0.79
A_3	0.98	1.01	1.06
H_V (Gpa)	12.48	13.52	16.74

$$B_V = \frac{2(C_{11} + C_{12}) + C_{33} + 4C_{13}}{9} \quad (16)$$

$$B_R = \frac{(C_{11} + C_{12})C_{33} - 2C_{13}^2}{C_{11} + C_{12} + 2C_{33} - 4C_{13}} \quad (17)$$

$$B_H = \frac{B_V + B_R}{2} \quad (18)$$

$$G_V = \frac{C_{11} + C_{12} + 2C_{33} - 4C_{13} + 12(C_{44} + C_{66})}{30} \quad (19)$$

$$G_R = \frac{5}{2} \frac{\left[(C_{11} + C_{12})C_{33} - 2C_{13}^2\right] C_{44}C_{66}}{3B_V C_{44}C_{66} + \left[(C_{11} + C_{12})C_{33} - 2C_{13}^2\right](C_{44} + C_{66})} \quad (20)$$

$$G_H = \frac{G_V + G_R}{2} \quad (21)$$

Where $B = B_H$ (the Hill bulk modulus) and $G = G_H$ (the Hill shear). The Young's modulus E and Poisson's ratio ν of a hexagonal structure are also calculated by using the following expressions [54]:

$$E = \frac{9BG}{3B + G} \quad (22)$$

$$\nu = \frac{3B - E}{6B} \quad (23)$$

The Young's modulus is considered as a measure of the material's ability to resist stress and pressure in the elastic deformation range [55]. More Young's modulus is bigger, more the deformation of matter is difficult. The values of the B, G and E magnitudes for our compounds Zr_3AlC_2, $(Zr_{0.5}Ti_{0.5})_3AlC_2$ and Ti_3AlC_2 are represented in Table 3. We can see that, when the concentration x increase, the values of B, G and E increase. The compound Ti_3AlC_2 present a higher ability to resist deformation, while it's the inverse in the case of the compound Zr_3AlC_2. The Poisson's ratio ν is frequently used to deduce the type of the chemical bonding. When its value is less than 0.25, the chemical bonding has a covalent, while if its value is more than 0.25, the bonding will be a typical ionic [56]. The calculated values of the Poisson's ratio ν are 0.255, 0.249 and 0.233 for Zr_3AlC_2, $(Zr_{0.5}Ti_{0.5})_3AlC_2$ and Ti_3AlC_2 respectively, which indicate that the chemical bonding nature is more ionic for Zr_3AlC_2, have a mixed nature for $(Zr_{0.5}Ti_{0.5})_3AlC_2$ and more covalent for Ti_3AlC_2. It's also possible to study the nature of the chemical bonding using the Cauchy pressure. When the value of Cauchy pressure is positive, then the ionic bonding is dominant, while the covalent bonding is dominant when its value is negative [57]. In hexagonal system, the Cauchy pressure is estimated for the different directions as follows:

$$P_x^{Cauchy} = C_{13} - C_{44} \quad (24)$$

$$P_y^{Cauchy} = C_{12} - C_{66} \quad (25)$$

From Table 3, it clear that for the Ti_3AlC_2 compound, all the values of Cauchy pressure P_x^{Cauchy} or P_y^{Cauchy} are negative, which confirm the more covalent character for this compound, while the compounds Zr_3AlC_2 and $(Zr_{0.5}Ti_{0.5})_3AlC_2$ have positive values of P_x^{Cauchy} and negative values of P_y^{Cauchy} which indicate the mixed nature for these compounds, especially in for the compound Zr_3AlC_2 where the ionic character is clear. In engineering science, calculating the Poisson ratio allow us to classify materials as brittle or ductile. If the Poisson ratio of a material is greater than the value 0.26, it is considered as ductile, otherwise if it is considered as brittle [58]. For our compounds, we have found that all Poisson ratio values are less than 0.26, which means that they are all classified as brittle. Another criterion called Pugh criterion can also make classification of ductile and brittle materials. When B/G is greater than 1.75, the material will be ductile, and if not, it will be considered brittle [59]. From our results of B/G ratio in Table 3, we obtained that all the B/G values are less than 1.75 which confirms that these compounds exhibit a brittle nature.

The calculation of the shear anisotropic factors of materials is extremely important to study the degree of durability related mainly to micro-cracks in crystals. In our hexagonal system, we have calculated three elastic anisotropy factors A_1, A_2 and A_3 [60], where A_1 for {100} planes between the [011] and [010] directions, A_2 for {010} shear planes between the [101] and.

[001] directions and A_3 for {001} shear planes between the [110] and [010] directions, where:

$$A_1 = \frac{C_{11} + C_{12} + 2C_{33} - 4C_{13}}{6C_{44}} \quad (26)$$

$$A_2 = \frac{2C_{44}}{C_{11} + C_{12}} \quad (27)$$

$$A_3 = \frac{C_{11} + C_{12} + 2C_{33} - 4C_{13}}{3(C_{11} - C_{12})} \quad (28)$$

All the values of A_1, A_2 and A_3 must be equal to 1 for an isotropic crystal while they differ from 1 for anisotropic crystal [61]. According to our results reported in Table 3, all the anisotropy factors are greater or smaller than 1, which indicates that the $(Zr_{1-x}Ti_x)_3AlC_2$ MAX phase compounds exhibit an anisotropy behavior.

Hardness is another mechanical property of a material related to the elastic and plastic response of a material. In general, hardness is an important indicator of corrosion resistance of materials, so the most corrosion-resistant materials are those with the greater hardness [62]. We have used the formula of Chen of Vickers's Hardness [63]:

$$H_V = 2\left(\frac{G^3}{B^2}\right)^{0.585} - 3 \quad (29)$$

The calculated results are found to equal 12.48 GPa, 13.52 GPa and 16.74 GPa for Zr_3AlC_2, $(Zr_{0.5}Ti_{0.5})_3AlC_2$ and Ti_3AlC_2, respectively. The hardness of Zr_3AlC_2 is the smallest among of the three compounds, and the hardness of Ti_3AlC_2 is the greatest among of them.

3.3. Effect of the pressure on the mechanical properties

We have also studied the effect of the pressure on the mechanical properties of our compounds $(Zr_{1-x}Ti_x)_3AlC_2$ (where x = 1, 0.5 and 1). Fig. 3 show change of the elastic constants under different pressures from 0 to 25 GPa. We can see that the elastic constants of our compounds increase when the pressure increase, but despite that, the mechanical stability condition is kept fulfilled. Fig. 4 shows the change of elastic modulus under different pressures from 0 to 25 GPa. We can notice that all the bulk modulus B, shear modulus G and Young's modulus E increase almost linearly when the pressure increases. That means these compounds maintain their mechanical stability under pressures up to 25 GPa.

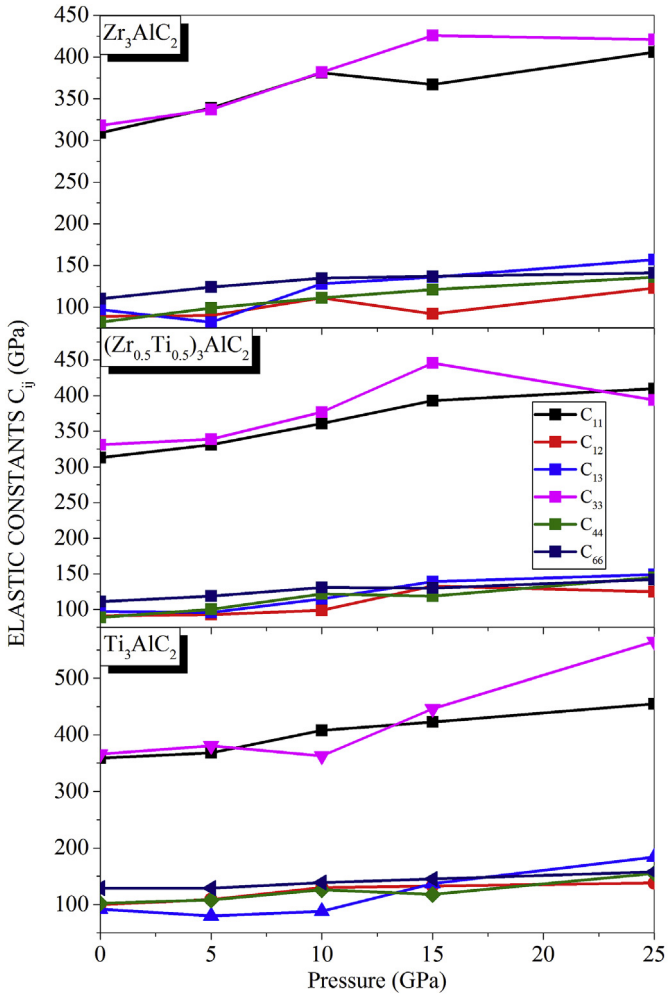

Fig. 3. Variation of the elastic constants Cij under different pressures from 0 to 25 GPa.

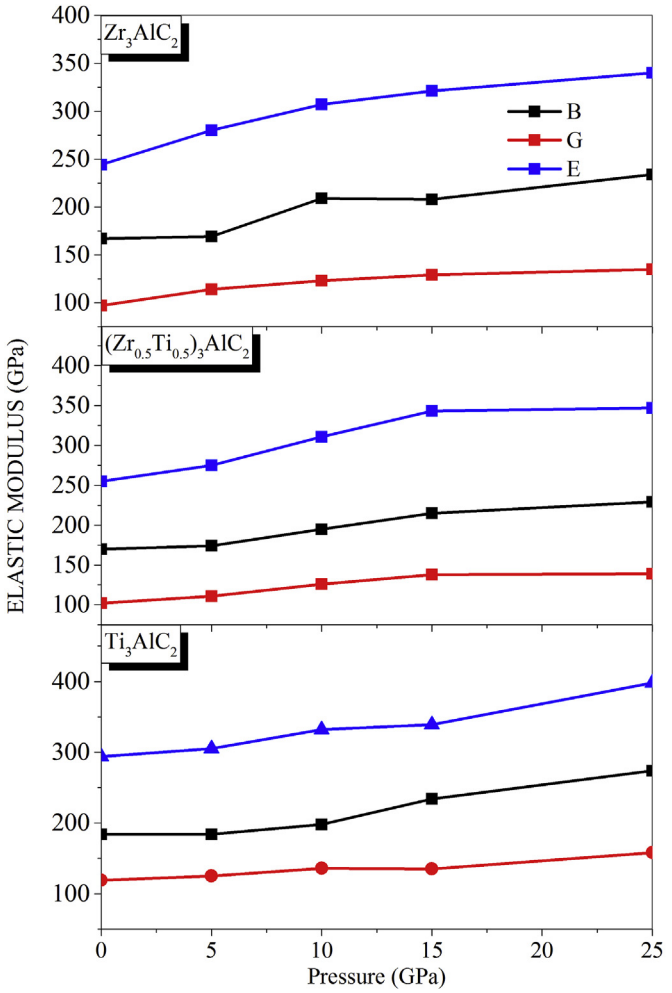

Fig. 4. Variation of the Bulk modulus B, shear modulus G and Young's modulus E under different pressures from 0 to 25 GPa.

3.4. Electronic properties

The calculation of the electronic properties of a material is extremely important, as it informs us about the electronic conductivity, the nature of the connections that are formed between the different elements of this material, and these properties include band structures, state density and charge densities. In Fig. 5, we illustrate the band structures for Zr_3AlC_2, $(Zr_{0.5}Ti_{0.5})_3AlC_2$ and Ti_3AlC_2 compounds along the high-symmetry axes of the first Brillouin zone. We can note from this figure that the three band structure are topologically identical and we can easily observe the overlap between the valence and conduction bands at the Fermi level of all these diagrams. Consequently, no band gap is found at the Fermi level and as a result all these compounds show metallic nature. We can also observe a great dispersion at both the valence and conduction bands. In order to further understanding the nature of the calculated band structures, we have also calculate the total density of states (TDOS) and partial density of states (PDOS) for the studied compounds in a wide energy interval [-6 eV, 6 eV] symmetric around the Fermi level. We illustrate in Fig. 6(a and b and c) the TDOS and PDOS of Zr_3AlC_2, $(Zr_{0.5}Ti_{0.5})_3AlC_2$ and Ti_3AlC_2, respectively. The Fermi level is taken as the origin of the energies. The TDOS results confirm the metallic nature for our compounds. We can divide the valence region into two parts: the first part where the valence band between −5.0 eV and −1.5 eV and the second part where the valence band between −1.5 eV and 0.0 eV. The first part is mostly dominated by the p-d of the transition element (Zr and Ti), *s*-Al and *p*-C for the three investigated compounds. The second part present a strong *p-d* hybridization between the *d* orbital of transition metal elements (Ti and Zr) and *p* orbital of Al. While, the conduction band are originated mainly to the *d*-Zr contributions with a minor contribution of s-p states of Al and p states of C. The presence of p-d and s-p hybridization reveal that the chemical bonding are mixed ionic-covalent for our compounds, which confirm the result obtained from mechanical properties. The hybridization *p-d* contribute to forming the metallicity of our compounds. It is important to emphasize that, to our knowledge; there are no experimental or theoretical results about the electronic properties for these compounds.

3.5. Thermodynamic properties

In solid states physics, the Debye temperature θ_D and the sound v velocity play a very important role to study the thermodynamic properties. The determination of both values is calculated as follows [64,65]:

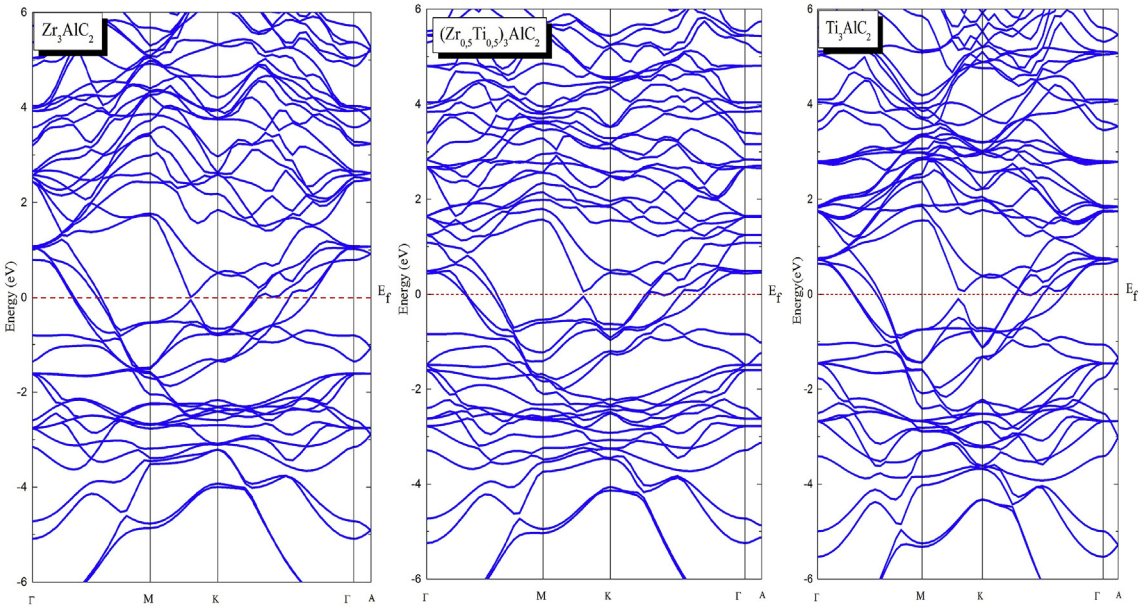

Fig. 5. The band structures for Zr_3AlC_2, $(Zr_{0.5}Ti_{0.5})_3AlC_2$ and Ti_3AlC_2 compounds along the high-symmetry axes of the first Brillouin zone.

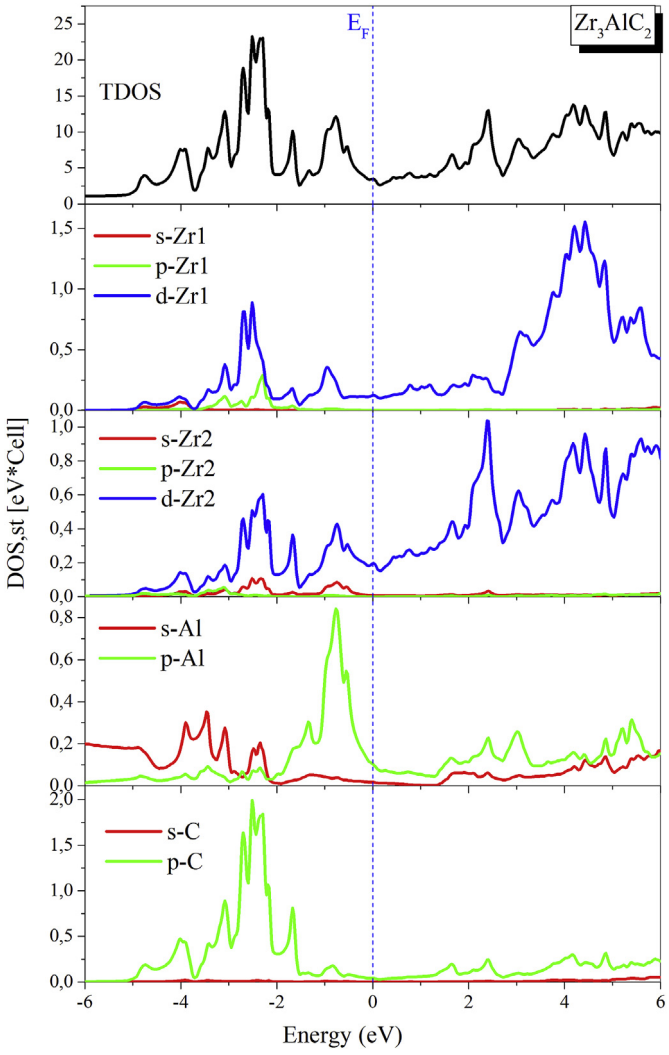

Fig. 6A. The Total and Partial density of states (TDOS, PDOS) of Zr_3AlC_2 compound.

$$\theta_D = \frac{h}{k_B}\left[\left(\frac{3n}{4\pi}\right)\frac{N_A\rho}{M}\right]^{\frac{1}{3}} \tag{30}$$

$$v_m = \left[\frac{1}{3}\left(\frac{2}{v_t^3}+\frac{1}{v_l^3}\right)\right]^{-\frac{1}{3}} \tag{31}$$

$$v_l = \left(\frac{3B+4G}{3\rho}\right)^{\frac{1}{2}} \tag{32}$$

$$v_t = \left(\frac{G}{\rho}\right)^{\frac{1}{2}} \tag{33}$$

where h is Plank's constant, k_B is Boltzmann's constant, n is the number of atoms per formulaunit, N_A is Avogadro's number, ρ is the density, M is the molecular weight, v_m is the average sound velocity, v_l and v_t are the longitudinal and transverse sound velocities, respectively. The values of ρ, v_t, v_l, v_m and θ_D are shown in Table 4. We can note the values of density ρ of $(Zr_{1-x}Ti_x)_3AlC_2$ are decrease when x increase where x = 0, 0.5 and 1. All the values of v_l, v_t and v_m and θ_D are increase with x. To the best of our knowledge, there is no experimental report in the literature about these quantities for our compounds up to now.

We have also evaluated the Debye temperature, bulk modulus and heat capacity under temperatures from 0 to 600 K and the pressure from 0 to 30 GPa by employing the quasi-harmonic Debye model as implemented in the Gibbs code [66], which is based on the estimation of the Debye temperature by using the following formulas [67]:

$$\theta_D = \frac{\hbar}{K_B}\left[6\pi^2 V^{\frac{1}{2}} r\right]^{\frac{1}{3}} f(\nu)\sqrt{\frac{B_s}{M}} \tag{34}$$

Where V is the molecular volume, M the molecular mass of the compound, k_B is the Boltzman constant and f (ν) the scaling function [68,69], that depends on the Poisson's ratio ν of the isotropic

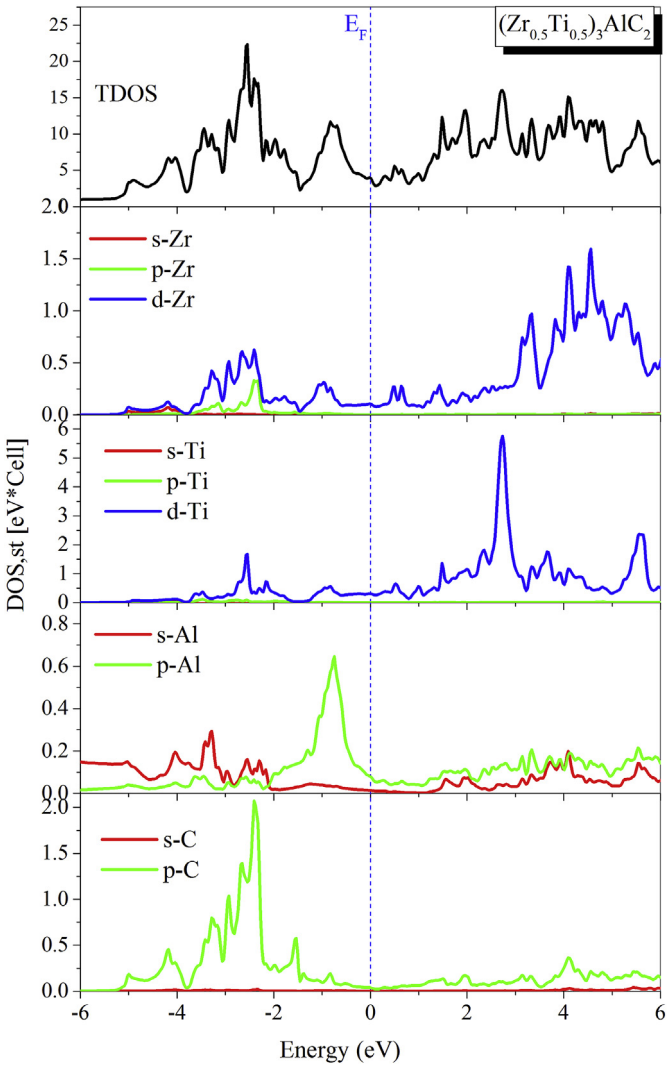

Fig. 6b. The Total and Partial density of states (TDOS, PDOS) of $(Zr_{0.5}Ti_{0.5})_3AlC_2$ compound.

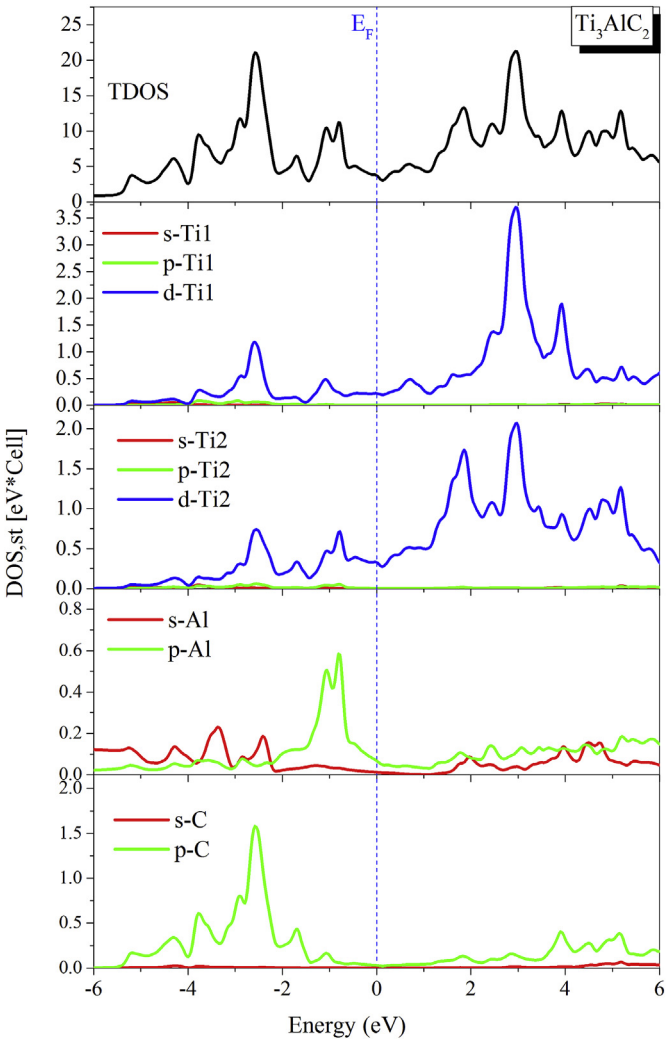

Fig. 6c. The Total and Partial density of states (TDOS, PDOS) of Ti_3AlC_2 compound.

material [70]:

$$f(\nu)=\left\{3\left[2\left(\frac{2}{3}\frac{1+\nu}{1-2\nu}\right)^{\frac{3}{2}}+\left(\frac{1}{3}\frac{1+\nu}{1-\nu}\right)^{\frac{3}{2}}\right]^{-1}\right\}^{\frac{1}{3}} \tag{35}$$

B_s the adiabatic bulk modulus given by the static compressibility:

$$B_s \cong B_{static}=V\left(\frac{d^2E(V)}{dV^2}\right) \tag{36}$$

Where E (V) is the total energy per unit cell for our compounds, determined from the ground-state calculation established in section 3.1. The heat capacity is given by:

$$C_V=3nk_B\left(4D\left(\frac{\theta_D}{T}\right)-\frac{\frac{3\theta_D}{T}}{e^{\frac{\theta_D}{T}}-1}\right) \tag{40}$$

Where $D\left(\frac{\theta_D}{T}\right)$ denote the Debye integral and n is the number of atoms per unit cell.

Table 4
Density (ρ in (g/cm^3), longitudinal, transverse and average sound velocity v_l, v_t and v_m in (Km/s) as well as Debye temperature θ_D in (K) for Zr_3AlC_2, $(Zr_{0.5}Ti_{0.5})_3AlC_2$ and Ti_3AlC_2 compounds.

Composition	ρ	v_l	v_t	v_m	θ_D	Remark
Zr_3AlC_2	5.59	7.29	4.17	4.64	546.8	Calc[a]
	5.61	12.74	4.57	5.19	613	Calc[b]
$(Zr_{0.5}Ti_{0.5})_3AlC_2$	4.93	7.88	4.55	5.05	615.8	Calc[a]
	5.07	14.16	5.14	5.83	718	Calc[b]
Ti_3AlC_2	4.22	9.01	5.31	5.89	749.9	Calc[a]
	4.22	15.48	5.64	6.40	815	Calc[b]

[a] Present work.
[b] Ref. [20].

The calculated Bulk modulus and the Debye temperature of Zr_3AlC_2, $(Zr_{0.5}Ti_{0.5})_3AlC_2$ and Ti_3AlC_2 are displayed in Figs. 7 and 8 (a, b and c), respectively. From these Figures, we can observe that the values of bulk modulus B and Debye temperature θ_D decrease slowly when the temperature increase under constant pressure, but they increase rapidly when the pressure increase under constant temperature for all our compounds. We point out that Debye temperature θ_D and Bulk modulus change similarly for all our compounds.

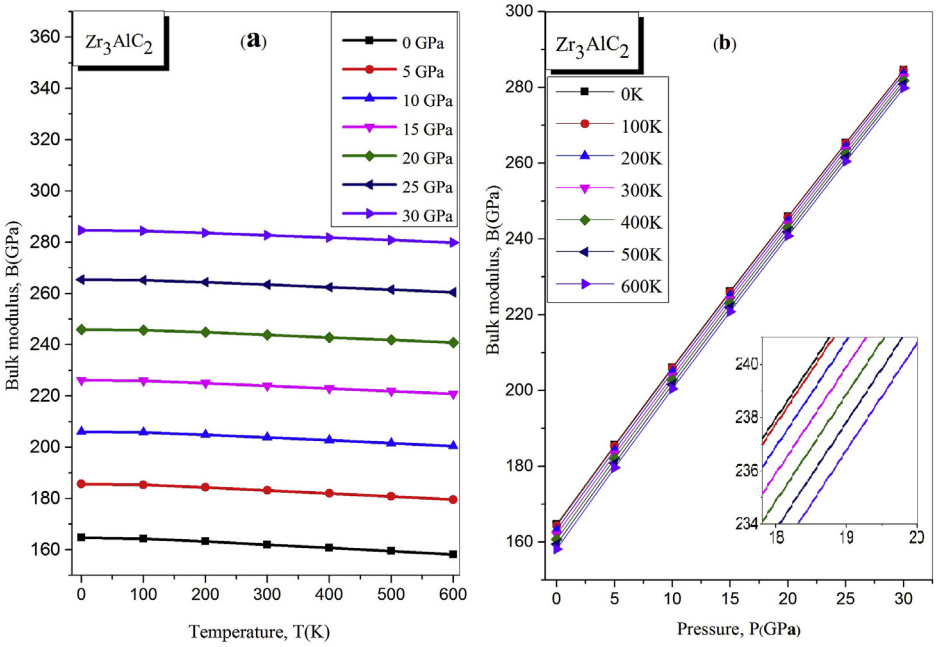

Fig. 7A. The Bulk modulus of Zr_3AlC_2 compound as a function of temperature and pressure.

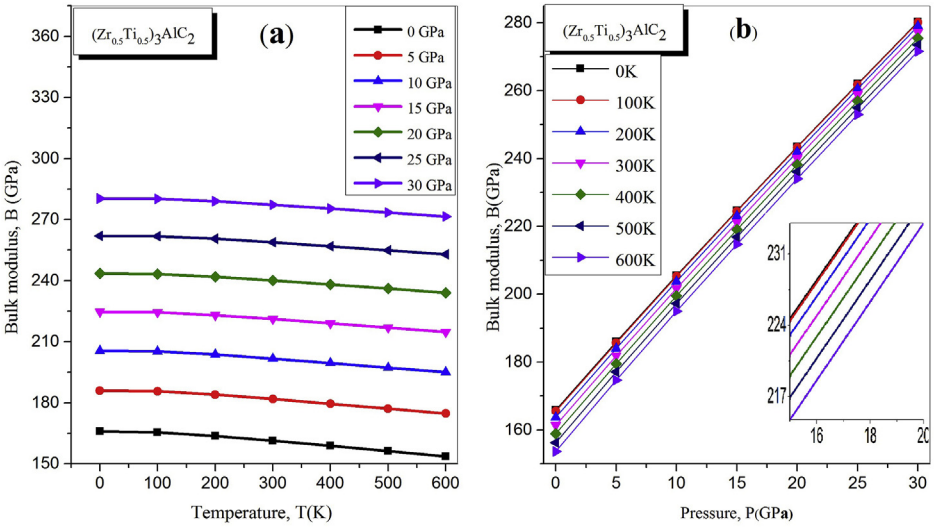

Fig. 7b. The Bulk modulus of $(Zr_{0.5}Ti_{0.5})_3AlC_2$ compound as a function of temperature and pressure.

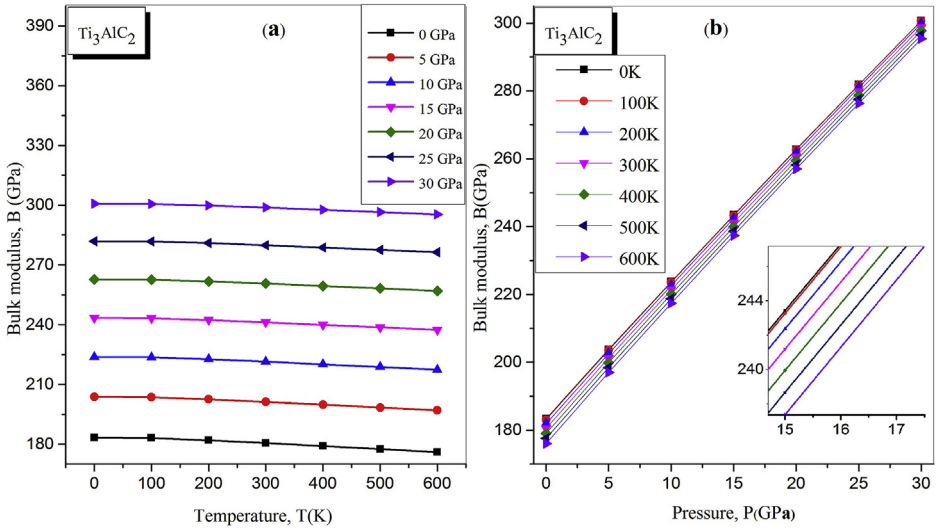

Fig. 7c. The Bulk modulus of Ti_3AlC_2 compound as a function of temperature and pressure.

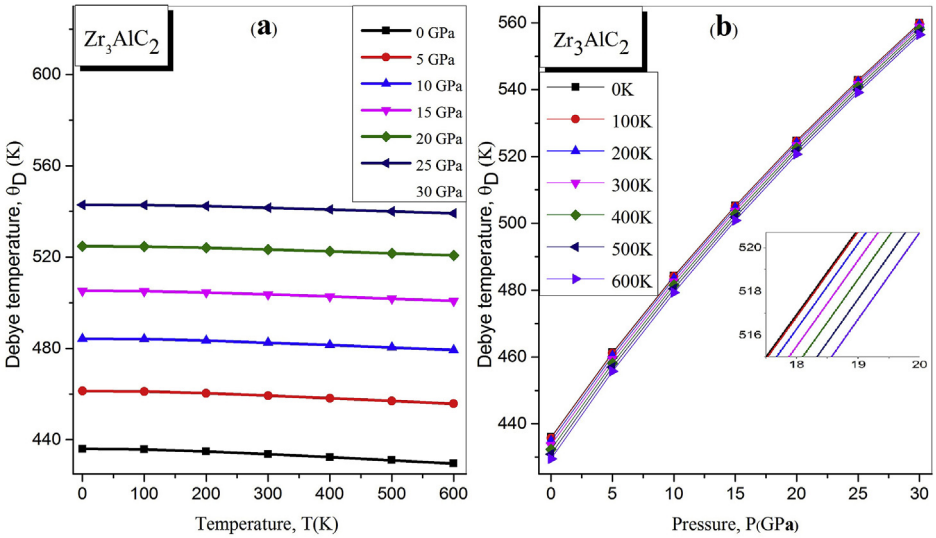

Fig. 8A. The Debye temperature of Zr_3AlC_2 compound as a function of temperature and pressure.

The heat capacity C_p and C_v are also investigated under the pressure and temperature changes. Figs. 9 and 10 (a, b and c)show the variation of the heat capacity C_p and C_v of Zr_3AlC_2 $(Zr_{0.5}Ti_{0.5})_3AlC_2$ and Ti_3AlC_2 as a function of temperature and pressure, respectively. We can note from these figures that the C_p and C_v values for all our compounds increase rapidly with increasing temperature when the temperature is inferior than 200K and continue to increase weakly as the temperature rises. The values of C_p and C_v decrease slowly when the pressure increases under a constant temperature for all of our compounds except when the temperature equals zero where all the values of C_p and C_v remain zero.

4. Conclusion

In summary, we have presented a report on the structural, electronic, mechanical and the thermodynamic properties of the MAX phases (Zr1-xTix)3AlC2 compounds by means of the ab-*initio* plane-wave (FP-LAPW) method. The equilibrium properties were calculated and compared with others work. The lattice constants a and c as function of pressure were evaluated. We found that, the compression along the (a,c)-axis decreases with linear dependence when the pressure increase. The results of the formation energy show that, the examined compounds are quite stable even at high temperatures. The obtained independent elastic constants confirm the stability of the $(Zr_{1-x}Ti_x)_3AlC_2$ compounds against any elastic deformation. The bulk modulus, shear modulus, Young's modulus E, Poisson's ratio, Cauchy pressure and Vickers hardness are calculated. The chemical bonding between the nearest neighbor atoms which is dominant is the ionic for Zr_3AlC_2, mixed ionic-covalent for $(Zr_{0.5}Ti_{0.5})_3AlC_2$ and covalent for Ti_3AlC_2. Also, all these compounds present a brittle nature and anisotropy behavior. The Hardness calculation show that, the Ti_3AlC_2 is harder than $(Zr_{0.5}Ti_{0.5})_3AlC_2$ and Zr_3AlC_2 compounds. Sine all the electronic

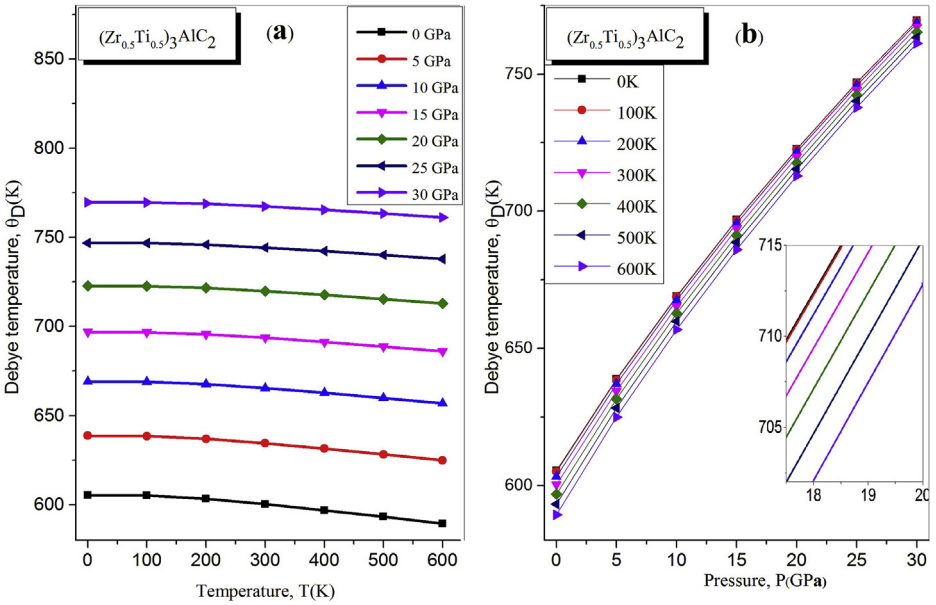

Fig. 8b. The Debye temperature of $(Zr_{0.5}Ti_{0.5})_3AlC_2$ compound as a function of temperature and pressure.

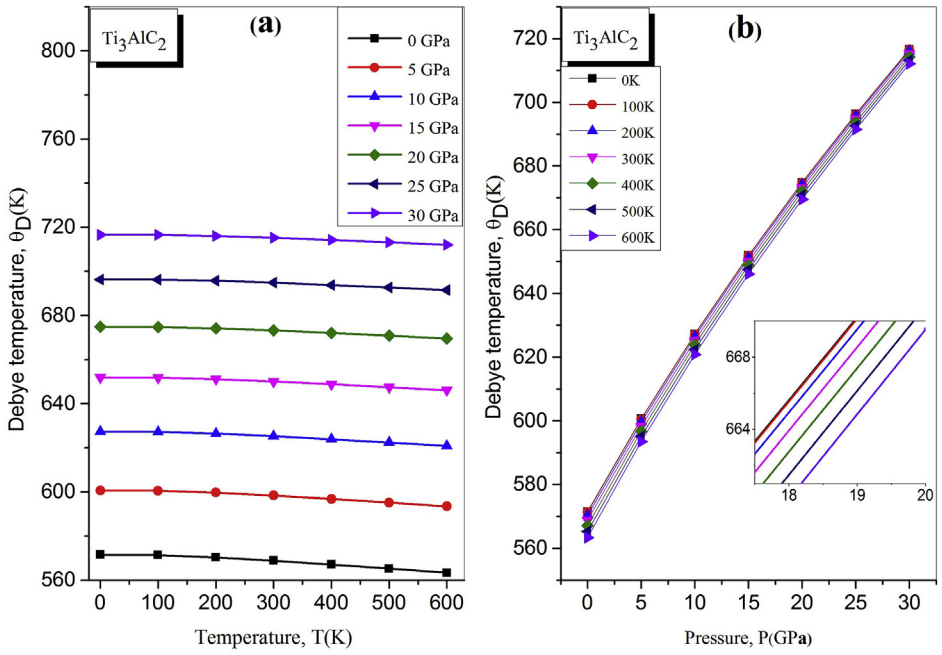

Fig. 8c. The Debye temperature of Ti_3AlC_2 compound as a function of temperature and pressure.

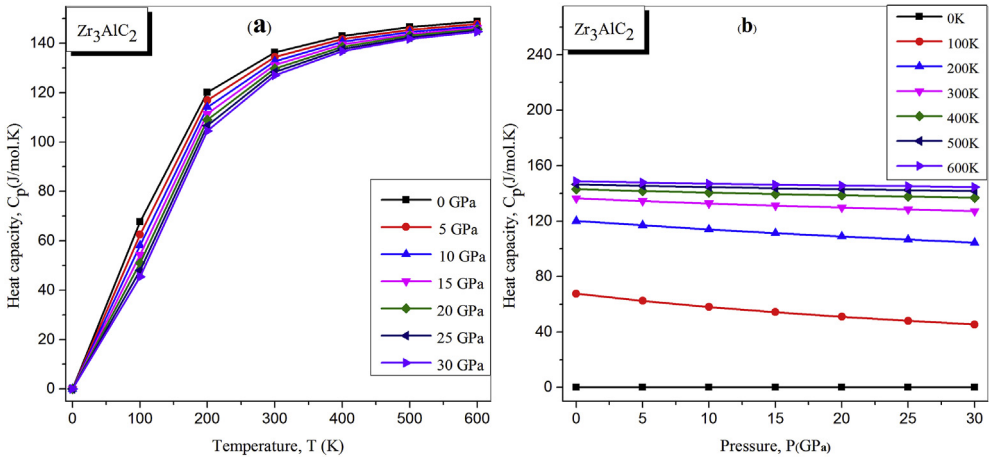

Fig. 9A. The Heat capacity Cp of Zr_3AlC_2 compound as a function of temperature and pressure.

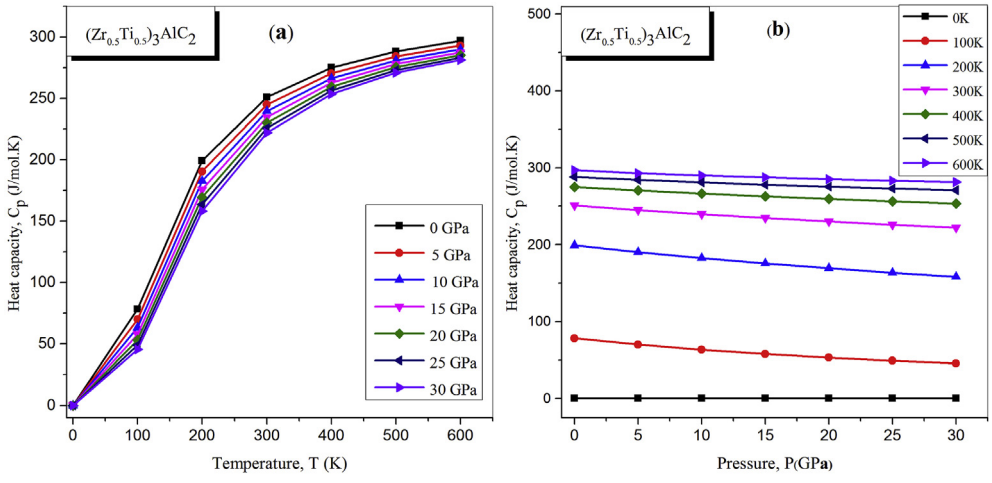

Fig. 9b. The Heat capacity Cp of $(Zr_{0.5}Ti_{0.5})_3AlC_2$ compound as a function of temperature and pressure.

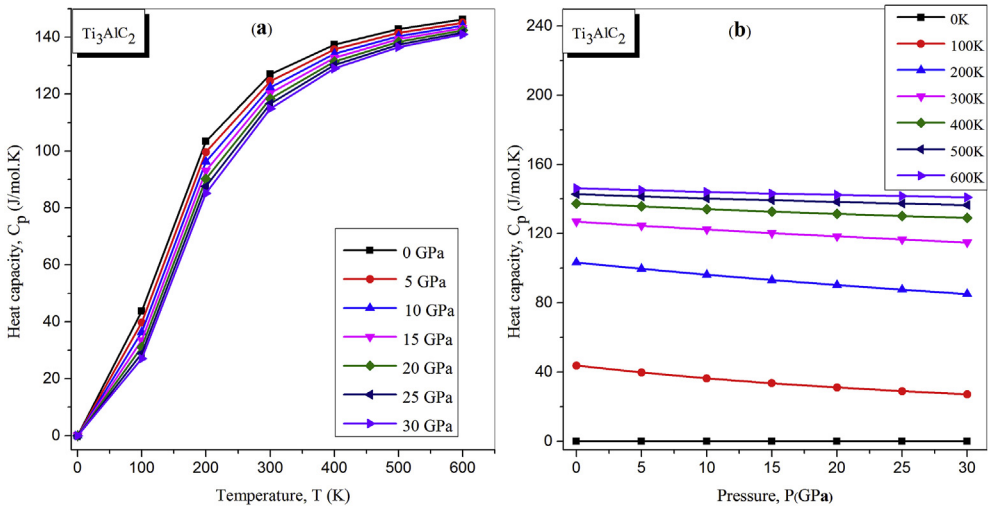

Fig. 9c. The Heat capacity Cp of Ti_3AlC_2 compound as a function of temperature and pressure.

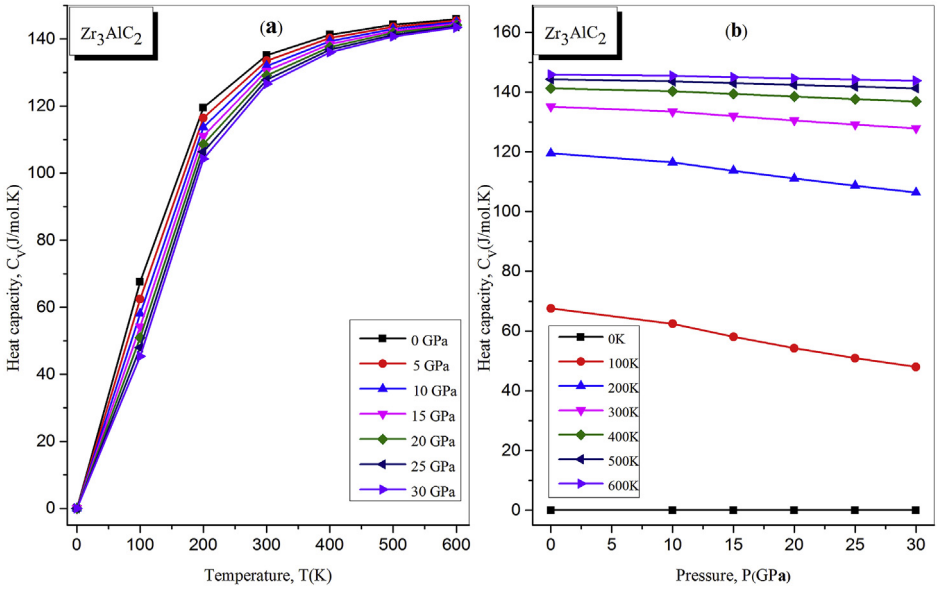

Fig. 10A. The Heat capacity Cv of Zr_3AlC_2 compound as a function of temperature and pressure.

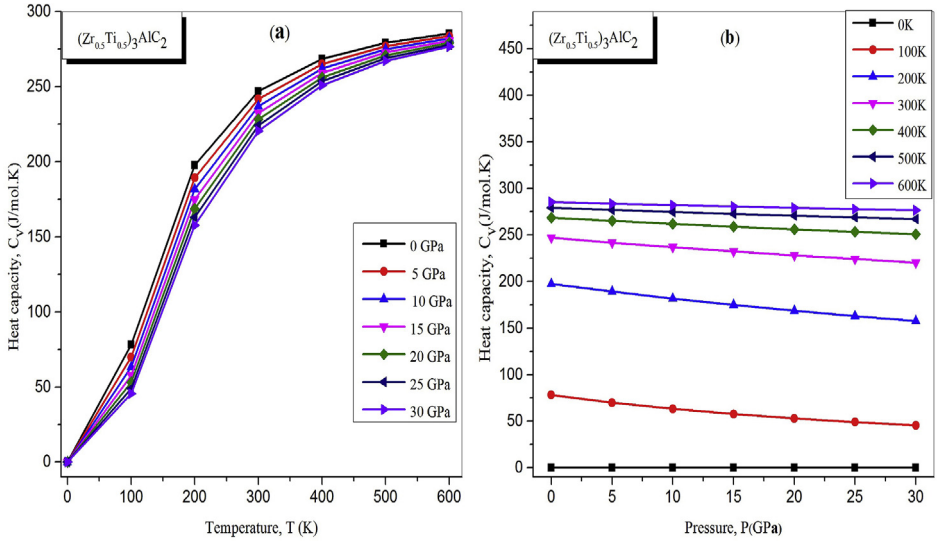

Fig. 10b. The Heat capacity Cv of $(Zr_{0.5}Ti_{0.5})_3AlC_2$ compound as a function of temperature and pressure.

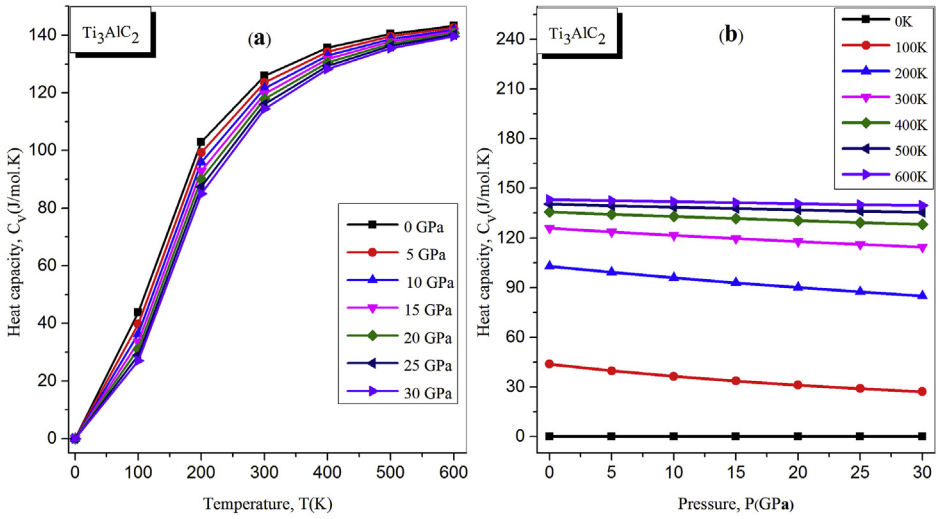

Fig. 10c. The Heat capacity Cv of Ti_3AlC_2 compound as a function of temperature and pressure.

structure haven't band gap at Fermi level so the studied compounds show a metallic behavior. The TDOS and PDOS curves reveal the existence of *p-d* and *s-p* hybridization. Finally, by the quasi-harmonic Debye model we have calculated the variation of the bulk modulus, Debye temperature and heat capacity as function of temperature and pressure. The bulk modulus and the Debye temperature in each compound increase significantly with increasing pressure and decrease slowly with increasing temperature. Conversely, the heat capacity increases with increasing temperature and slightly decreasing with increasing temperature.

Declaration of competing interest

The authors declare that they have no known competing financial interests or personal relationships that could have appeared to influence the work reported in this paper.

References

[1] M.W. Barsoum, M. Radovic, Annu. Rev. Mater. Res. 41 (2011) 195–227.
[2] W. Jeitschko, H. Nowotny, F. Benesovsky, Monatsh. Chem. 94 (1963) 1201.
[3] H. Nowotny, Prog. Solid State Chem. 2 (1970) 27.
[4] M.W. Barsoum, L. Farber, I. Levin, A. Procopio, T. El-Raghy, A. Berner, American Ceramic Society 82 (1999) 2545–2547.
[5] C. Hu, F. Li, J. Zhang, J. Wang, J. Wang, Y. Zhou, Scripta Mater. 57 (2007) 893–896.
[6] M.W. Barsoum, T. El-Raghy, Am. Sci. 89 (2001) 334–343.
[7] H. Yoo, M.W. Barsoum, T. El-Raghy, Nature 407 (2000) 581.
[8] T. Lapauw, J. Halimc, J. Lu, T. Cabioc'h, L. Hultman, M.W. Barsoum, K. Lambrinou, J. Vleugels, Euro. Ceram. Soc 36 (2016) 943.
[9] E. Zapata-Solvas, S.-R.G. Christopoulos, N. Ni, D.C. Parfitt, D. Horlait, M.E. Fitzpatrick, A. Chroneos, W.E. Lee, J. Am. Ceram. Soc. 100 (2017) 1377.
[10] T. El-Raghy, M.W. Barsoum, A. Zavaliangos, S.R. Kolidindi, J. Am. Ceram. Soc. 82 (1999) 2855.
[11] M.W. Barsoum, L. Farber, T. El-Raghy, Metall. Mater. Trans. 30 (1999) 1727.
[12] D. Tallman, Acta Mater. 85 (2014) 132.
[13] Gokhan Surucua, Aytac Erkisi, Mater. Res. Express 4 (2017), 106520.
[14] Gokhan Surucu, Aysenur Gencer, Xiaotian Wang, Ozge Surucu, J. Alloys Compd. 819 (2020), 153256.
[15] Aysenur Gencera, Gokhan Surucu, Mater. Res. Express 5 (2018), 076303.
[16] Surucu Gokhan, Colakoglu Kemal, Deligoz Engin, Korozlu Nurettin, J. Electron. Mater. 45 (2016) 4256–4264.
[17] Gokhan Surucu, Aytac Erkisi, BORON 3 (2018) 24–32.
[18] Gokhan Surucu, Mater. Chem. Phys. 203 (2018) 106–117.
[19] M.A. Hadi, Y. Panayiotatos, A. Chroneos, J. Mater. Sci. Mater. Electron. 28 (2016) 3386–3393.
[20] M.A. Hadi, M. Roknuzzaman, A. Chroneos, S.H. Naqib, A.K.M.A. Islam, R.V. Vovk, K. Ostrikov, Comput. Mater. Sci. 137 (2017) 318.
[21] P. Hohenberg, W. Kohn, Phys. Rev. B 136 (1964) 864.
[22] W. Kohn, L.S. Sham, Phys. Rev. 140 (1965) 113.
[23] J.C. Slater, Adv. Quant. Chem. 1 (1994) 5564.
[24] P. Blaha, K. Schwarz, G.K.H. Madsen, D. Kvasnicka, J. Luitz, WIEN2K, an Augmented Plane Wave +Local Orbitals Program for Calculating Crystal Properties, 2001, ISBN 3-9501031-1-2.
[25] S. Aouimer, M. Ameri, D. Bensaid, N.E. Moulay, A.Z. Bouyakoub, F.Z. Boufadi, I. Ameri, Y. Al-Douri, Acta Phys. Pol. 136 N°1 (2019) 127–134.
[26] A. Bouhemadou, D. Allali, K. Boudiaf, B. Al Qarni, S. Bin-Omran, R. Khenata, Y. Al Douri, J. Alloys Compd. 774 (2019) 299–314.
[27] Friha Khelfaoui, Mohammed Ameri, Djillali Bensaid, Ibrahim Ameri, Yarub Al-Douri, J. Supercond. Nov. Magnetism 31 (2018) 3183–3192.
[28] M.H. Benkabou, M. Harmel, A. Haddou, A. Yakoubi, N. Baki, R. Ahmed, Y. Al-Douri, S.V. Syrotyuk, H. Khachai, R. Khenata, C.H. Voon, Mohd Rafie Johan, Chin. J. Phys. 56 (2018) 131–144.
[29] Z. Souadia, A. Bouhemadou, O. Boudrifa, S. Bin-Omran, R. Khenata, Y. Al Douri, High Pres. Res. 37 (Issue 4) (2017) 558–578.
[30] Kada Bidai, Mohammed Ameri, Slamani Amel, Ibrahim Ameri, Y. Al-Douri, Dinesh Varshney, C.H. Voon, Chin. J. Phys. 55 (Issue 5) (2017) 2144–2155.
[31] K. Bidai, M. Ameri, I. Ameri, D. Bensaid, A. Slamani, A. Zaoui, Y. Al-Douri, Arch. Metall. Mater. 62 (N° 2) (2017) 865–871.
[32] Nadjia Tayebi, Kada Bidai, Mohammed Ameri, Slamani Amel, Ibrahim Ameri, Y. Al-Douri, Dinesh Varshney, Chin. J. Phys. 55 (2017) 769–779.
[33] A. Bennadji, M. Ameri, D. Hachemane, Y. Al-Douri, I. Ameri, D. Varshney, C.H. Voon, Chin. J. Phys. 55 (2017) 386–399.
[34] Kada Bidai, Mohammed Ameri, Zaoui Ali, Ibrahim Ameri, Yarub Al-Douri, Chin. J. Phys. 54 (2016) 678–694.
[35] Mohammed Ameri, Faiza Bennar, Slamani Amel, Ibrahim Ameri, Y. Al-Douri, Dinesh Varshney, Phase Transitions 89 (2016) 1236–1252.
[36] Samir Mustapha Laoufi, Amina Touia, Mohammed Ameri, Ibrahim Ameri, Fatima Boufadi, Keltouma Boudia, Amel Slamani, Fadila Belkharroubi, Y. Al-Douri, Optik 127 (2016) 7382–7393.
[37] A. Benkabou, H. Bouafia, B. Sahli, B. Abidri, M. Ameri, S. Hiadsi, D. Rached, B. Bouhafs, N. Benkhettou, Y. Al-Douri, Chin. J. Phys. 54 (2016) 33–41.
[38] Kada Bidai, Mohammed Ameri, Djillali Bensaid, Slamani Amel, Ibrahim Ameri, Y. Al-Douri, Optik 127 (2016) 5155–5162.
[39] Nadhira Bioud, Optik 127 (2016) 4559–4573.
[40] S. Daho, M. Ameri, Y. Al Douri, D. Bensaid, D. Varshney, I. Ameri, Mater. Sci. Semicond. Process. 41 (2016) 102–108.
[41] A. Reggad, R. Lardjani, R. Baghdad, B. Bouhafs, Physica B 526 (2017) 89–95.
[42] J.P. Perdew, K. Burke, M. Ernzerhof, Phys. Rev. Lett. 77 (1996) 3865.
[43] S. Berri, D. Maouche, F. Zerarga, Y. Medkour, Physica B 407 (2012) 3328–3334.
[44] M. Pietzka, J. Schuster, J. Phase Equil. 15 (1994) 392.
[45] 2Doptimize Package Is provided by M. Jamal as Part of the Commercial Code WIEN2K. http://www.wien2k.at/.
[46] Gokhan Surucu, Cagil Kaderoglu, Engin Deligoz, Haci Ozisik, Mater. Chem. Phys. 189 (2017) 90–95.
[47] A.H. Reshak, Moreteza jamal, Int. J. Electrochem. Sci. 8 (2013) 12252–12263.
[48] E. Zapata, M.A. Hadi, D. Horlait, D.C. Parfitt, A. Thibaud, A. Chroneos, W.E. Lee, J. Am. Ceram. Soc. 100 (2017) 3393–3401.
[49] H. Rached, D. Rached, S. Benalia, A.H. Reshak, M. Rabah, R. Khenata, S. Bin Omran, Mater. Chem. Phys. 143 (2013) 93–108.
[50] J. Wang, J. Wang, Y. Zhou, C. Hu, Acta Mater. 56 (2008) 1511–1518.
[51] R. Hill, Proc. Phys. Soc. 65 (1952) 349–354.
[52] W. Voigt, Leipzig: Teubner, 1928, pp. 95–100.
[53] A. Reuss, Z. Angew. Math. Mech. 9 (1929) 49–58.
[54] X. TaO, J. Yang, L. Xi, Y. Ouyang, J. Solid State Chem. 194 (2012) 179–187.
[55] Y. Tu, Y. Wang, Solid State Commun. 151 (2011) 238–241.

[56] A. Yildirim, H. Koc, E. Deligoz, Chin. Phys. B 21 (2012), 037101.
[57] M. Jamal, N. Kamali Sarvestani, A. Yazdani, A.H. Reshak, RSC Adv. 4 (2014) 57903–57915.
[58] G. Vaitheeswaran, V. Kanchana, A. Svane, A. Delin, J. Phys. Condens. Matter 19 (2007), 326214.
[59] S.F. Pugh, Phil. Mag. 45 (1954) 823.
[60] H.M. Ledbetter, J. Phys. Chem. 6 (1977) 1181.
[61] Z.E. Biskri, H. Rached, M. Bouchear, D. Rached, J. Mech, Behav. Biomed. Mater 32 (2014) 345–350.
[62] A.L. Ding, C.M. Li, J. Wang, J. Ao, Z.-Q. Chen, Chin. Phys. B 23 (2014), 096201.
[63] X.Q. Chen, H. Niu, D. Li, Y. Li, Intermetallics 19 (2011) 1275–1281.
[64] M.H. Elahmar, H. Rached, D. Rached, R. Khenata, G. Murtaza, S. Bin Omran, W.K. Ahmed, J. Magn. Magn Mater. 393 (2015) 165–174.
[65] M. Benkabou, H. Rached, A. Abdellaoui, D. Rached, R. Khenata, M.H. Elahmar, B. Abidri, N. Benkhettou, S. Bin-Omran, J. Alloys Compd. 647 (2015) 276–286.
[66] M.A. Blanco, E. Francisco, V. Luaña, Comput. Phys. Commun. 158 (2004) 57.
[67] A.G. McLellan, The Classical Thermodynamics of Deformable Materials, vol. 165, Cambridge University Press, Cambridge, 1980.
[68] E. Francisco, J.M. Recio, M.A. Blanco, A. Martín Pendás, J. Phys. Chem. 102 (1998) 1595.
[69] E. Francisco, G. Sanjurjo, M.A. Blanco, Phys. Rev. B 63 (2001), 094107.
[70] J.P. Poirier, Introduction to the Physics of the Earth's Interior, Cambridge University Press, 1991.

Materials Chemistry and Physics 260 (2021) 124189

Contents lists available at ScienceDirect

Materials Chemistry and Physics

journal homepage: www.elsevier.com/locate/matchemphys

The Vanadium-doping effect on physical properties of the Zr_2AlC MAX phase compound

Ahmed Azzouz-Rached [a,c], Habib Rached [a,b,*], Ismail Ouadha [b], Djamel Rached [b], Abderrahmane Reggad [d]

[a] Department of Physics, Faculty of Exact Sciences and Informatics, Hassiba Benbouali University of Chlef, Algeria
[b] Magnetic Materials Laboratory, Faculty of Exact Sciences, Djillali Liabes University of Sidi Bel-Abbes, Algeria
[c] Laboratory for Theoretical Physics and Material Physics, Department of Physics, Faculty of Exact Sciences and Informatics, Hassiba Benbouali University of Chlef, Algeria
[d] C2MO, Engineering Physics Laboratory, Faculty of Matter Sciences, Ibn Khaldoun University, Tiaret, Algeria

HIGHLIGHTS

- Based on the first-principle calculation, the V-doped Zr_2AlC compounds have been investigated.
- The elastic stabilities reveal that these compounds are stable against any elastic deformations.
- The mechanical properties class the studied compounds as Brittle, Stiff and hard materials.
- The electronic structure analysis divulge that all our compounds exhibit a metallic behavior with strong *p-d* hybridization.

ARTICLE INFO

Keywords:
First-principle calculations
Transition metal
MAX Phases compounds
Mechanical properties
Thermodynamic properties

ABSTRACT

The Vanadium substitutions effect on physical properties of Zr_2AlC MAX phase compounds have been studied using the first-principle method. The equilibrium ground states of properties were calculated and compared with available experimental, and theoretical data. The formation energy has been calculated in order to evaluate the stability of our compounds especially which are un-synthesized ones yet. The elastic constants are calculated by the Hex-elastic package and revealed that our compounds are mechanically stable. The obtained elastic modulus and anisotropy factor divulged that the compressibility along the a-axis is stronger than that along the c-axis. All the studied materials represent a strong elastic anisotropy. The macroscopic mechanical properties class the compounds as brittle, stiff, and hard materials. The electronic structure indicated that, all our compounds exhibit a metallic behavior, and this metallicity is due to the strong *p-d* covalent bonding. Furthermore, the effect of temperature, and pressure on the heat capacity, Debye's temperature, entropy, and the volume at ambient condition are calculated by the quasi-harmonic Debye model. It is important to emphasis that, the investigated properties of the quaternary MAX phase compounds have not been calculated. Therefore, our results can be considered as a first quantitative theoretical prediction.

1. Introduction

In the latest years, an extraordinary development has been made by way of the manner of chemists, physicists, and technologists to examine, and to develop new substances among them the MAX phase [1]. Recently, a good number of MAX phases have been theoretically, and experimentally investigated due to their properties which combine metallic, and ceramic behaviors [2,3], and also for their good mechanical properties at high temperatures [4]. The MAX phase materials are known to enter into many industrial applications for their desirable property [5], such as in aerospace, automotive, defense, medical, and nuclear reactors [6–8].

Generally, these classes of materials crystallize in hexagonal structure with a stoichiometric composition (which is the general formula of type-structure) is $M_{n+1}AX_n$ (where M is an early transition metal, A is an element from group III-A, and IV-A, X is either C or N and n = 1, 2 and 3)

* Corresponding author. Department of Physics, Faculty of Exact Sciences and Informatics, Hassiba Benbouali University of Chlef, Algeria.
E-mail address: habib_rached@yahoo.fr (H. Rached).

https://doi.org/10.1016/j.matchemphys.2020.124189
Received 3 April 2020; Received in revised form 11 September 2020; Accepted 20 December 2020
Available online 23 December 2020

[2,9]. There was no interest in this phase until 1996, with the first publication of Barsoum's [10]. Thereafter, a large range of these compounds are investigated. It was found that, they present many points in common for the corresponding carbides, and nitrides at the level of the thermal, elastic, and electric [6,11]. However, the mechanical properties are extremely different, they are mechanically stable with lower hardness values, and resist to thermal shocks. It's certainly a tenacious material, having a terrific and excessive resistance to temperature [12]. A. Bouhemadou et al. [13], studied using the pseudo-potential plane--waves method the effect of high pressures, up to 20 GPa, on the structural, and elastic properties of Zr_2AlX and Ti_2AlX, with (X = C and N). By the full-potential plane-wave method Yakoubi et al. [9], investigated the ground states properties, and the electronic structure of Zr_2AlX (X = C and N) compounds. Yakoubi demonstrated that, strength and electrical properties in these materials are principally governed by the metallic planes. The $Zr_2(Al_{0.58}Bi_{0.42})C$, $Zr_2(Al_{0.2}Sn_{0.8})C$, and $Zr_2(Al_{0.3}Sb_{0.7})C$ MAX nanolaminates have been studied by using the pseudo potential plane-wave PP-PW method in order to evaluate their structural, elastic, and electronic properties [4]. Mahbuba Roksana Khatun et al. [14], reported on the Mulliken bond population, Vickers hardness, thermodynamic, and optical properties of MAX phases V_2AC (A = Al, Ga). Khatun revealed that these compounds could be good candidate materials to reduce solar heating up to ~15 eV.

In order to widen previous theoretical, and experimental works on Zr_2AlC and V_2AlC compounds and enriched literature for the first time by new quaternary MAX phase $(Zr_{1-x}Vx)_2AlC$ in the objective to propose new materials that have not been studied before and which may have an extraordinary properties. For this purpose, we have studied the effect of Vanadium atom substitution for Zirconium based MAX-phase Zr_2AlC on the structural, electronic, mechanical, and thermodynamic properties.

2. Computational method

The calculations were done by using the full potential linearized augmented plane waves within the density functional theory (DFT) and implemented in the Wien2k code [15,16]. The local density approximation (LDA) parameterized by Perdew and Wang [17] was considered for exchange and correlation potentials V_{XC}. We reported in Table 1 all the parameters used in the calculations for the $(Zr_{1-x}Vx)_2AlC$ compounds such as the convergence parameter $R_{MT} \times K_{max}$ which controlling the size of the basis sets (where K_{max} is the maximum reciprocal lattice vector, and R_{MT} is the smallest muffin-tin radius), the magnitude of the largest vector responsible in the Fourier expansion of density G_{max}, and the number of special k-points in the Irreducible first Brillouin zone IBZ. The self-consistent calculation cycle (SCF) is performed iteratively until convergence energy 0.00001 is reached. The muffin-tin (MT) sphere was considered up to $l_{max} = 10$. The Monkorst-Pack method in the Irreducible first Brillouin Zone (IBZ) was performed in this work [18].

The crystal structures of $(Zr_{1-x}V_x)_2AlC$ are hexagonal type with space group P63/mmc (#194). The C atoms occupied the positions:

$$\left((0;0;0)\ and\ \left(0;0;\frac{1}{2}\right)\right)$$

The Al atoms occupied the positions:

$$\left(\left(\frac{1}{3};\ \frac{2}{3};\ \frac{3}{4}\right)\ \text{and}\ \left(\frac{2}{3};\ \frac{1}{3};\ \frac{1}{4}\right)\right)$$

While the Zr atoms occupied the positions:

$$\left(\left(\frac{1}{3};\ \frac{2}{3};\ z\right),\ \left(\frac{2}{3};\ \frac{1}{3};\ z+\frac{1}{2}\right),\ \left(\frac{2}{3};\ \frac{1}{3};\ -z\right)\ and\ \left(\frac{1}{3};\ \frac{2}{3};\ -z+\frac{1}{2}\right)\right)$$

Where z is the free internal parameter. The crystalline structures of the compounds are shown in Fig. 1.

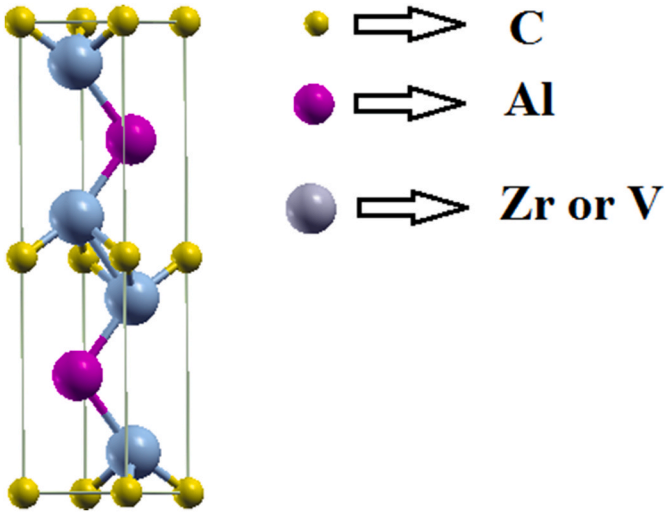

Fig. 1. The crystal structure of the $(Zr_{1-x}V_x)_2AlC$ MAX phase compounds.

Table 1
The parameters used during the calculation for $(Zr_{1-x}V_x)_2AlC$ compounds.

Compounds	$R_{MT} \times K_{max}$	G_{max}	Electronic configuration	R_{MT}	k-point	Separation Energy (Rydberg)
Zr_2AlC	9	15	Zr:[Kr]$5s^2 4d^2$ Al:[Ne]$3s^2 3p^3$ C:[He]$2s^2 2p^2$	Zr: 2.09 Al: 2.32 C: 1.71	230	−6
$(Zr_{0.75}V_{0.25})_2AlC$	9	14	Zr:[Kr]$5s^2 4d^2$ V:[Ar] $4s^2 3d^3$ Al:[Ne]$3s^2 3p^3$ C:[He]$2s^2 2p^2$	Zr: 2.05 V:2.05 Al: 2.37 C:1.68	200	−8
$(Zr_{0.50}V_{0.50})_2AlC$	9	14	Zr:[Kr]$5s^2 4d^2$ V:[Ar] $4s^2 3d^3$ Al:[Ne]$3s^2 3p^3$ C:[He]$2s^2 2p^2$	Zr:1.99 V:1.99 Al:2.31 C:1.63	200	−8
$(Zr_{0.25}V_{0.75})_2AlC$	9	14	Zr:[Kr]$5s^2 4d^2$ V:[Ar] $4s^2 3d^3$ Al:[Ne]$3s^2 3p^3$ C:[He]$2s^2 2p^2$	Zr:1.98 V:1.98 Al:2.27 C:1.62	200	−8
V_2AlC	9	15	V:[Ar] $4s^2 3d^3$ Al:[Ne]$3s^2 3p^3$ C:[He]$2s^2 2p^2$	V:1.43 Al:2.04 C:1.75	200	−6

3. Results and discussions

3.1. Ground states properties

To calculate the ground-states equilibrium of properties we started by doing the relaxation of all the structure in order to optimize the internal parameter in the first step. Secondly, we calculated the geometric optimization of the compounds by using the 2D-optimize package developed by Jamal Morteza [19] and fitted them by the Birch-Murnaghan's equation of states [20].

The results of lattice constants (a, c), the internal parameter (z), the bulk modulus (B_0), and its pressure derivative (B') with LDA approximations are reported with some other experimental, and theoretical results in Table 2. Through these results, we found that the results are in reasonable agreement with all other works reported for the ternary compounds. In order to evaluate the stability of the compounds especially, un-synthesized ones, we calculated the formation enthalpy by using the following equation [21,22]:

$$\Delta E_{f\,(Zr_{1-x}V_x)_2AlC} = E_{tot\,(Zr_{1-x}V_x)_2AlC} - (2(1-x)E_{Zr} + 2xE_V + E_{Al} + E_C) \quad (1)$$

Where $\Delta E_{f\,(Zr_{1-x}V_x)_2AlC}$ is the formation enthalpy of $(Zr_{1-x}V_x)_2AlC$, E_{tot} is the total energy per unit cell of the bulk compounds, $E(X = Zr, V, Al$ and $C)$; it represents the total energy per atom of the element in pure solid state, and x is the V-doped concentration ($x = 0, 0.25, 0.5, 0.75$ and 1.0). The values obtained of the formation enthalpy are -0.637 eV, -0.550 eV, -0.401 eV, -0.419 eV, and -0.587 eV for Zr_2AlC, $(Zr_{0.75}V_{0.25})_2AlC$, $(Zr_{0.50}V_{0.50})_2AlC$, $(Zr_{0.25}V_{0.75})_2AlC$, and V_2AlC, respectively. All the formation enthalpies are negative, which indicates that the examined compounds are quite stable even at high temperatures. Fig. 2 shows the variation of the lattice parameter as a function of V-doped concentration (x). From this figure, we observe that, an increase in V concentration of the quaternary compound leads to a decrease in lattice parameter. We can interpret that by the atomic radius difference between Zr and V. From the results of the bulk modulus, we observe an increase in compressibility module with the increase of the V concentration, which means that the quaternary compound becomes less compressible, and less resistant to fracture when the V concentration increases. Fig. 3 reports the variation of minimum energy as a function of V concentration x for $(Zr_{1-x}V_x)_2AlC$. We note that, an increase of the V concentration of the quaternary compound leads to an increase in the minimum energy. This increase could be due to the electronegativity difference between Zr, and V. According to our research; there are no experimental or theoretical results about the quaternary compounds. This strongly confirms that the calculations, for the investigated quaternary compounds, reported here are new.

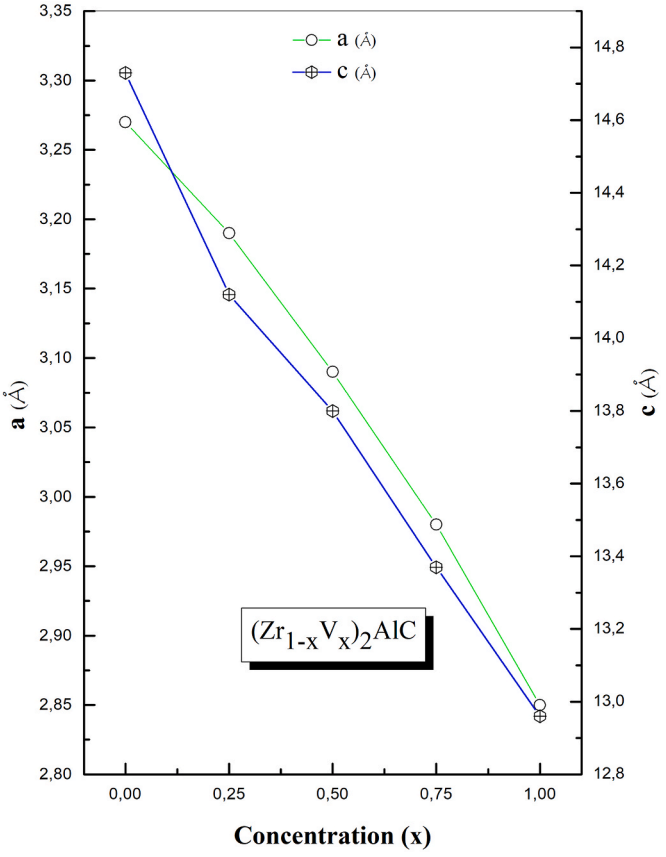

Fig. 2. The lattice parameter variation as a function of V-doped concentration (x).

3.2. Mechanical properties

3.2.1. Elastic constants

Hook's law is recognized as a linear relationship between stress σ_{ij}, strain tensor ε_{kl}, and elastic constants C_{ijkl}.

$$\sigma_{ij} = C_{ijkl}\,\varepsilon_{kl} \quad (2)$$

Table 2
The lattice parameters (a(Å) and c(Å)), bulk modulus B (**GPa**), pressure derivative of the bulk modulus (B') and internal parameter z (Zr, V) for $(Zr_{1-x}V_x)_2AlC$ compounds.

Compounds	Method	Source	a (Å)	c (Å)	B (GPa)	B′	z (Zr, V)
Zr_2AlC	FP-LAPW LDA	Our work	**3.27**	**14.73**	**161.727**	**3.481**	**0.081**
	CASTEP PP-PW	[13]	**3.26899**	**14.40815**	**134**	**3.89**	**0.08646**
	Experimental XRD	[1]	**3.3237**	**14.5705**	-	-	**0.0871**
	Experimental SAED		**3.3**	**14.6**	-	-	-
	Experimental NPD		**3.3239**	**14.556**	-	-	**0.0898**
	FP-LAPW LDA	[9]	**3.2104**	**14.246**	**176.28**	**4.04**	**0.0869**
	CASTEP PP-PW	[24]	**3.3174**	**14.6304**	**124.04**	**4.0836**	**0.0861**
	CASTEP PP-PW	[25]	**3.319**	**14.6045**	-	-	-
	CASTEP PP-PW	[4]	**3.319**	**14.604**			**0.0864**
$(Zr_{0.75}V_{0.25})_2AlC$	FP-LAPW LDA	Our work	**3.1874**	**14.118**	**168.4347**	**3.6357**	-
$(Zr_{0.50}V_{0.50})_2AlC$	FP-LAPW LDA	Our work	**3.0936**	**13.801**	**177.0276**	**4.1425**	-
$(Zr_{0.25}V_{0.75})_2AlC$	FP-LAPW LDA	Our work	**2.9781**	**13.370**	**196.3967**	**3.8083**	-
V_2AlC	FP-LAPW LDA	Our work	**2.8499**	**12.955**	**230.2683**	**3.9130**	**0.0861**
	GGA-PW-PP	[26]	**2.895**	**13.015**	-	-	-
	GGA-PAW	[27]	**2.95**	**13.29**	**197**	**4.12**	**0.083**
	Experimental	[28]	**2.909**	**13.12**	-	-	-
	Experimental	[29]	**2.91**	**13.13**	-	-	**0.086**
	Experimental	[30]	**2.91**	**13.17**	-	-	-
	CASTEP PP-PW	[14]	**2.907**	**13.147**	-	-	-

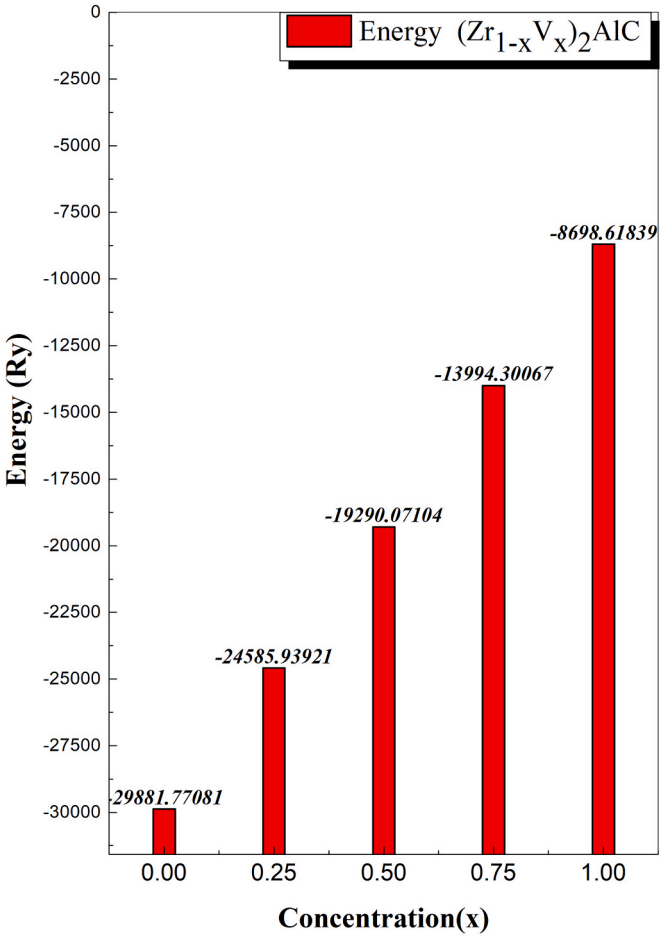

Fig. 3. The minimum energy (**Ry**) variation as a function of V-doped concentration (x).

Using this law we can specify five independent elastic constants C_{ij} for the hexagonal symmetry, namely C_{ij} in addition to the sixth one expressed by:

$$C_{66} = \frac{1}{2}(C_{11} - C_{12}) \tag{3}$$

To determine the elastic constants of the compounds at their equilibrium lattice constants we used the Hex-elastic package established by Jamal Morteza [23]. From this package the elastic constants are derived by means of a Taylor expansion of the total energy $E(V, \varepsilon_i)$ with respect to the small strain ε_i of the lattice [23]:

$$E(V, \varepsilon_i) = E_0(V_0, 0) + V_0\left(\sum_i \tau_i \xi_i \varepsilon_i + \frac{1}{2}\sum_{ij} c_{ij}\varepsilon_i\xi_i\varepsilon_j\xi_j\right) + O(\varepsilon^3) \tag{4}$$

The E_0, and V_0 are the energy, and the volume of unstrained crystal, respectively. The factor ξ_i, takes the value 1 if the index i is equal to 1, 2 or 3 and the value 2 if it is equal to 4, 5 or 6. In the above equation τ_i are related to the strain ε_i. For our systems, the total energy $E(V, \varepsilon_i)$ is modified by applying five distortions defined as follows:

$$D_1 = \begin{pmatrix} 1+\varepsilon & 0 & 0 \\ 0 & 1+\varepsilon & 0 \\ 0 & 0 & 1 \end{pmatrix} \tag{5}$$

$$D_2 = \begin{pmatrix} \left(\frac{1+\varepsilon}{1-\varepsilon}\right)^{\frac{1}{2}} & 0 & 0 \\ 0 & \left(\frac{1-\varepsilon}{1+\varepsilon}\right)^{\frac{1}{2}} & 0 \\ 0 & 0 & 1 \end{pmatrix} \tag{6}$$

$$D_3 = \begin{pmatrix} 1 & 0 & 0 \\ 0 & 1 & 0 \\ 0 & 0 & 1+\varepsilon \end{pmatrix} \tag{7}$$

$$D_4 = \begin{pmatrix} 1 & 0 & \varepsilon \\ 0 & 1 & 0 \\ \varepsilon & 0 & 1 \end{pmatrix} \tag{8}$$

$$D_5 = \begin{pmatrix} (1+\varepsilon)^{-\frac{1}{3}} & 0 & 0 \\ 0 & (1+\varepsilon)^{-\frac{1}{3}} & 0 \\ 0 & 0 & (1+\varepsilon)^{\frac{2}{3}} \end{pmatrix} \tag{9}$$

The energy under these distortions can be obtained by the following equations:

$$E(V, \varepsilon) = E(V_0, 0) + V_0\delta(\tau_1 + \tau_2) + V_0\left((C_{11} + C_{12})\varepsilon^2 + O(\varepsilon^3)\right) \tag{10}$$

$$E(V, \varepsilon) = E(V_0, 0) + V_0\left((C_{11} - C_{12})\varepsilon^2 + O(\varepsilon^3)\right) \tag{11}$$

$$E(V, \varepsilon) = E(V_0, 0) + V_0\delta(\tau_3) + V_0\left(\frac{C_{33}}{2}\varepsilon^2 + O(\varepsilon^3)\right) \tag{12}$$

$$E(V, \varepsilon) = E(V_0, 0) + V_0\delta(\tau_5) + V_0\left(2(C_{55})\varepsilon^2 + O(\varepsilon^3)\right) \tag{13}$$

$$E(V, \varepsilon) = E(V_0, 0) + V_0\left((C_{zz})\frac{\varepsilon^2}{9} + O(\varepsilon^3)\right) \tag{14}$$

$$C_{zz} = C_{11} + C_{12} + 2C_{33} - 4C_{13} \tag{15}$$

The values of all the elastic constants calculated for our compounds are reported in Table 3. It is clear from the table that the findings are in excellent agreement with that obtained from other study [24–30]. To get a mechanical stability, the following criteria, known as the Born Huang criteria, must be satisfied [31]:

$$C_{55} > 0, (C_{11}–C_{12}) > 0, (C_{11}+C_{33}+C_{12}) > 0, (C_{11}+C_{12})\,C_{33} - 2C_{13}^2 > 0 \tag{16}$$

We can mention that it has been suggested by J. Wang et al. that the Born-Huang criteria are valid only for the stability analysis of an unstressed lattice and not for the stressed one [33,34].

We remark that the calculated elastic constants completely satisfy the criteria of the mechanical stability at a zero pressure, which reveal that all the studied materials are stable against any elastic deformations. One can observe that, the (C_{13}/C_{12}) ratio is larger than the (C_{33}/C_{11}) ratio which can be explained by the existence of a strong covalent bonding in the [100] than [001] direction. The current findings reveal that C_{11} is larger than C_{33} for Zr_2AlC, $(Zr_{0.75}V_{0.25})_2AlC$, $(Zr_{0.25}V_{0.75})_2AlC$, and V_2AlC compounds, which indicates that, the compression along the a, and b-axes are more difficult than that along the c-axis, contrary to the results of $(Zr_{0.5}V_{0.5})_2AlC$ compound; the a and b-axes are more compressible than the c axis. One can also remark that, C_{11} and C_{33} are considerably higher than all other elastic constants, which divulge that the compounds present a strong elastic anisotropy and indicating that the deformation resistances along the axial direction are stronger than the deformation resistances in shape. The variation of the elastic constants as function of V-doped concentration (x) are plotted in Fig. 4. This clearly illustrates an increase in the elastic coefficients

Table 3
The calculated elastic constants C_{ij} **(GPa)** for $(Zr_{1-x}V_x)_2AlC$ compounds.

Compounds	Method	Source	C_{11}	C_{12}	C_{13}	C_{33}	C_{55}	C_{66}
Zr_2AlC	FP-LAPW LDA	Our work	**261.91**	**63.55**	**84.40**	**260.56**	**103.27**	**99.18**
	CASTEP PP-PW	[13]	**278**	**64**	**67**	**235**	**97**	**107**
	CASTEP PP-PW	[4]	**258**	**67**	**63**	**221**	**91**	-
	CASTEP PP-PW	[25]	**258**	**67**	**63**	**221**	**91**	-
$(Zr_{0.75}V_{0.25})_2AlC$	FP-LAPW LDA	Our work	**301.05**	**79.39**	**115.83**	**295.81**	**137.64**	**110.83**
$(Zr_{0.5}V_{0.5})_2AlC$	FP-LAPW LDA	Our work	**324.91**	**84.27**	**115.72**	**332.11**	**158.49**	**120.32**
$(Zr_{0.25}V_{0.75})_2AlC$	FP-LAPW LDA	Our work	**346.80**	**105.72**	**150.60**	**343.14**	**163.18**	**120.53**
V_2AlC	FP-LAPW LDA	Our work	**389.78**	**126.64**	**140.06**	**377.74**	**181.40**	**131.57**
	GGA-PAW	[32]	**338**	**92**	**148**	**328**	**155**	-
	GGA-PW-PP	[26]	**346**	**71**	**106**	**314**	**151**	**138**
	CASTEP PP-PW	[14]	**345.4**	**61.6**	**100.5**	**312.4**	**147.6**	-

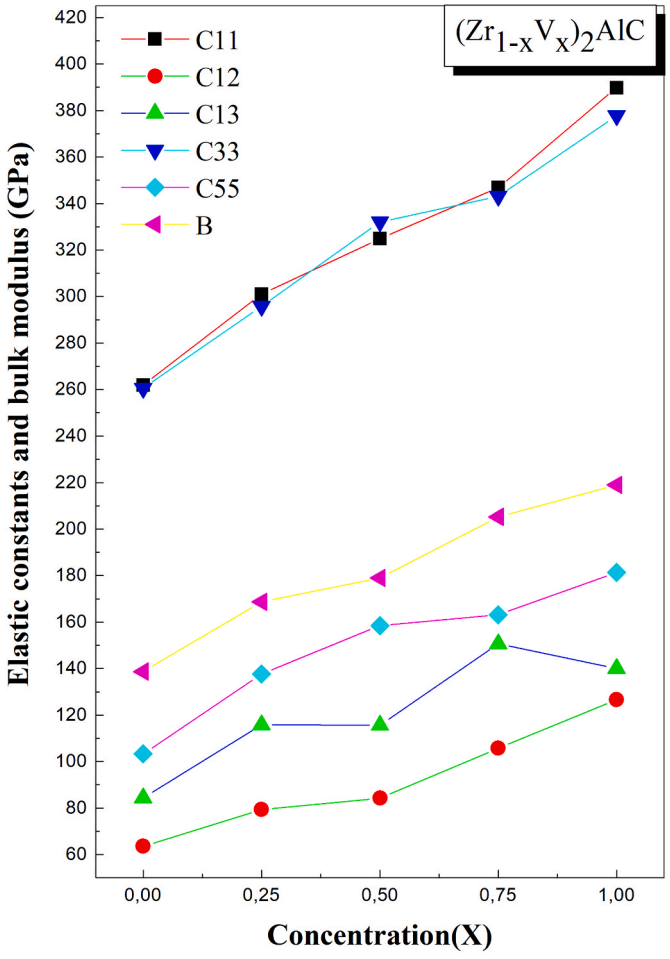

Fig. 4. The variations of the elastic constants and bulk modulus as a function of V-doped concentration (x).

when increasing Vanadium concentration.

3.2.2. Anisotropy factor

Secondly, we estimated an important parameters called the shear anisotropy parameters. For the hexagonal lattice, One defines three parameters expressed by the following relations [35]:

$$A_1 = \frac{(C_{11} + C_{12} + 2C_{33} - 4C_{13})}{6C_{55}} \tag{17}$$

$$A_2 = \frac{2C_{55}}{(C_{11} - C_{12})}$$

$$A_3 = A_1.A_2 = \frac{(C_{11} + C_{12} + 2C_{33} - 4C_{13})}{3(C_{11} - C_{12})} \tag{18}$$

Where A_1 for the {1 0 0} plane between the [011] and [010] directions, A_2 for the {0 1 0} plane between the [101] and [001] directions, and A_3 for the {0 0 1} plane between the [110] and [010] directions. The anisotropy factor, which indicates in which direction the MAX phase is more compressible, is defined as follows:

$$\frac{k_c}{k_a} = \frac{(C_{11} + C_{12} - 2C_{13})}{(C_{33} - C_{13})} \tag{19}$$

The calculated values of the shear anisotropic parameters as well as that of anisotropy factor are summarized in Table 4. From this result; all the values of A_i are close to 1, which indicate the degree of elastic anisotropy, as it determines that the middle plane is the most important between the three parameters. We see that the calculated value of the anisotropy factor k_c/k_a of our compounds is less than 1; indicating that the compressibility along the a-axis is stronger than that along the c-axis.

3.2.3. Elastic modulus and hardness

In order to evaluate the macroscopic mechanical properties of the compounds we have calculated the elastic modulus by using the Voigt, Reuss and Hill approximations [36–38]. The Bulk modulus B_V, B_R, B_H, and Shear modulus G_V, G_R, G_H are defined by the following relations:

Voigt's approximation

$$B_V = \frac{1}{2}(2(C_{11} + C_{12}) + 4C_{13} + C_{33}) \tag{20}$$

$$G_V = \frac{1}{30}(C_{11} + C_{12} + 2C_{33} - 4C_{13} + 12C_{55} + C_{66}) \tag{21}$$

Table 4
The shear anisotropic parameters for the three different shear planes (A_1, A_2 *and* A_3) and anisotropy factor $\frac{k_c}{k_a}$ ratio for $(Zr_{1-x}V_x)_2AlC$ compounds.

Compounds	Method	Source	A_1	A_2	A_3	$\frac{k_c}{k_a}$
Zr_2AlC	FP-LAPW LDA	Our work	**0.8214**	**1.04123**	**0.8553**	**0.8893**
	CASTEP PP-PW	[13]	-	-	-	-
	CASTEP PP-PW	[25]	**0.94**	**0.95**	**0.90**	**1.26**
	CASTEP PP-PW	[4]	**0.53**	**1.80**	**0.95**	**0.58**
$(Zr_{0.75}V_{0.25})_2AlC$	FP-LAPW LDA	Our work	**0.6159**	**1.2419**	**0.7650**	**0.8266**
$(Zr_{0.5}V_{0.5})_2AlC$	FP-LAPW LDA	Our work	**0.6420**	**1.3172**	**0.8456**	**0.8213**
$(Zr_{0.25}V_{0.75})_2AlC$	FP-LAPW LDA	Our work	**0.5478**	**1.3538**	**0.7416**	**0.7859**
V_2AlC	FP-LAPW LDA	Our work	**0.6538**	**1.3787**	**0.9014**	**0.9941**

Reuss's approximation

$$B_R = \frac{(C_{11}+C_{12})C_{33}-2C_{13}^2}{C_{11}+C_{12}+2C_{33}-4C_{13}} \quad (22)$$

$$G_R = \frac{5}{20}\times\frac{C_{55}C_{66}\left[(C_{11}+C_{12})C_{33}-2C_{13}^2\right]}{3B_V C_{44}C_{66}+\left\{(C_{11}+C_{12})C_{33}-2C_{13}^2\right\}(C_{55}+C_{66})\}} \quad (23)$$

Hill's approximation

$$B_H = \frac{(B_V+B_R)}{2} \quad (24)$$

$$G_H = \frac{(G_V+G_R)}{2} \quad (25)$$

One can deduce the Young's modulus E, and Poisson's ratio υ given by the following relationships [39,40]:

$$E = \frac{9BG}{3B+G} \quad (26)$$

$$\upsilon = \frac{3B-2G}{2(3B+G)} \quad (27)$$

The results of the calculated elastic modulus from the Hill's approximation are reported in Table 5. The values of various physical quantities (Bulk, shear, and Young's modulus) increase with the increasing of V-doped concentration (x). The V_2AlC is relatively more incompressible, and stiffer and have the greater resistance to shear deformations. From the table, it is clear that the calculated values of the Poisson's ratio are less than 0.25 for all the materials, which indicate a covalent character in inter-atomic bounding for these materials. Moreover, the value of Poisson's ratio can also be used to distinguish between brittle and ductile behavior [41]. The calculated values of Poisson's ratio which are less than 0.26 are indicative of brittle response to applied stress. In addition to the Poisson's ratio a critical value of Pugh's ratio (K = G/B ~ 0.57) separate between the brittle and ductile nature of materials [42]. It's obvious from the results that the values are greater than 0.57 for all the compounds, which indicate a brittle behavior for these materials which is consistent with Poisson's ratio results. Cauchy pressure of any crystal is quite important in crystal physics. It gives information about the ionic/covalent bonding of the materials by value of Cauchy pressure positive/negative, respectively [43]. In hexagonal materials, the Cauchy pressure can be estimated for the two different directions:

$$P_X^{Cauchy} = C_{13} - C_{55} \quad (28)$$

$$P_Z^{Cauchy} = C_{12} - C_{66} \quad (29)$$

All the values of Cauchy pressure P_x^{Cauchy}, and P_y^{Cauchy} are negative, these results confirm the covalent character of our compounds. We can note that the three criteria give the same result about the nature of the chemical bonding which approves that the three parameters (Cauchy pressure, the Poisson's ratio, and Pugh's ratio) are related.

Another parameter which is closely related to bulk and shear moduli of materials, namely Vickers hardness can be calculated by using Chen's formula [44]:

$$H_V = 2\left(K^2G\right)^{0.585} - 3 \quad (30)$$

From the results, the values of V_2AlC, and $(Zr_{0.5}V_{0.5})_2AlC$ compounds exceeds the value of 20 GPa which indicate that, these compounds are hard materials.

3.2.4. Debye temperature

The Debye temperature (θ_D) is an important parameter. The θ_D can be estimated from the average sound velocity proposed by Anderson [45], which is related by the elastic modulus. The formulas used to calculate θ_D are expressed in the following relationships:

$$\theta_D = \frac{h}{k_B}\left[\frac{3n}{4\pi}\left(N_a\cdot\frac{\rho}{M}\right)\right]^{\frac{1}{3}}\cdot v_m \quad (31)$$

$$v_m = \left[\frac{1}{3}\left(\frac{2}{v_t^3}+\frac{1}{v_l^3}\right)\right]^{\frac{-1}{3}} \quad (32)$$

$$v_l = \left(\frac{3B+4G}{3\rho}\right)^{\frac{1}{2}} \quad (33)$$

$$v_t = \left(\frac{G}{\rho}\right)^{\frac{1}{2}} \quad (34)$$

Where k_B, h, n, N_A, ρ, M, v_m, v_l, and v_t are Boltzmann's constant, Planck's constant, number of atoms in unit cell, Avogadro's number, density, molecular weight, the average sound velocity, longitudinal and transverse sound velocity, respectively. The results of these parameters (θ_D, v_m, v_l, and v_t) are recapitulated in Table 6. The data indicate that the density decreases when the V-doped concentration (x) increases, which leads to an increase in Debye temperature and average sound velocity. We can deduce that when the V-doped concentration (x) increases the compounds become stiffer.

The variations of the wave velocity and Debye temperature with vanadium concentration are plotted in Fig. 5. One can observe that the wave velocity as well Debye temperature increase when the V concentration increases.

We have also interested to investigate the melting temperature *Tm* and Grüneisen parameter γ, which are another important parameters for these type of materials. The Grüneisen parameter describes how the thermal properties of a material vary with the volume of crystal. The low values of Grüneisen parameter indicates that the compounds possess a

Table 5

The calculated bulk modulus B_H **(GPa)**, shear modulus G_H **(GPa)**, Young's modulus E **(GPa)**, Poisson's ratio *v*, Pugh's ratio $\frac{G_H}{B_H}$, Vickers hardness H_V **(GPa)**, and Cauchy pressure P_X^{Cauchy}, and P_Z^{Cauchy} for $(Zr_{1-x}V_x)_2AlC$ compounds.

Compounds	Method	Source	B_H	G_H	$\frac{G_H}{B_H}$	E	H_v	υ	P_X^{Cauchy}	P_Z^{Cauchy}
Zr_2AlC	FP-LAPW LDA	Our work	**138.70**	**97.67**	**0.704**	**237.31**	**16.356**	**0.21**	**−18.87**	**−35.62**
	CASTEP PP-PW	[13]	**131.6**	**99.5**	-	**238.4**	-	**0.19**	-	-
	CASTEP PP-PW	[25]	**125**	**92**	-	**222**	**16.7**	**0.20**	-	-
	CASTEP PP-PW	[4]	**124**	**91**	**0.73**	**219**	**16.37**	**0.24**	-	-
$(Zr_{0.75}V_{0.25})_2AlC$	FP-LAPW LDA	Our work	**168.67**	**114.48**	**0.678**	**280.08**	**17.344**	**0.22**	**−21.81**	**−31.44**
$(Zr_{0.5}V_{0.5})_2AlC$	FP-LAPW LDA	Our work	**178.98**	**129.87**	**0.725**	**313.74**	**20.685**	**0.20**	**−42.77**	**−36.05**
$(Zr_{0.25}V_{0.75})_2AlC$	FP-LAPW LDA	Our work	**205.26**	**128.07**	**0.623**	**318.06**	**16.687**	**0.241**	**−12.58**	**−14.80**
V_2AlC	FP-LAPW LDA	Our work	**218.98**	**146.53**	**0.669**	**359.53**	**20.120**	**0.226**	**−41.33**	**−4.92**
	GGA-PWPP	[26]	**175**	**139**	-	**261**	-	-	-	-
	CASTEP PP-PW	[14]	**169.7**	**135.7**	-	**321.0**	-	-	-	-
	GGA-PAW	[32]	**195.0**	**124.5**	**0.79**	**307.9**	-	**0.236**	-	-

Table 6
The calculated density ρ **(g/cm^3)**, longitudinal, transverse, and average elastic wave velocity v_l, v_t, v_m**(m/s)** and the Debye temperatures Δ_D θ_D**(*K*)** for $(Zr_{1-x}V_x)_2AlC$ compounds.

Compounds	Method	Source	ρ	v_l	v_t	v_m	θ_D
Zr_2AlC	FP-LAPW LDA	Our work	**5.3619**	**7082.11**	**4268.01**	**4719.42**	**544.908**
	CASTEP PP-PW	[25]	**5.278**	**6849.13**	**4174.41**	**4610.71**	**529.70**
	CASTEP PP-PW	[13]	**5.56**	**6891**	**4228**	**4667**	**544**
$(Zr_{0.75}V_{0.25})_2AlC$	FP-LAPW LDA	Our work	**5.3119**	**7726.85**	**4612.12**	**5104.69**	**609.183**
$(Zr_{0.5}V_{0.5})_2AlC$	FP-LAPW LDA	Our work	**5.2596**	**8182.63**	**4969.27**	**5490.64**	**673.497**
$(Zr_{0.25}V_{0.75})_2AlC$	FP-LAPW LDA	Our work	**5.2068**	**8498.16**	**4959.51**	**5500.72**	**699.412**
V_2AlC	FP-LAPW LDA	Our work	**5.1339**	**8984.52**	**5343.52**	**5916.25**	**782.824**
	GGA-PAW	[32]	**4.81**	**8863**	**5087**	**5369**	**731**
	CASTEP PP-PW	[14]	**4.84**	-	-	-	**710**

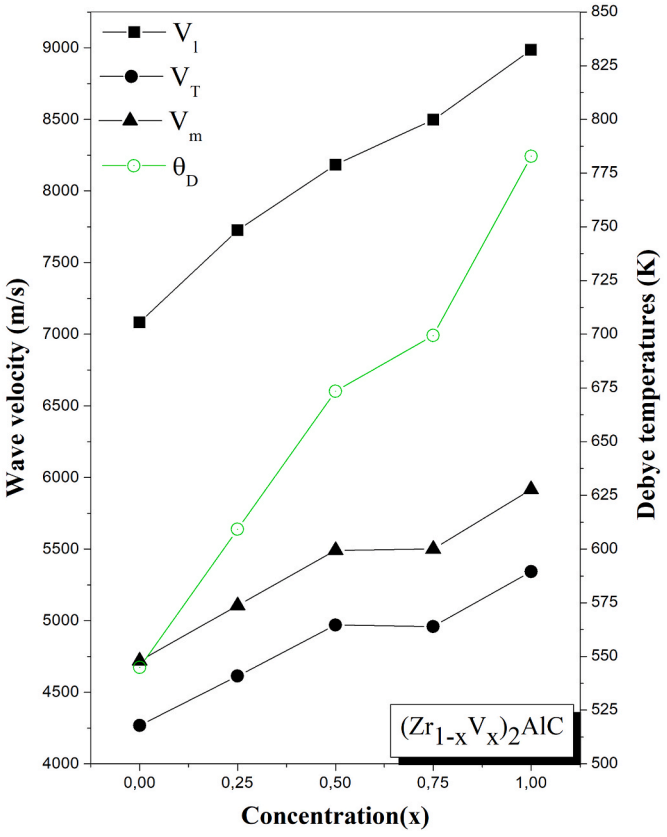

Fig. 5. The variations of the wave velocity and Debye temperature as a function of V-doped concentration (x).

rather stiff lattice and a good thermal conductivity. The Tm and γ are related by the elastic constants and the Poisson's ratio, respectively [46, 47]:

$$Tm = 354 + \frac{3}{2}(2C_{11} + C_{33}) \tag{35}$$

$$\gamma = \frac{3}{2}\frac{(1+v)}{(2-3v)} \tag{36}$$

The calculated values of melting temperature and Grüneisen parameter are indicated in Table 7. From these findings, we observe that the V_2AlC compound exhibit the highest value of melting temperature indicating that this compound presents a strong bonding and good thermal conductivity compared to others.

Table 7
The Melting temperature Tm (**K**) and Grüneisen's parameter **γ** for $(Zr_{1-x}V_x)_2AlC$ compounds.

Compounds	Method	Source	Tm	γ
Zr_2AlC	FP-LAPW LDA	Our work	**1530.57**	**1.340**
	CASTEP PP-PW	[25]	**1459**	**1.30**
$(Zr_{0.75}V_{0.25})_2AlC$	FP-LAPW LDA	Our work	**1700.88**	**1.378**
$(Zr_{0.5}V_{0.5})_2AlC$	FP-LAPW LDA	Our work	**1826.91**	**1.3129**
$(Zr_{0.25}V_{0.75})_2AlC$	FP-LAPW LDA	Our work	**1909.071**	**1.457**
V_2AlC	FP-LAPW LDA	Our work	**2089.965**	**1.3917**

3.3. Electronic properties

In this part, we investigate the electronic structure of the compounds, which provides important information about the nature of chemical bonding, electrical resistivity, electronic conductivity and optical absorption. Firstly, we calculated the band structure of the herein studied compounds along the higher symmetry points in the first Brillouin zone (BZ). The results of band structure are shown in Fig. 6 and Fig. 7 for the ternary and quaternary MAX phase compounds, respectively. From these figures, it is obvious that the band structure is topologically identical and presents a great dispersion at the valence and conduction bands. One can also observe that at the Fermi level there is a significant overlap between the valence and conduction bands for the five investigated compounds. This confirms the metallic nature for the materials. Secondly, the total density of states (TDOS) and the projected density of states (PDOS) were studied in a wide energy interval [-10 eV, 7 eV] symmetric around the Fermi level. The TDOS and PDOS of the ternary

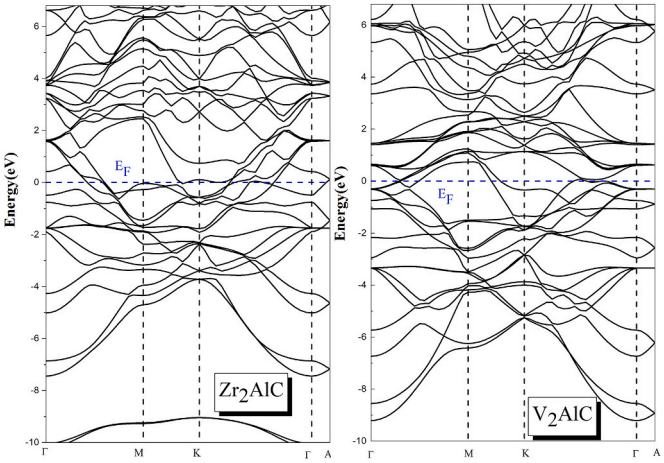

Fig. 6. The band structure of Zr_2AlC and V_2AlC compounds.

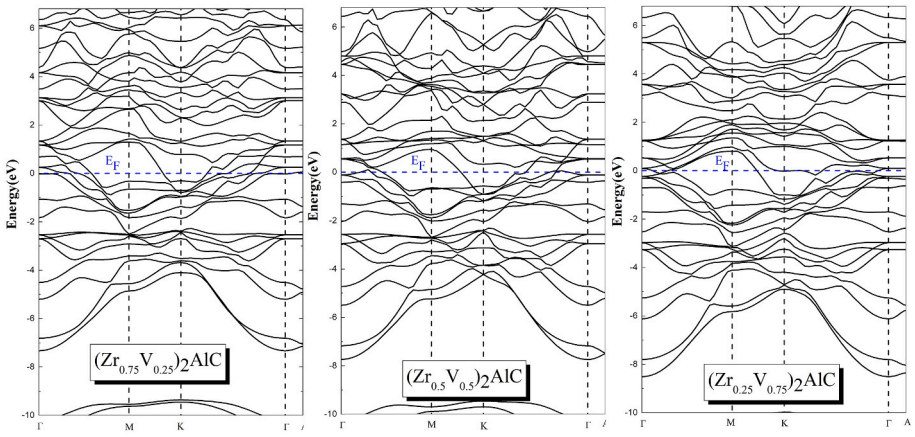

Fig. 7. The band structures of $(Zr_{1-x}V_x)_2AlC$ compounds (with x = 0.25, 0.50 and 0.75).

and quaternary compounds are illustrated in Fig. 8 and Fig. 9, respectively. The metallic nature of the compounds is confirmed by the non-vanishing value of the TDOS at the Fermi level. Furthermore, from the PDOS results, we can split the DOS spectrum into three main regions for the materials. The region located in lower valence band presents the *s-p* hybridization between the *s* orbital and *p* orbital of C and Al atoms, respectively. While, the second region located near the Fermi level we can observe that the *d*-(Zr, V) and *p*-C states are strongly mixed which reveal the presence of a strong covalent bonding in this region. This strong covalent bonding is mainly origin of the metallicity of our compounds. The remaining region contains weaker covalent bonding between *d*-Zr and *p*-Al states. All these observations confirm the obtained findings from the mechanical properties.

3.4. Thermodynamic properties

The thermodynamic properties were investigated in the temperature range from 0 to 450 K and in the pressure range from 0 to 30 GPa. We used the Gibbs2 package [48] based upon the quasi-harmonic Debye model [49]. The Debye model consists of linking the elastic properties of solid to its acoustic vibration in the center of Brillouin zone.

The calculation of the heat capacity allows to get an insight on the vibrational properties of materials. The heat capacity of $(Zr_{1-x}V_x)_2AlC$ as functions of temperature and pressure at constant volume and pressure (Cv and Cp) are plotted in Fig. 10 and Fig. 11, respectively. At low temperatures, the heat capacities increase when temperature increases and at higher temperatures the effect of anharmonic Cv is deleted, and Cv tends towards to the limit of Dulong-petit limit common to all investigated materials at 0 GPa. When the pressure increases the heat capacity decreases at 300 K. The investigation of the Debye temperature (θ_D) as a function of temperature at 0 GPa and pressure at 300 K for the compounds is plotted in Fig. 12. It mentions that the V_2AlC compound has a higher θ_D than the others and there is no effect on θ_D below temperature 225 K and when the temperature is higher than 225 K, the values of θ_D show slight decrease at zero pressure whereas at ambient temperature (300 K), we notice that θ_D increases with when pressure increases. The influence of the pressure is more significant than that of the temperature on θ_D of $(Zr_{1-x}V_x)_2AlC$. The entropy (S) as a function of temperature and pressure is plotted in Fig. 13. It shows that the entropy increases with increasing in temperature and decreases with increasing in pressure. We also noticed that the entropy is more sensitive to the temperature than to the pressure. The variation of the volume as functions of the temperature and pressure are presented in Fig. 14 for $(Zr_{1-x}V_x)_2AlC$. It is clearly seen that the volume exhibits a very moderate decrease with pressure at 300 K and a slight increase with temperature at a small rate which indicates that our compounds are far from (Tm) melting point and the structural integrity is preserved at 0 GPa, which means that pressure is more significant than temperature at ambient conditions (0 GPa and 300 K).

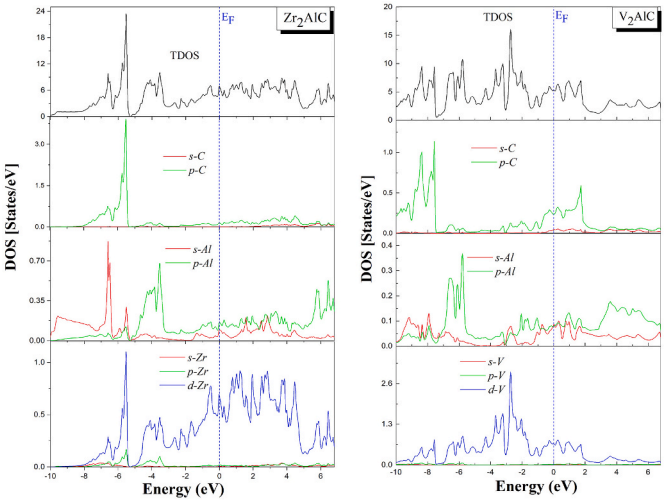

Fig. 8. The total and partial densities of states for Zr_2AlC and V_2AlC compounds.

4. Conclusion

The ab-*initio* plane-wave (FP-LAPW) method as implemented in Wien2k was used to study the structural, electronic, mechanical and thermodynamic properties of the MAX phase $(Zr_{1-x}V_x)_2AlC$ compounds. Firstly, the internal parameter and lattice parameters were optimized. It was found that, the compression along the (a, c)-axis decreased gradually when V-doped concentration (x) increased. The formation energy was calculated in order to determine the stability of the compounds. Secondly from the mechanical properties we obtained that the studied compounds are stable against any elastic deformation. The mechanical properties revealed that our compounds are brittle and stiff materials. The calculation of the electronic properties showed a metallic behavior with the presence of a strong covalent bond. Within the quasi-harmonic Debye model, the effect of temperature and pressure on the heat capacity, Debye's temperature, entropy and the volume were calculated at ambient condition. These parameters were found to be more influenced by pressure than temperature. The findings are in reasonable agreement with reported works for the ternary compounds. However, the investigated properties for the quaternary MAX phase were not reported before.

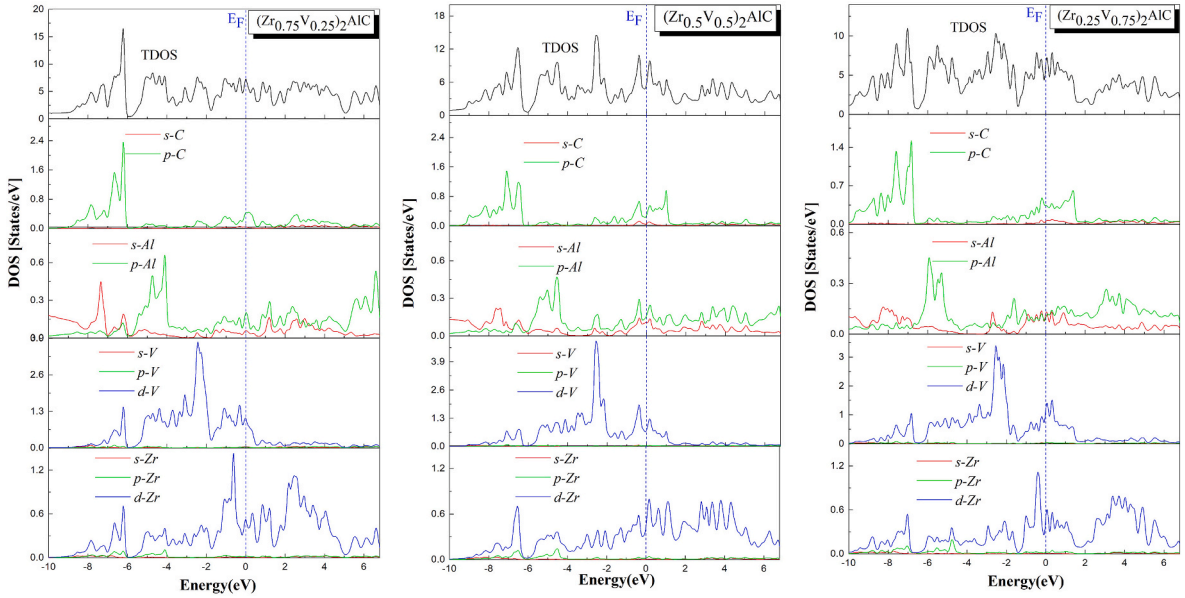

Fig. 9. The total and partial densities of states for $(Zr_{1-x}V_x)_2AlC$ compounds (with x = 0.25, 0.50 and 0.75).

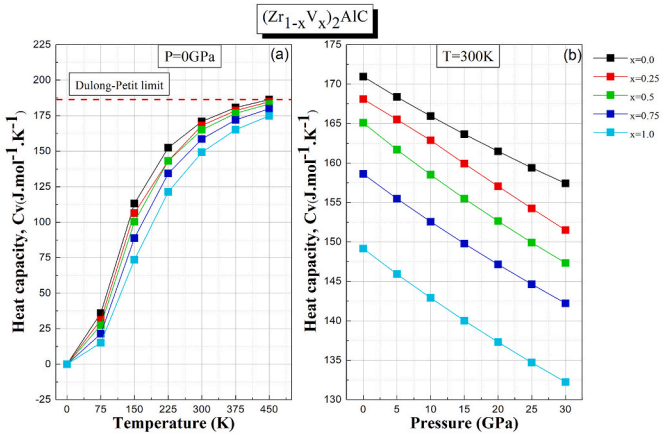

Fig. 10. The Heat capacity at a constant volume of $(Zr_{1-x}V_x)_2AlC$ as a function of temperature at zero pressure (a) and as a function of pressure at room temperature (b).

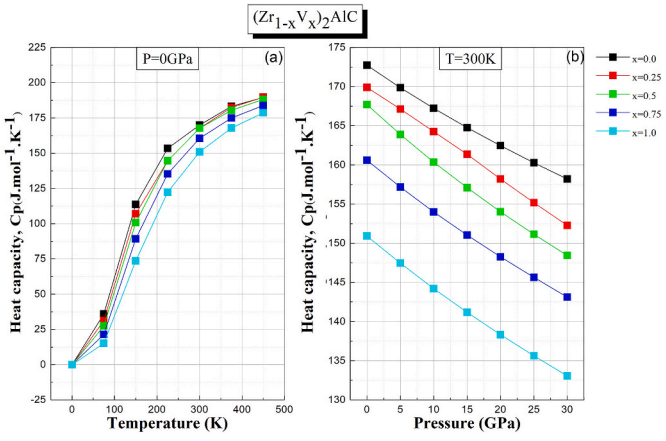

Fig. 11. The Heat capacity at a constant pressure of $(Zr_{1-x}V_x)_2AlC$ as a function of temperature at zero pressure (a) and as a function of pressure at room temperature (b).

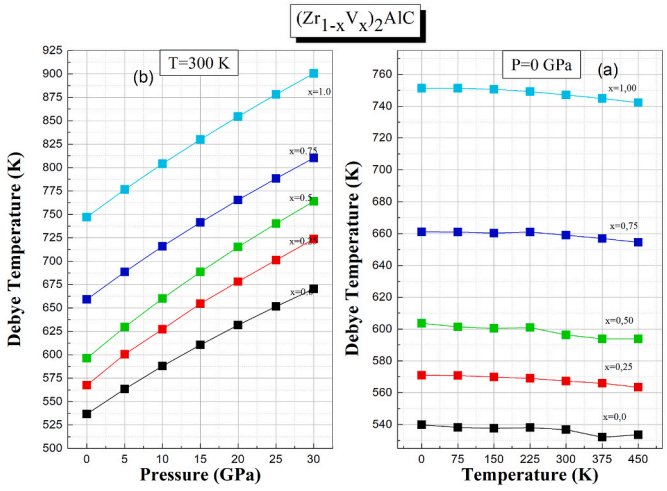

Fig. 12. The Debye temperature of $(Zr_{1-x}V_x)_2AlC$ as a function of temperature at zero pressure (a) and as a function of pressure at room temperature (b).

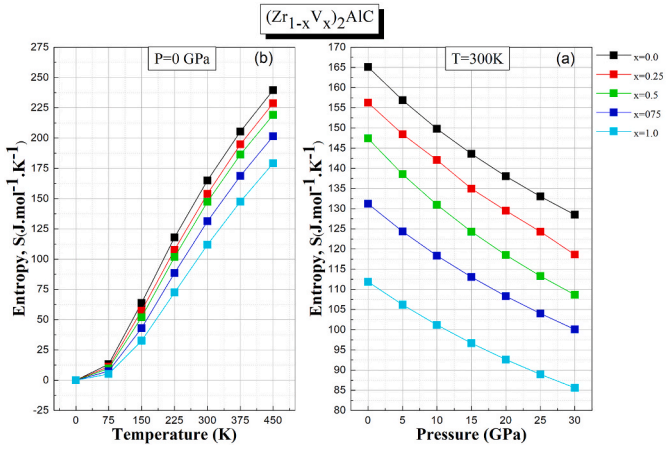

Fig. 13. The entropy of $(Zr_{1-x}V_x)_2AlC$ as a function of temperature at zero pressure (a) and as a function of pressure at room temperature (b).

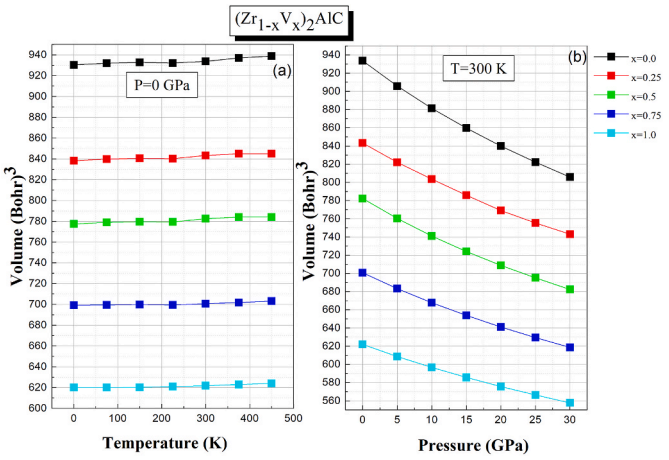

Fig. 14. The volume of $(Zr_{1-x}V_x)_2AlC$ as a function of temperature at zero pressure (a) and pressure at room temperature (b).

CRediT authorship contribution statement

Ahmed Azzouz-Rached: All the authors were involved in the preparation of the manuscript. Individual contributions to the present manuscript. **Habib Rached:** contributed to the majority of the 1st manuscript (calculation, writing the 1st manuscript). **Ismail Ouadha:** Supervision, and contributed to the major revision of the manuscript and contributed to the interpretation of the results. **Djamel Rached:** developed the theoretical framework. **Abderrahmane Reggad:** developed the theoretical framework.

Declaration of competing interest

The authors declare that they have no known competing financial interests or personal relationships that could have appeared to influence the work reported in this paper.

Acknowledgements

This work was financially supported by DGRSDT (The general directorate for scientific research and technological development "**ALGERIA**") under PRFU project [No. **B00L02UN220120190002**].The authors are very grateful to **BOUHEKKA Ahmed** from Ahmed Ben Yahia El-Wancharissi University Center of Tissemsilt (Algeria) for his helpful assistance in improving the English language of the manuscript.

References

[1] T. Lapauw, K. Lambrinou, T. Cabioc'h, J. Halim, J. Lu, A. Pesach, J. Vleugels, J. Eur. Ceram. Soc. 36 (2016) 1847–1853.
[2] M.W. Barsoum, Prog. Solid State Chem. 28 (2000) 201–281.
[3] M.W. Barsoum, MAX Phases : Properties of Machinable Ternary Carbides and Nitrides, Wiley-VCH Verlag GmbH & Co, Weinheim, Germany, 2013.
[4] M.A. Ali, M.M. Hossain, N. Jahan, A.K.M.A. Islam, S.H. Naqib, Comput. Mater. Sci. 131 (2017) 139–145.
[5] E. Zapata-Solvas, S.-R.G. Christopoulos, N. Ni, D.C. Parfitt, D. Horlait, M. E. Fitzpatrick, A. Chroneos, W.E. Lee, J. Am. Ceram. Soc. 100 (2017) 1377.
[6] T. El-Raghy, M.W. Barsoum, A. Zavaliangos, S.R. Kolidindi, J. Am. Ceram. Soc. 82 (1999) 2855.
[7] M.W. Barsoum, L. Farber, T. El-Raghy, Metall. Mater. Trans. 30 (1999) 1727–1738.
[8] D.J. Tallman, E.N. Hoffman, E.N. Caspi, B.L. Garcia-Diaz, G. Kohse, R.L. Sindelar, M.W. Barsoum, Acta Mater. 85 (2015) 132–143.
[9] A. Yakoubi, L. Beldi, B. Bouhafs, M. Ferhat, P. Ruterana, Solid State Commun. 139 (2006) 485–489.
[10] M.W. Barsoum, T. El-Raghy, J. Am. Ceram. Soc. 79 (1996) 1953–1956.
[11] P. Eklund, M. Beckers, U. Jansson, H. Högberg, L. Hultman, Thin Solid Films 518 (2010) 1851–1878.
[12] M. Haftani, M.S. Heydari, H.R. Baharvandi, N. Ehsani, Int. J. Refract. Metals Hard Mater. 61 (2016) 51–60.
[13] A. Bouhemadou, R. Khenata, M. Chegaar, Eur. Phys. J. B 56 (2007) 209–215.
[14] M.R. Khatun, M.A. Ali, F. Parvin, A.K.M.A. Islam, Results Phys. 7 (2017) 3634–3639.
[15] P. Blaha, K. Schwarz, J. Luitz, WIEN97: A Full Potential Wave Package for Calculating Crystal Properties, Vienna University of Technology, Austria, 2001.
[16] P. Blaha, K. Schwarz, G.K.H. Madsen, D. Kvasnicka, J. Luitz, in: K. Schwarz (Ed.), WIEN2k: an Augmented Plane Wave+Local Orbitals Program for Calculating Crystal Properties, 'TechnischeUniversität Wien', Austria, 2001.
[17] J.P. Perdew, Y. Wang, Phys. Rev. B 46 (1992) 12947–12954.
[18] H.J. Monkhorst, J.D. Pack, Phys. Rev. B 13 (1976) 5188–5192.
[19] 2Doptimize package is provided by M. Jamal as part of the commercial code WIEN2K, http://www.wien2k.at/.
[20] F.D. Murnaghan, Proc. Natl. Acad. Sci. Unit. States Am. 30 (1944) 244–247.
[21] Gokhan Surucu, Mater. Chem. Phys. 203 (2018) 106–117.
[22] H. Rached, S. Bendaoudia, D. Rached, Mater. Chem. Phys. 193 (2017) 453–469.
[23] M. Jamal, Hex-elastic, 2012. http://www.wien2k.at/reg_user/unsupported/cubic-elast/.
[24] F. Luo, Z. Guo, X. Zhang, C. Yuan, L. Cai, Chin. J. Chem. Phys. 28 (2015) 263–268.
[25] M.A. Ali, M.M. Hossain, M.A. Hossain, M.T. Nasir, M.M. Uddin, M.Z. Hasan, A.K.M. A. Islam, S.H. Naqin, J. Alloys Compd. 743 (2018) 146–154.
[26] J. Wang, Y. Zhou, Phys. Rev. B 69 (2004) 214111.
[27] Z. Sun, R. Ahuja, S. Li, J.M. Schneider, Appl. Phys. Lett. 83 (2003) 899–901.
[28] J.C. Schuster, H. Nowotny, C. Vaccaro, J. Solid State Chem. 32 (1980) 213–219.
[29] J.C. Schuster, H. Nowotny, C. Vaccaro, J. Solid State Chem. 32 (1980) 213–219.
[30] C. Wang, T. Yang, J. Xiao, S. Liu, J. Xue, Am. Ceram. Soc. 99 (2016) 1769–1777.
[31] M. Born, Math. Proc. Camb. Phil. Soc. 36 (1940) 160.
[32] Z. Sun, S. Li, R. Ahuja, J.M. Schneider, Solid State Commun. 129 (2004) 589–592.
[33] J. Wang, S. Yip, S.R. Phillpot, D. Wolf, Phys. Rev. Lett. 71 (1993) 4182.
[34] J. Wang, S. Yip, S.R. Phillpot, D. Wolf, Phys. Rev. B 52 (1995) 12627.
[35] H.M. Ledbetter, J. Phys. Chem. 6 (1977) 1181–1203.
[36] W. Voigt, Lehrburch der Kristallphysik, Teubner, Leipzig, 1928.
[37] A. Reuss, Z. Angew. Math. Mech. 9 (1929) 49.
[38] R. Hill, Proc. Phys. Soc. 65 (1952) 349–354.
[39] A. Bouhemadou, Braz. J. Phys. 40 (2010) 52–57.
[40] M.A. Ali, A.K.M.A. Islam, M.S. Ali, J. Sci. Res. 4 (2012) 1–10.
[41] I.N. Frantsevich, F.F. Voronov, S.A. Bokuta.Naukova Dumka, Kiev, 1983, pp. 60–180.
[42] S.F. Pugh, The London, Edinburgh, and Dublin Philosophical Magazine and, J. Sci. 45 (1954) 823–843.
[43] M. Jamal, N. Kamali Sarvestani, A. Yazdani, A.H. Reshak, RSC Adv. 4 (2014) 57903–57915.
[44] V. Belomestnykh, E. Teslevva, Tech. Phys. 49 (2004) 1098–1100.
[45] O.L. Anderson, J. Phys. Chem. Solid. 24 (1963) 909–917.
[46] M.E. Fine, L.D. Brown, H.L. Marcus, Scripta Metall. 18 (1984) 951–956.
[47] V. Belomestnykh, E. Tesleva, Tech. Phys. 49 (2004) 1098–1100.
[48] A. Otero-de-la-Roza, D. Abbasi-Pérez, V. Luaña, Comput. Phys. Commun. 182 (2011) 2232–2248.
[49] R. Fox, Br. J. Hist. Sci. 4 (1968) 1–22.